NASA CR-134506
UCRL-51466

FILAMENT-WOUND KEVLAR 49/EPOXY PRESSURE VESSELS

T. T. Chiao
M. A. Hamstad
M. A. Marcon
J. E. Hanafee

November 9, 1973

Prepared for U.S. Atomic Energy Commission under contract No. W-7405-Eng-48

LAWRENCE
LIVERMORE
LABORATORY

University of California/Livermore

PREPARED FOR NATIONAL AERONAUTICS
AND SPACE ADMINISTRATION

NASA-LEWIS RESEARCH CENTER
CONTRACT C-13980-C
R. F. LARK, PROJECT MANAGER

Printed in the United States of America
Available from
National Technical Information Service
U. S. Department of Commerce
5285 Port Royal Road
Springfield, Virginia 22151
Price: Printed Copy $___*; Microfiche $0.95

*Pages	NTIS Selling Price
1-50	$4.00
51-150	$5.45
151-325	$7.60
326-500	$10.60
501-1000	$13.60

TID-4500, UC-4
Chemistry

LAWRENCE LIVERMORE LABORATORY
University of California/Livermore, California/94550

UCRL-51466

FILAMENT-WOUND KEVLAR 49/EPOXY PRESSURE VESSELS

T. T. Chiao
M. A. Hamstad
M. A. Marcon
J. E. Hanafee

MS. date: November 9, 1973

1. Report No.	2. Government Accession No.	3. Recipient's Catalog No.
NASA CR-134506		

4. Title and Subtitle	5. Report Date
Filament-Wound Kevlar 49/Epoxy Pressure Vessels	November 9, 1973
	6. Performing Organization Code

7. Author(s)	8. Performing Organization Report No.
T. T. Chiao, M. A. Hamstad, M. A. Marcon and J. E. Hanafee	UCRL-51466
	10. Work Unit No.

9. Performing Organization Name and Address	11. Contract or Grant No.
Lawrence Livermore Laboratory Livermore, California 94550	C-13980-C
	13. Type of Report and Period Covered Contractor Report April 1, 1972 - June 30, 1973

12. Sponsoring Agency Name and Address	14. Sponsoring Agency Code
National Aeronautics and Space Administration Washington, D. C. 20546	

15. Supplementary Notes

Project Manager, R. F. Lark
Materials and Structures Division
NASA-Lewis Research Center
Cleveland, Ohio 44135

16. Abstract

The performance of an organic fiber (Kevlar 49) has been investigated. First, a detailed study of the strength of fiber/epoxy strands was completed. Variables studied included: fiber uniformity, strength distribution at room and LN_2 temperatures, stress-strain characteristics, strain rate effect on the fiber strength, stress-rupture behavior, and ageing under no load. Second, the composite performance in filament-wound pressure vessels was studied. Variables studied included: spherical vs cylindrical vessels, cylinderical vessel design and size, winding patterns, reproducibility, pressurization rate, fatigue, and effect of liquid hydrogen temperatures. Third, a study was made of the acoustic emission generated during tensile tests of the fiber/epoxy strands, tensile tests of fiber/epoxy elongated NOL rings, burst tests at room temperature of the cylindrical and spherical pressure vessels, and vessel fatigue tests. Fourth, a microstructural characterization of the failure mode of the fiber was carried out using transmission and scanning electron microscopy and optical microscopy. Fracture surfaces of bare fibers were compared with epoxy impregnated strands from tensile tests, pressure vessels, and NOL rings.

17. Key Words (Suggested by Author(s))	18. Distribution Statement
Kevlar 49 fiber Filament winding Pressure vessels Advanced composites Metallic liners Acoustic emission	Unclassified, Unlimited

19. Security Classif. (of this report)	20. Security Classif. (of this page)	21. No. of Pages	22. Price*
Unclassified	Unclassified	66	$3.00

* For sale by the National Technical Information Service, Springfield, Virginia 22151

NASA-C-168 (Rev. 6-71)

Contents

FILAMENT-WOUND KEVLAR 49/EPOXY PRESSURE VESSELS

Abstract

The performance of an organic fiber (Kevlar-49) has been investigated. First, a detailed study of the strength of fiber/epoxy strands was completed. Variables studied included: fiber uniformity, strength distribution at room and LN_2 temperatures, stress-strain characteristics, strain rate effect on the fiber strength, stress-rupture behavior, and ageing under no load. Second, the composite performance in filament-wound pressure vessels was studied. Variables studied included: spherical vs cylindrical vessels, cylinderical vessel design and size, winding patterns, reproducibility, pressurization rate, fatigue, and effect of liquid hydrogen temperatures. Third, a study was made of the acoustic emission generated during tensile tests of the fiber/epoxy strands, tensile tests of fiber/epoxy elongated NOL rings, burst tests at room temperature of the cylindrical and spherical pressure vessels, and vessel fatigue tests. Fourth, a microstructural characterization of the failure mode of the fiber was carried out using transmission and scanning electron microscopy and optical microscopy. Fracture surfaces of bare fibers were compared with epoxy impregnated strands from tensile tests, pressure vessels, and NOL rings.

Introduction

Filament-wound pressure vessels offer significant weight savings over the more conventional metal pressure vessels. For applications where weight is critical a filament-wound vessel may be the only possible design choice.

In the last few years a number of new fibers have been introduced by the various manufacturers. To date the fiber with the highest specific strength is called Kevlar 49 (previously designated PRD-49-III). Thus, it is of great interest to study the performance of this fiber in a typical composite such as a filament-wound pressure vessel.

The specific objective, under which the work reported here was carried out, was to develop a filament wound ultra light-weight composite vessel for the containment of cryogenic propellants and pressurant gases. The intended-use temperature of the vessel ranges from -253°C to ambient temperature.

An extensive investigation of the fiber,

the epoxy matrix, filament wound pressure vessels, and a possible non-destructive acoustic emission test method has been completed.

Fiber/Epoxy Strand Characterization

A broad-ranged investigation of Kevlar-49 fibers has been carried out. The chemical details of this organic fiber have not been revealed by the manufacturer. We have tried to identify the chemical structure, and suspect that it is poly-p-benzamide (-CO-⟨⟩-NH-). Elemental analysis from our laboratory together with recent data in the literature[1] justify our belief. The analytical results are shown in Table 1.

Approximate values for the impurity elements present in the fiber are shown in Table 2.

The claimed typical bare fiber properties, when tested in strand form with a 25.4-cm gage and a twist of 1.2 turns/cm, are summarized in Table 3. The average cross-sectional area of the single strand based on fiber measurements is 2.82×10^{-4} cm^2.

A number of tensile properties of Kevlar 49 in an epoxy matrix have been investigated. We were interested in the fiber uniformity, its strength distribution at room and LN_2 temperatures, stress-strain characteristics, the strain rate effect on the fiber strength, the stress-rupture behavior, and ageing behavior under no load.

During this study we made over 6000 fiber/epoxy strands using the filament

Table 1. Elemental analysis of Kevlar 49.

Elements	Theoretical, %	Analysis, %
C	70.5	69.58
H	4.2	4.28
N	11.78	11.66
O	13.52	14.35
Ash	—	0.13

Table 2. Impurities in Kevlar 49.

Elements	ppm
Ca	500
Ma	50
Na	50
Si	40
Fe	20
Al	15
Pb	4
Ti	4
B	2
Cu	2
Sr	0.7
Ag	0.2
Mn	0.2

Table 3. Bare fiber properties.[a]

Strength	2758 MPa (400 ksi)
Elongation	2.0%
Modulus	131.0 GPa (19×10^6 psi)
Density	1.45 g/cm^3
Moisture regain	1.5%
Finish	None
Filament diameter	11.7 μm (4.6×10^{-4} in.)
No. of filaments/end	285

[a]Producers twist ≈ 1 turn per 30 cm.

Table 4. Effect of cure cycle on the tensile properties of ERL 2258/ZZL 0820 epoxy.

Hardener content, p/100	Gel and cure cycle, h/°C [a]	No. of specimens	At maximum (= at rupture)					Secant modulus			
			Strength			Elongation		At 0.5% strain		At 1% strain	
			MPa	(psi)	CV, % [b]	%	CV, % [b]	GPa (ksi)	CV, % [b]	GPa (ksi)	CV, % [b]
31	4/90 + 6/150	26	71.7	(10 400)	6.1	1.9	7.7	4.16 (604)	3.9	4.06 (589)	3.1
31	4/90 + 6/160	13	103	(15 000)	7.9	4.6	17.3	3.65 (530)	9.9	3.49 (506)	13.7
	4/90 + 2/160	28	114	(16 500)	1.7	6.2	9.6	3.84 (557)	1.9	3.70 (536)	1.4
31	4/90 + 6/168	20	106	(15 400)	5.5	5.7	16.9	3.71 (538)	1.0	3.54 (514)	0.5
31	4/90 + 6/180	23	100	(14 500)	6.8	5.2	17.2	3.67 (532)	1.9	3.48 (505)	1.5
	4/90 + 2/180	15	104	(15 100)	7.1	4.7	17.4	3.66 (531)	3.3	3.54 (514)	2.4
31	4/90 + 6/188	23	88.9	(12 900)	6.7	3.9	13.5	3.82 (554)	6.7	3.57 (517)	3.2

[a] There is a 1-h ramp from the gel temperature to the cure temperature. Cooling of the mold to room temperature is normally done in 2 h.

[b] Coefficient of variation.

winding process; these strands were representative samples taken from over 27 kg (61 spools) of single-end fiber. All 61 spools were preproduction material.

EPOXY

A popular epoxy system, Union Carbide ERL 2258/ZZL 0820 (100/30), was arbitrarily picked as the matrix material.* The cure schedule for all specimens was constant throughout the study: gel at 93°C for 3 h, then cure at 163°C for 2 h.

The pure cast resin had a maximum strength of 114 MPa (16.5 ksi), a rupture elongation of 6.2%, and a modulus of 3.84 GPa.

Table 4 summarizes the tensile properties of this epoxy for other gel and cure cycles, and Fig. 1 summarizes the corresponding stress-strain curves. For further details on this epoxy system see Ref. 2.

*Reference to a company or product name does not imply approval or recommendation of the product by the University of California or the U.S. Atomic Energy Commission to the exclusion of others that may be suitable.

STRAND SPECIMEN PREPARATION

A spool of fiber was first dried in a vacuum oven for a minimum of 24 h at 82°C; approximately one layer was stripped from the outside and discarded. Then the fiber was epoxy impregnated and wound into strand specimens using a small filament winder. Good impregnation of the fiber strands was assured by a combination of heating, mechanical working, and vacuum degasing operations. One hundred strand specimens were made from each of the 61 fiber spools. From one of these spools, selected at random, one thousand more specimens were made to study the effects of strain rate and LN_2 temperature on fiber tensile strength as well as stress-rupture properties. After curing, the specimens were cut from the winding frame and stored in a dry atmosphere until tested.

An alignment fixture was used to define a 25.4-cm gage length between two sets of clamps holding the specimens. The specimens were bonded in the mechanical clamps with a room-temperature epoxy adhesive. By a combination of bonding and slight mechanical

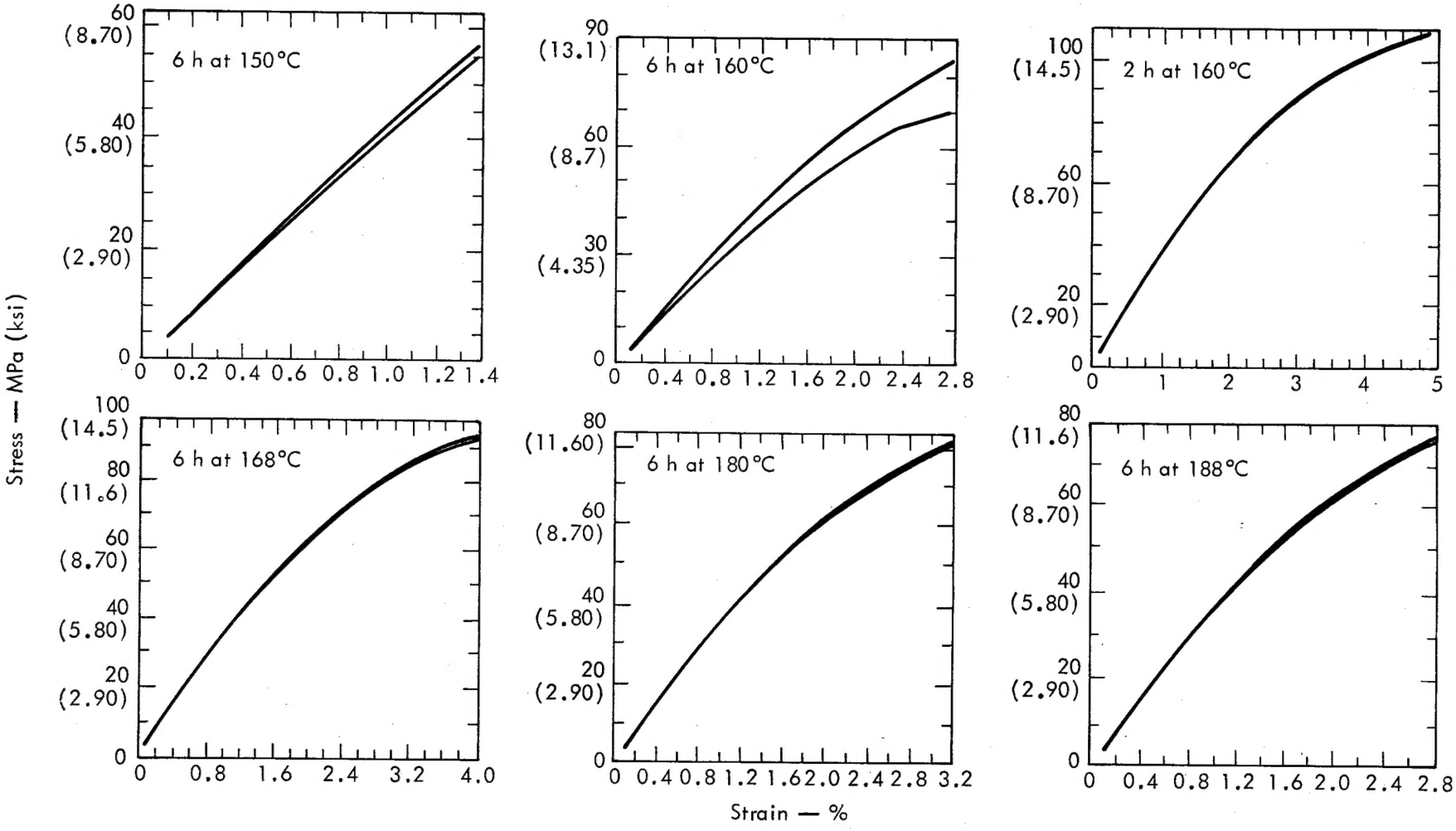

Fig. 1. Stress-strain curves after various cure cycles. All cycles begin with a gelling cycle of 4 h at 90°C. The two lines in each plot show the 95% confidence limits.

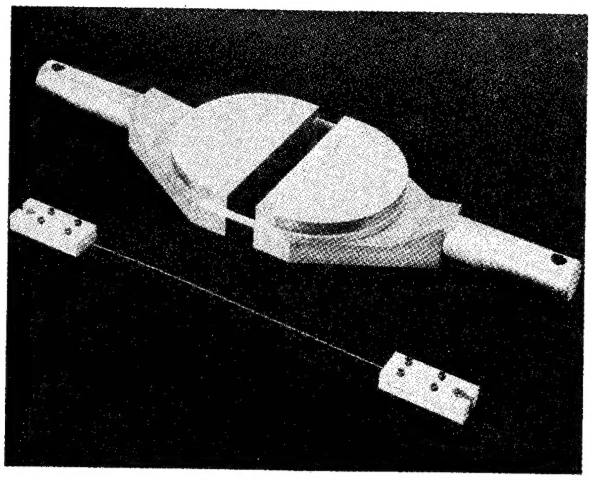

Fig. 2. Uniaxial composite specimens: ring (top) and strand (bottom).

clamping, we were able to test the large number of specimens without difficulty. Figure 2 shows the resulting specimen.

SAMPLING

The linear mass of the fiber on each spool was based on the average mass of three 2.54-m bare fiber specimens taken from the spool prior to test specimen fabrication. Five fiber/epoxy strands were selected at random from each of the first 24 spools for ultimate tensile stress determination only. Of the remaining 37 spools, 10 specimens were taken from each for stress, strain, and modulus determination. In every case, one random fiber/epoxy strand from each spool was used to determine the fiber content.

TESTING

Tensile tests were carried out on a standard test machine at a crosshead rate of 2.2×10^{-2} cm·s^{-1}. For modulus and strain measurements, we confirmed the compliance of our tensile machine by using various gage length specimens.[3,4] The modulus data were further confirmed using accurate strain-measuring linear variable differential transformers.

The study of strain rate effects on the fiber strength was carried out by varying the crosshead speed. Thus, the strain rates were calculated by dividing the gage length (25.4 ± 0.05 cm) by the crosshead speed. This method of course, is subject to debate. However, considering the relatively low breaking loads of the strands vs the machine capacity, and the impracticality of using strain gages on so many strands, we feel that it is justifiable for comparative purposes.

The effect of LN_2 temperature on the fiber strength was determined by immersing the test specimens directly in LN_2. A diagram of the test setup is shown in Fig. 3.

The apparatus for the stress-rupture tests is shown in Fig. 4. Briefly the

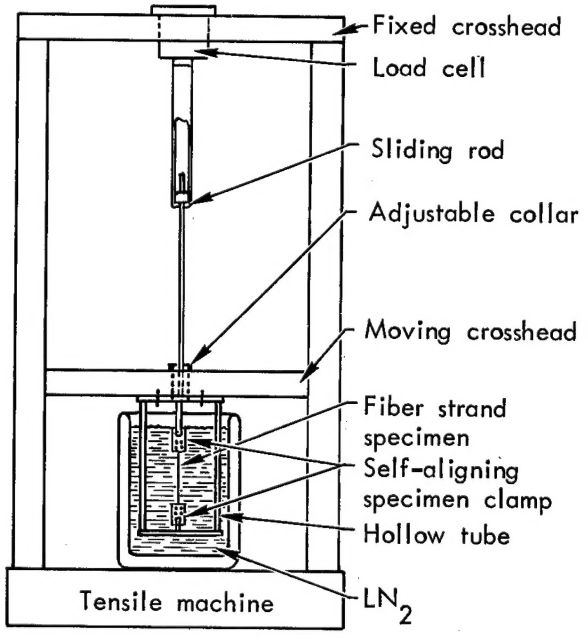

Fig. 3. Tensile test of fiber strand at LN_2 temperature.

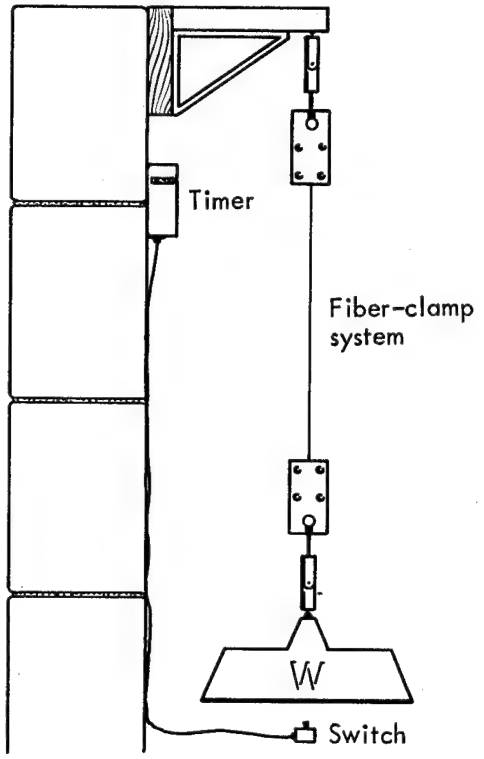

Fig. 4. Design concept of stress-rupture test apparatus.

fiber-clamp system is suspended between self-aligning universal joints. The upper U-joint is attached to a rigid bracket from a concrete wall and the lower U-joint is attached to a weight. When the specimen breaks, the weight drops on a switch that stops the timer. Some of the 400 test units housed in our specially designed Laboratory are shown in Fig. 5. Many of the design features were verified and discussed in detail previously.[5]

Our stress-rupture laboratory is in a specially constructed building in a remote area. The floor is suspended, above a concrete slab, on steel beams from the perimeter of the building. The test positions are attached to steel-reinforced concrete walls connected to the thick concrete slab under the floor. Thus, the floor does not come in direct contact with the walls that support the test apparatus, and the specimens under test are isolated from shock caused by the weight dropping from a ruptured specimen. Load release interaction between specimens through the top support was found to be minimal (1.1% of the applied load).

The test building is continuously monitored for ground shock by a siesmograph that is mounted atop one of the concrete walls. The most violent earth tremor recorded during the tests produced 2.9×10^{-4} g's and was not detected in the stress-rupture data.

The normal temperature in this laboratory ranged between 22 and 28°C; extremes of 9 and 41°C occurred for a few days as the result of equipment failure. The relative humidity fluctuated from 24 to 37% with extremes of 10 and 56% for a few hours.

RESULTS AND DISCUSSION: STRANDS

Since hundreds of tests were involved, a tabular data presentation was not practical. Instead, we made extensive use of probability plots. For easy comparison, the abscissa was arbitrarily normalized to the median value in each case.

The fiber volume content of the strand specimens varied more than we expected (11.0%). Figure 6 shows the scatter. Its effect on the fiber strength in a strand was not determined.

The bare fiber mass per linear length (the textile term, denier, is g/9000 m) is an indirect measurement of the filament diameter variation. Fiber mass variation together with fiber density (1.45 g/cm^3 at room temperature) allow a check of the

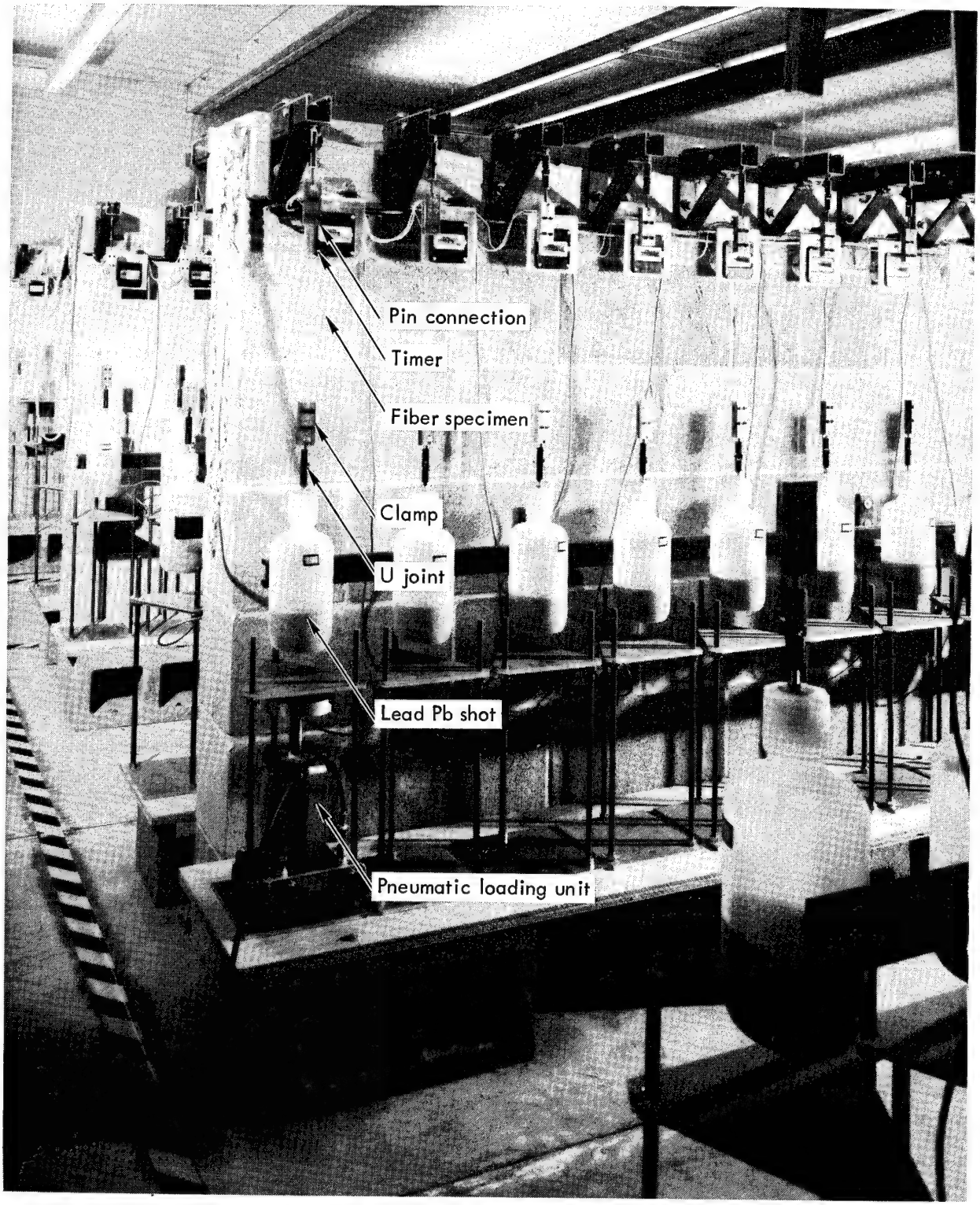

Fig. 5. Stress-rupture apparatus in Laboratory B.

cross-sectional area variation of the strands, such as shown in Fig. 7. It is clear that the fiber is quite uniform. It appears that the average area of 2.82 $\times 10^{-4}$ cm^2 can be used as a constant to represent the single-end strand for

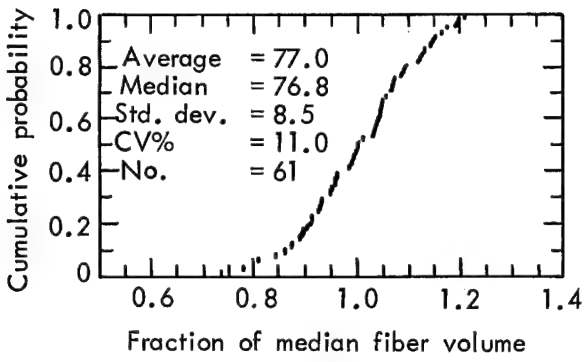

Fig. 6. Distribution of volumetric fiber content of the test specimens — organic fiber/epoxy strands.

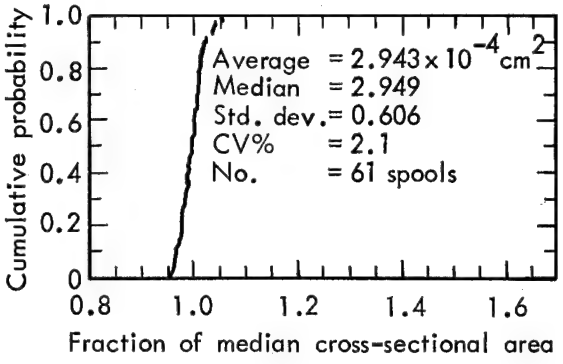

Fig. 7. Cross sectional area variation of single-end fiber strands.

engineering calculations. Photomicrographs of the strands (Fig. 8) further confirm the fiber uniformity.

The fiber strength distribution from 61 spools, based on the average cross-sectional area of each individual spool, is shown in Fig. 9. There are a few low values. The scatter, however, is reasonably narrow. The output of the tensile tester was recorded on magnetic tape for computer processing and plotting of the stress-strain data for the majority of the specimens. These results are summarized in Fig. 10. The strain values were corrected based on a constant compliance of 7.68×10^{-7} m/N. Modulus calculations were based on the stress at 1% strain. Figure 11 is a typical stress-strain curve showing the average curve. The X's represent the rupture values and the scatter. The same data for the epoxy is also shown.

The strain rate effect on the fiber strength is of interest to many researchers. Table 5 shows such data based on specimens from only one spool of fiber. The rate effect, if any, is minimal.

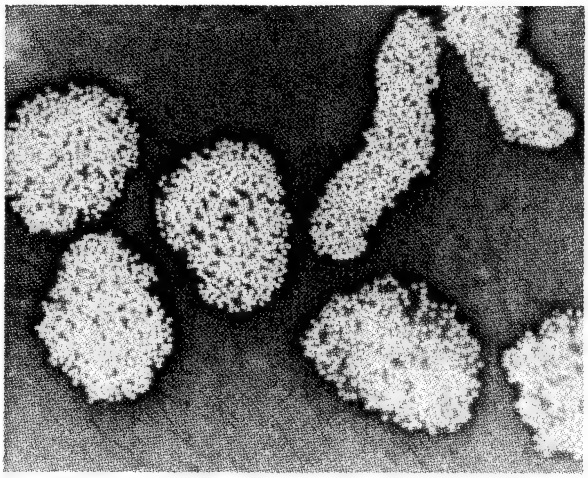

(a)

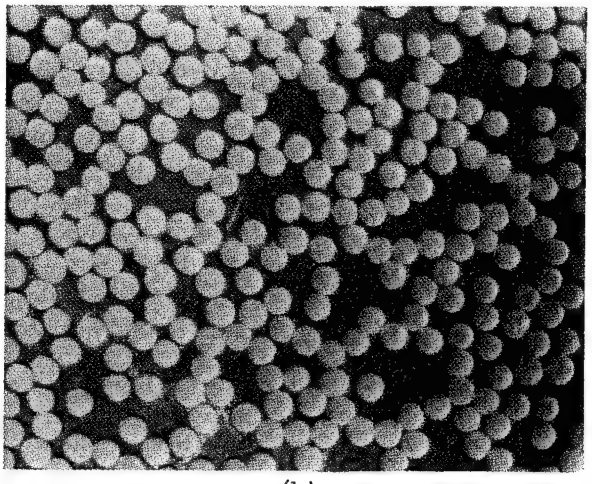

(b)

Fig. 8. Photomicrograph of the cross section of the organic fiber/epoxy strands (top, 100X, bottom 500X).

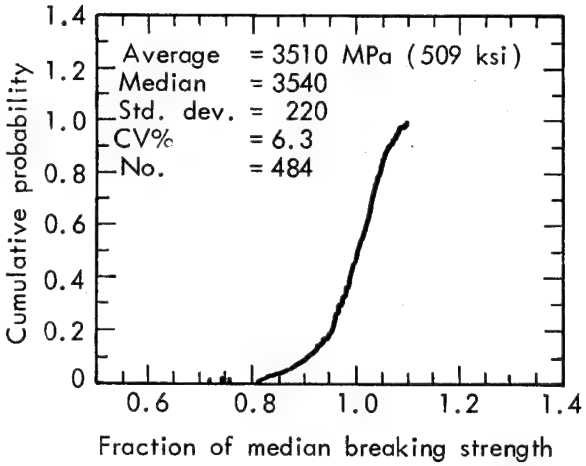

Fig. 9. Fiber strength distribution of the organic fiber/epoxy strands.

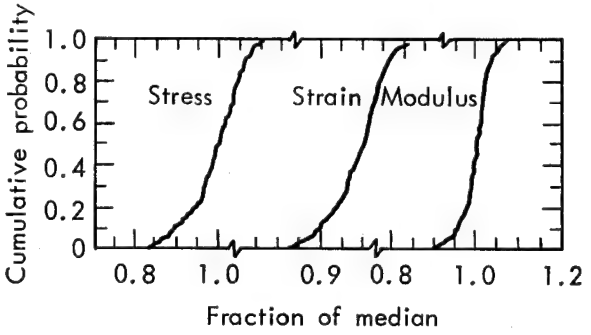

		Stress	Strain	Modulus
Average	= 3490 MPa	506 ksi	2.40%	138 GPa
Median	= 3520	510	2.42	138
Std. dev.	= 230	33	0.16	5
CV %	=	6.5	6.7	3.3
No.	=	363	363	363

Fig. 10. Tensile properties from 37 spools of the organic fiber.

Using specimens from the same spool of fiber, we also checked the effect of LN_2 temperature on the fiber strength of strands. Table 6 is a summary of the data. The fiber strength reduction at LN_2 temperature is not significant, considering the data scatter at the low temperature.

The specimens for the stress-rupture testing were carefully characterized while we were obtaining the stress-rupture data.

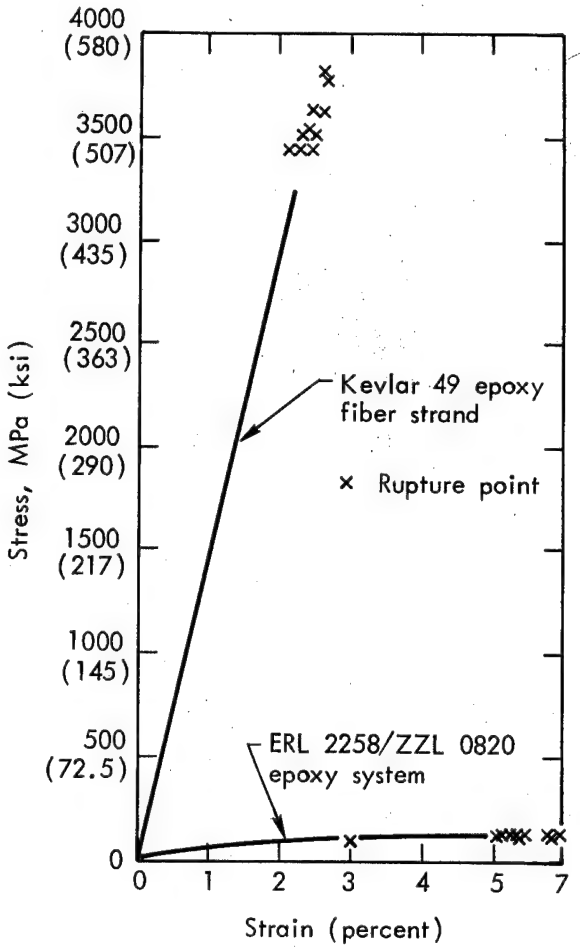

Fig. 11. Typical stress-strain curve of the fiber/epoxy strands and the epoxy system.

The volumetric fiber content of these epoxy-impregnated strand specimens was carefully controlled. As can be seen in Fig. 12, the coefficient of variation (CV) is less than 3%.

The average strand cross-sectional area of this fiber was calculated to be 2.82×10^{-4} cm^2 (4.36×10^{-5} in.^{2}) based on both the fiber specific gravity of 1.45 and an average fiber mass distribution of 4.086×10^{-4} g/cm. The latter figure was based on five strands. We used this cross-sectional area as a constant to convert any fiber tensile load to tensile stress.

Table 5. Strain rate effect on the ultimate tensile stress of the organic fiber/epoxy strands.

Strain rate[a], cm·cm·s	Av tensile strength[b], MPa (ksi)	95% conf. limits, MPa (ksi)	Standard deviation, MPa (ksi)	CV, %	No. of specimens
0.08	3230 (468)	± 83 (±12)	66 (9.6)	2.1	5
0.03	3190 (463)	±166 (±24)	135 (19.6)	4.2	5
0.017	3500 (507)	±179 (±26)	143 (20.7)	4.1	5
0.008	3410 (494)	±152 (±22)	123 (17.9)	3.6	5
0.0017	3430 (497)	±186 (±27)	149 (21.6)	4.4	5
0.0008	3440 (499)	± 83 (±12)	68 (9.9)	2.0	5
0.00017	3450 (501)	± 28 (±4)	21 (3.1)	0.6	5
0.00008	3380 (490)	±207 (±30)	164 (23.8)	4.9	5
0.000017	3250 (471)	±131 (±19)	121 (17.6)	3.7	6
0.000008	3280 (476)	±110 (±16)	88 (12.8)	2.7	5

[a]Crosshead speed divided by 25-cm gage length.

[b]All strands from one spool; the average cross-section area of 2.82×10^{-4} cm^2 was used to calculate stress.

[c]Rate normally used for fiber strength determination.

The variation of the breaking force of the fiber/epoxy strands at 21°C is summarized in Fig. 13. In terms of fiber ultimate stress, the average is 3480 MPa (505.2 ksi) with a CV of 2.5%. Throughout our study, this value was used as the reference stress.

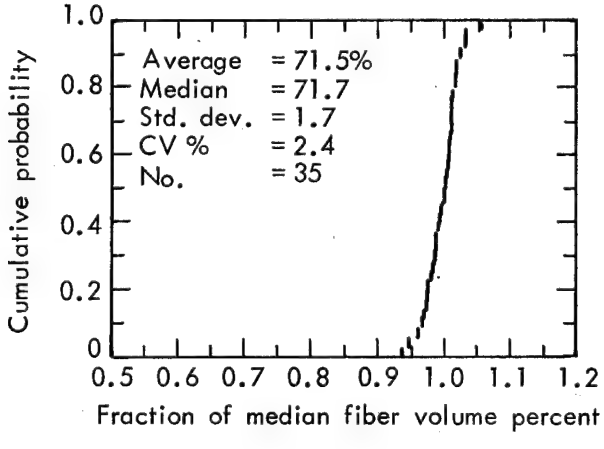

Fig. 12. Variation of the volumetric fiber content of stress-rupture strands.

Our data on aging of the fiber strands under no load in our test environment is shown in Table 7. We are uncertain about

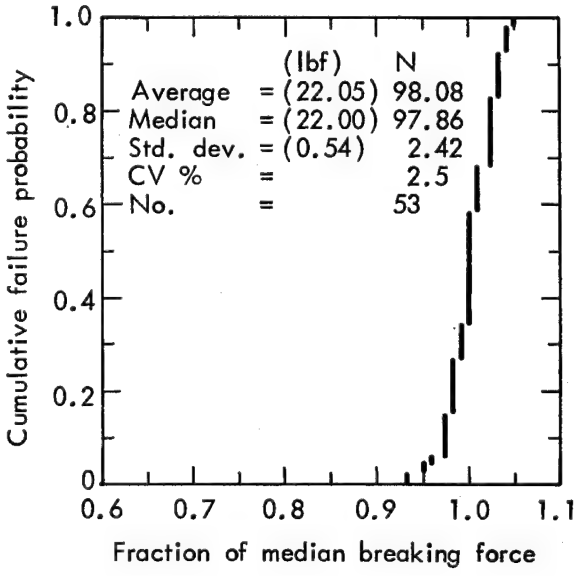

Fig. 13. Variation of breaking force of stress-rupture fiber/epoxy strands.

Table 6. Fiber strength of the organic fiber/epoxy strands.

Temperature, °C	Fiber strength, MPa (ksi)	95% confidence limits, MPa (ksi)	No. of specimens	CV, %
21	3480 (505)	±23 (±3.4)	53	2.5
-196	3350 (486)	±68 (±9.9)	27	5.2

the slight reduction of the average breaking force of the strands after nearly 2 yr of storage. This work is being continued.

Our stress-rupture experiment includes tests of the fiber/epoxy strands at seven stress levels based on the ultimate breaking stress: 90, 87, 84, 80, 70, 60, and 50%. Tests at the four higher levels are completed (Fig. 14), while tests at the lower levels are continuing. Failure contour lines based on available data are shown in Fig. 15.

There is no concensus on whether simple stress-rupture data on strands can be applied to a real composite structure. However, we feel there is at least a possibility that these data may provide the designer with a basis for selecting a material system for a particular composite structure.

The stress-rupture behavior of the Kevlar 49/epoxy system is less of a problem than the S-glass/epoxy material system. Our available data on the two material systems are compared in Fig. 16. For a constant time-to-failure, the Kevlar 49/epoxy material can be loaded at a slightly higher percentage of its ultimate stress than that of the S-glass/epoxy system. Actually, the rate of degradation under load of the organic/epoxy system is approximately half that of the S-glass/epoxy system.

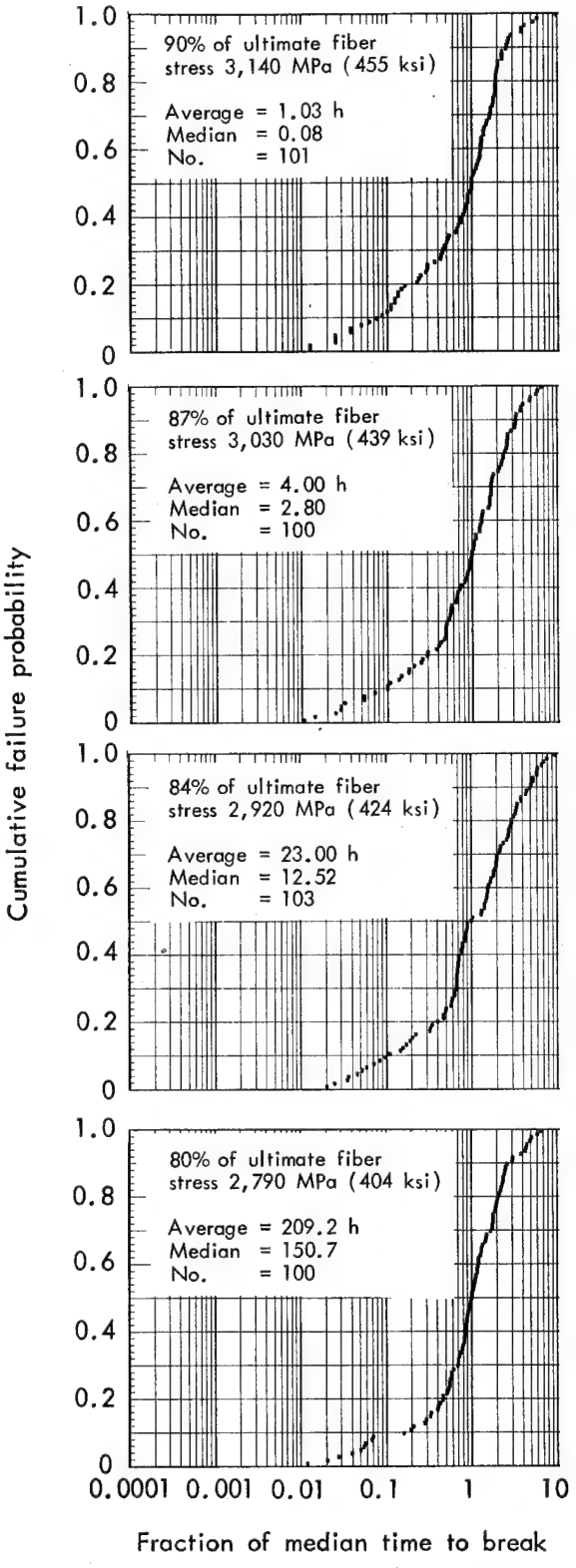

Fig. 14. Stress-rupture of the fiber/epoxy strands.

ELONGATED RINGS

A unidirectional specimen slightly more complex than the strand is the elongated NOL ring[6] shown in Fig. 2. The same vacuum winding process used

Table 7. Aging of Kevlar 49/epoxy strands, no load conditions.

Date	Average breaking force N	(lbf)	No. of specimens	Standard deviation N	(lbf)	CV, %
Oct. 1971	98.08	(22.05)	53	2.42	(0.54)	2.5
May 1972[a]	96.79	(21.76)	5	2.42	(0.54)	2.0
Nov. 1972[a]	93.50	(21.02)	5	1.60	(0.36)	1.7
July 1973[a]	88.61	(19.92)	5	4.14	(0.93)	4.7
July 1973[b]	92.08	(20.70)	5	4.00	(0.90)	3.5

[a]Strands stored under same conditions as stress/rupture specimens.

[b]Strands from dry specimen bank.

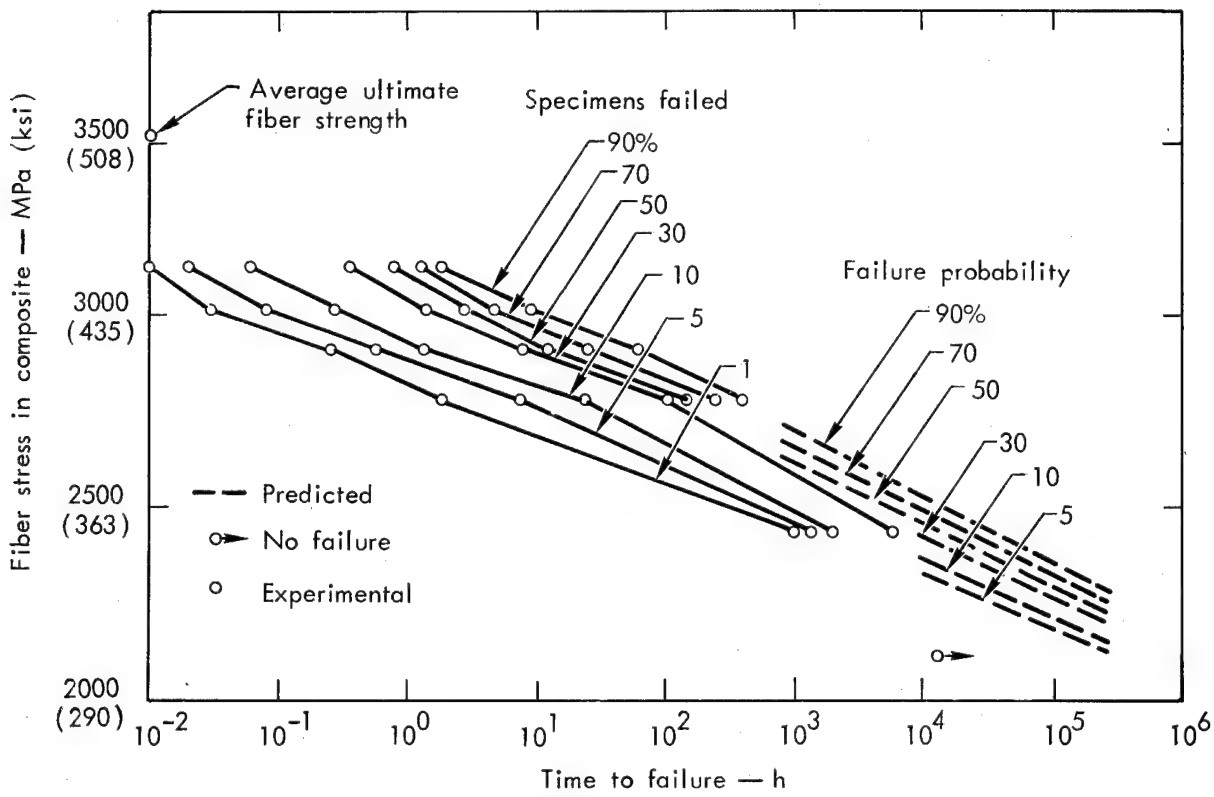

Fig. 15. Stress-rupture failure contour lines of the fiber/epoxy strands.

for strands was also used to fabricate these specimens. We tested 10 rings and got an average fiber strength of 2880 MPa (417 ksi) with a 5.4% coefficient of variation (CV) and an average rupture strain of 2.4% with a 4.5% CV. This strength reduction of 20% from strand to ring specimen was also observed with S-glass composites.[7]

CONCLUSIONS

The typical strength of Kevlar 49 in an epoxy matrix is 3510 MPa (509 ksi) at

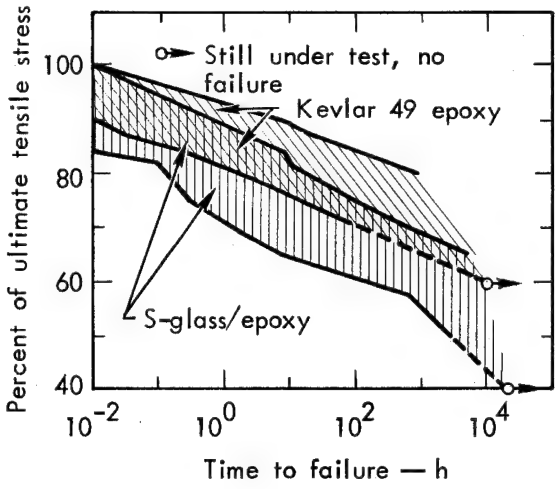

Fig. 16. Stress-rupture failure of the fiber/epoxy and S-glass/epoxy strands.

21°C. The fiber uniformity in terms of filament diameter, denier, and cross-sectional area is quite acceptable as an engineering material. Both LN_2 temperature and strain rate have little effect on the fiber strength. At room temperature and in a reasonably dry atmosphere, Kevlar 49/epoxy strands are subject to stress-rupture similar to the S-glass/epoxy composites. The higher the applied stress, the shorter the life of a composite. An increase in applied stress of approximately 138 MPa (20 ksi) reduces the life of the Kevlar 49/epoxy strands by a factor of 10. Ageing in a dry atmosphere under no load does not seem to significantly reduce the tensile strength of Kevlar 49/epoxy strands.

Considering its high modulus, high strength, and low density, this fiber is at present the most attractive reinforcement for fiber composites in tensile-critical applications where shear stress is minimal.

Filament-Wound Pressure Vessels, 10.2 cm Diameter

We continued the evaluation of Kevlar 49/epoxy composites by studying 10.2-cm filament-wound vessels of various designs. The two objectives of this study were to further evaluate the fiber properties in a shell structure, and to obtain information for designing vessels of the highest performance. We studied how five variables affected the performance of the vessels:

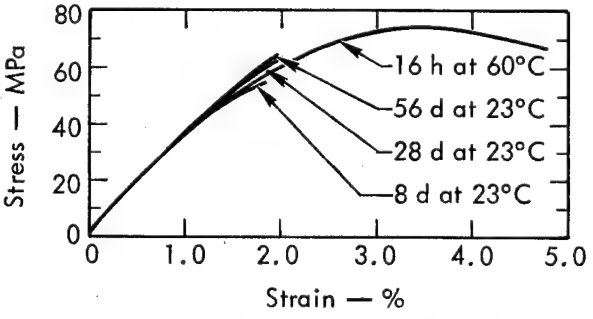

Fig. 17. Tensile properties of DER 332/Jeffamine T-403 (100:36) at room temperature cures vs 60°C cure.

- pressurization rate,
- length-to-diameter ratio (L/D),
- boss-to-diameter ratio (d/D),
- the various dome contours,
- interspersing of the wraps.

In addition, the reproducibility of the winding process was verified by winding a group of 21 identical vessels.

EXPERIMENTAL

Materials

We used the same ERL 2258 epoxy system used in the strand tests except for interspersed vessels. For the latter vessels we used a room-temperature curable epoxy, Dow DER 332/Jefferson Chemical Jeffamine T-403 (100/36) as the matrix material. Table 8 summarizes the tensile properties of this system for different gel and cure cycles; Fig. 17

Table 8. Tensile properties of DER 332/Jeffamine T-403 cured at various conditions.

Cure cycle, time/°C	No. of specimens	At maximum				At rupture				Secant modulus to 0.01 strain	
		Strength		Elongation		Strength		Elongation			
		MPa (psi)	CV, %	%	CV, %	MPa (psi)	CV, %	%	CV, %	MPa (ksi)	CV, %
8 d/23	8	52.6 (7 629)	4.2	1.7	5.6	52.6 (7 629)	4.2	1.7	5.6	3447 (500)	1.4
14 d/23	7	55.8 (8 092)	4.5	1.7	7.4	55.8 (8 092)	4.5	1.7	7.4	3654 (530)	5.1
28 d/23	8	62.2 (9 017)	4.4	2.1	6.3	62.2 (9 017)	4.4	2.1	6.3	3447 (500)	3.3
56 d/23	7	64.0 (9 286)	5.1	2.0	5.7	64.0 (9 286)	5.1	2.0	5.7	3516 (510)	1.6
24 h/50	7	73.4 (10 640)	1.8	3.7	0.8	66.6 (9 663)	5.5	4.6	10.4	3240 (470)	3.1
16 h/60	6	72.9 (10 570)	0.7	3.6	2.2	65.3 (9 466)	3.9	4.9	7.2	3240 (470)	1.5
8 h/70	7	72.7 (10 550)	0.9	3.6	5.5	67.7 (9 822)	1.4	4.7	8.2	3310 (480)	10.0

summarizes the corresponding stress-strain curves. For further details on this epoxy system see Ref. 8.

The cure schedule for the ERL 2258 matrix specimens was essentially constant throughout the study: gel at 60°C for 16 to 20 h, then cure at 163°C for 2 h. For the DER 332 matrix specimens, gel at room temperature for 16 h, then cure at 74°C for 3 h.

The Kevlar 49 fiber was from the 61 preproduction fiber spools, which were characterized in the strand study.

Vessel Designs

We studied various vessel designs with a constant diameter of 10.2 cm. Using an in-plane dome contour, we studied L/D ratios of 1.375, 2, and 3 as shown in Fig. 18(a). Maintaining L/D constant with the in-plane dome contour, we studied d/D ratios of 0.104, 0.166, and 0.234, as shown in Fig. 18(b). Finally, with a constant d/D of 0.104 and a cylindrical section of 7.6 cm, we varied the dome contours of the 10.2-cm vessels to in-plane, helical and hemispherical, as shown in Fig. 18(c). The dome contour coordinates were scaled down from ASTM-D 2585-68. A drawing of the vessel [left hand vessel of Fig. 18(a)] is shown in Fig. 19.

Modes of Failure

When a pressurized vessel is not locally reinforced, there are three typical failure modes: hoop, knuckle, and fitting, as shown in Fig. 20. However, changing the vessel design alters the mode of failure. Figure 21 shows the results of two design changes: (1) Additional hoop reinforcements placed at the equators

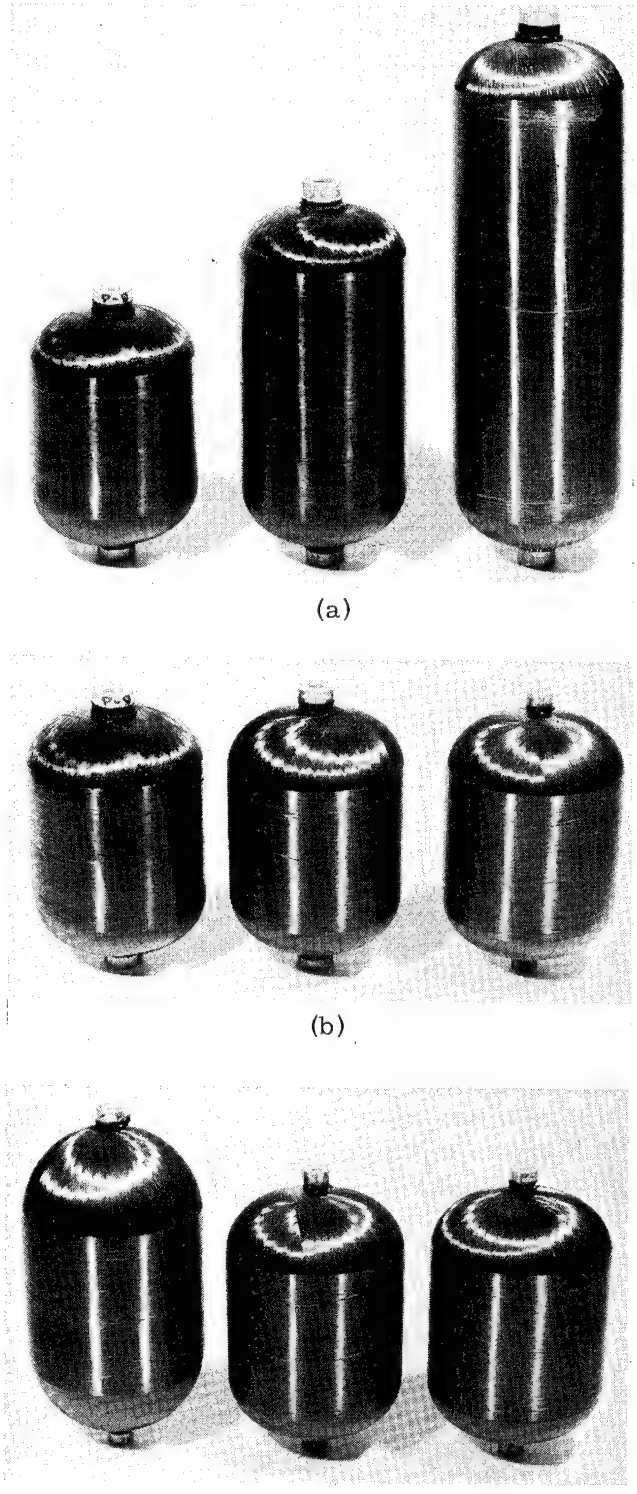

Fig. 18. Designs of 10.2-cm vessels.
(a) L/D of 1.375, 2, and 3.
(b) d/D of 0.104, 0.166, and 0.234 at constant L of 14 cm.
(c) hemispherical, helical, and in-plane dome contour with cylindrical section ~7.6 cm.

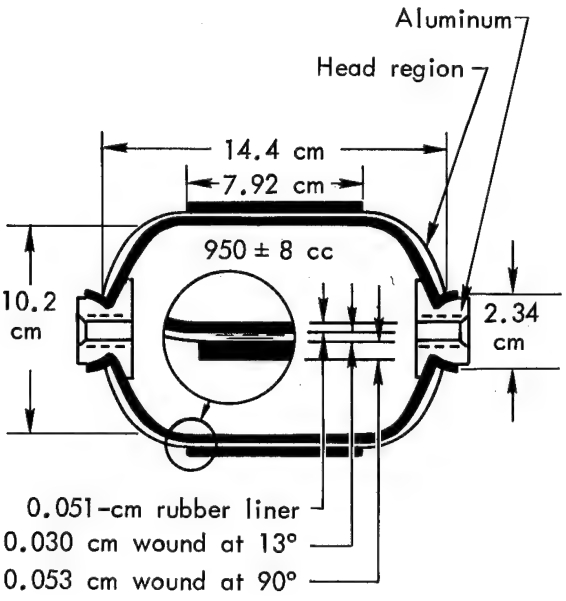

Fig. 19. Design of the 10.2-cm vessel.

confine combined hoop and axial failure to the center section of the vessel with in-plane domes, (2) When the vessel domes are changed to hemispherical, failure still occurs at one of the reinforced equators.

Filament Winding

Vessels were fabricated using a numerically controlled winding machine. Both the fiber package and the resin impregnation were kept inside a vacuum chamber controlled at approximately 670 Pa (5 mm Hg). We used about 2.3 N tension for winding of the single-end strand.

For axial winding, we used a constant wide-band pattern[9] with 0.88-cm sequential bands, except for the groups of vessels with a L/D of 3. Because of its high slip-angle (defined as the difference between the winding angle and the angle corresponding to the fiber geodesic path), we had to use 0.63-cm bands to minimize the winding slippage. Our winding machine enabled us to wind wide-bands automatically from one spool of fiber.

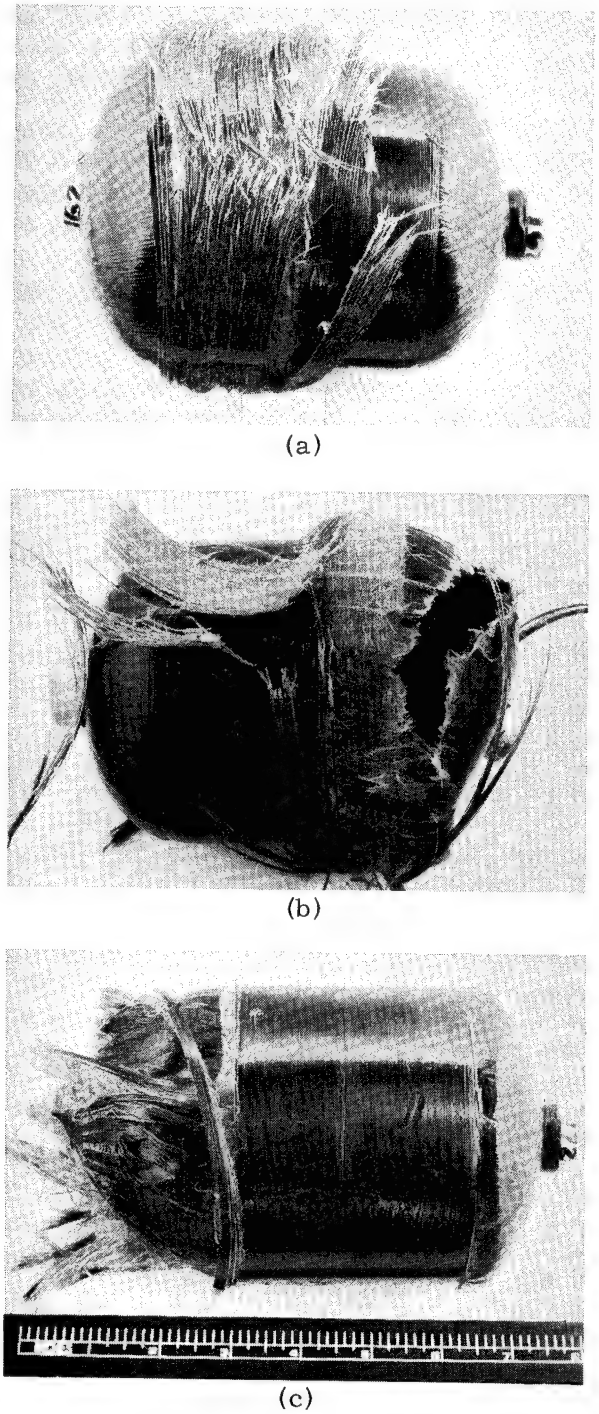

(a) (b) (c)

Fig. 20. Typical modes of failure of 10.2-cm vessels with no equator and knuckle reinforcements; (a) hoop, (b) knuckle, and (c) fitting.

Internal pressure, Δp, and thermal expansion, ΔT, techniques were used to

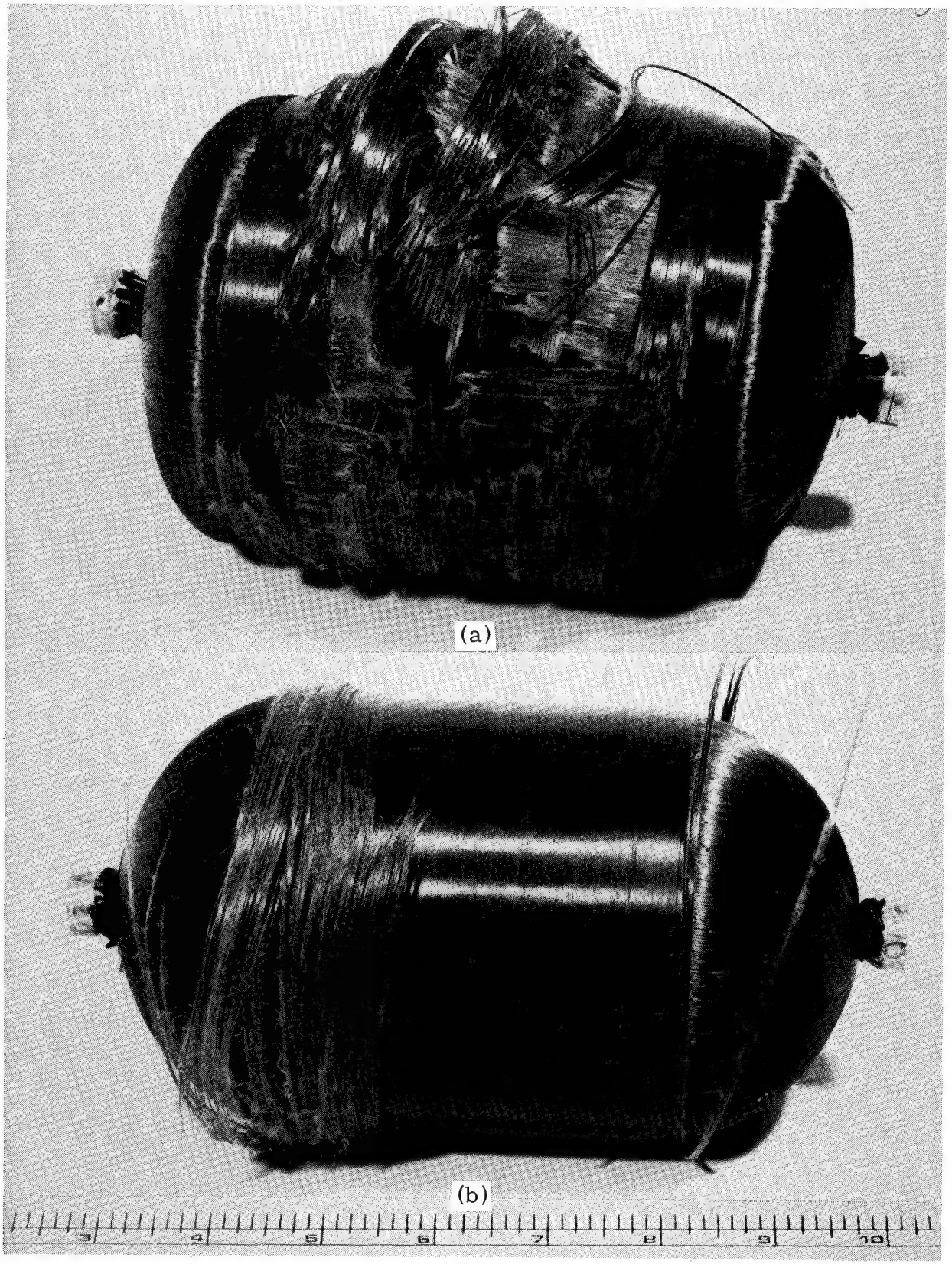

Fig. 21. Changing mode of failure due to different 10.2-cm vessel designs; (a) localized reinforcements at both equators with in-plane dome contours, (b) same localized reinforcements, but with hemispherical contours.

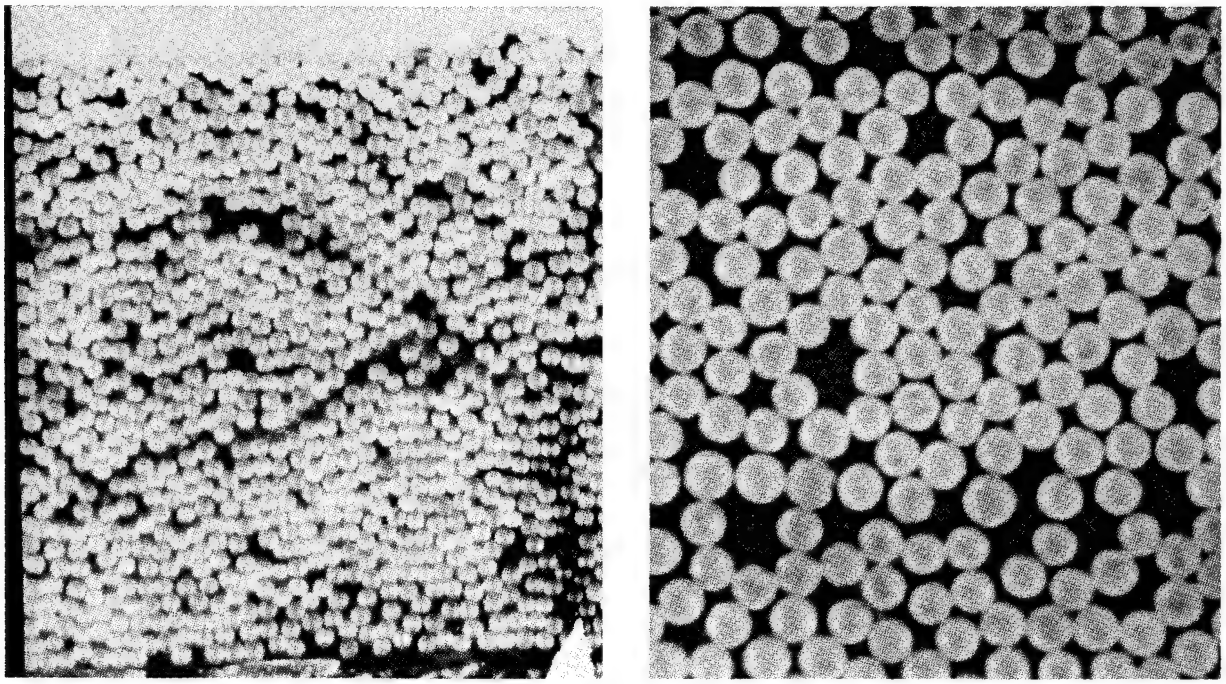

250×

500×

(a)

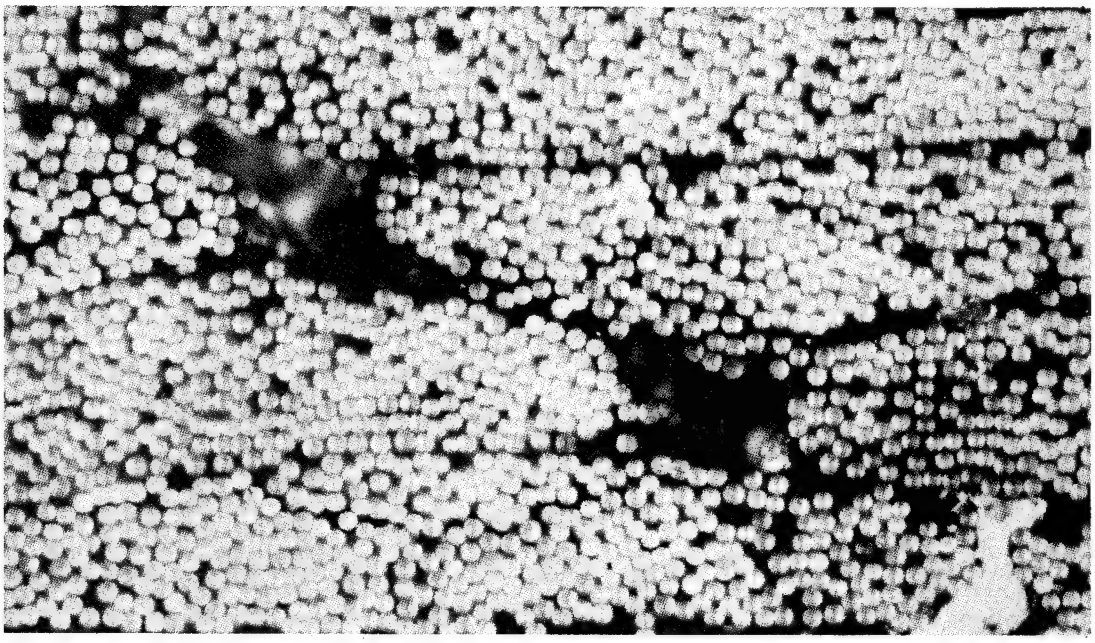

250×

(b)

Fig. 22. Photomicrographs of a vessel: (a) four layers of hoop winding, (b) four layers of axial winding.

deform a standard 10.2-cm vessel for a holographic interferometry study. Photographic results of holometry indicated nonuniform deformations in several areas of the vessel. We therefore decided that localized reinforcements at the equators and knuckles of a vessel were necessary for high vessel performance.

Composite Quality

The quality of the composite in terms of void content and resin distribution can be evaluated from Fig. 22. Our previous photomicrographs of fiber/epoxy strands (Fig. 8) did not show any voids; the same is true for the hoop winding. Figure 22(a) is typical for all groups of vessels; however, for the axial winding, there are some voids in the composite. Figure 22(b) represents the worst example in terms of the voids and poor resin distribution of the composite.

Testing

The vessels were first filled with fluid, and then tested at a constant rate of 0.12 MPa/s using a closed-loop pressure control system. The pressure in the vessel was sensed by an electronic pressure transducer located near the vessel. During pressurization the vessel was placed in a steel tube, shown in Fig. 23, inside a chamber. This tube protects the circumferential strain-measurement instrumentation as well as the acoustic emission transducer.

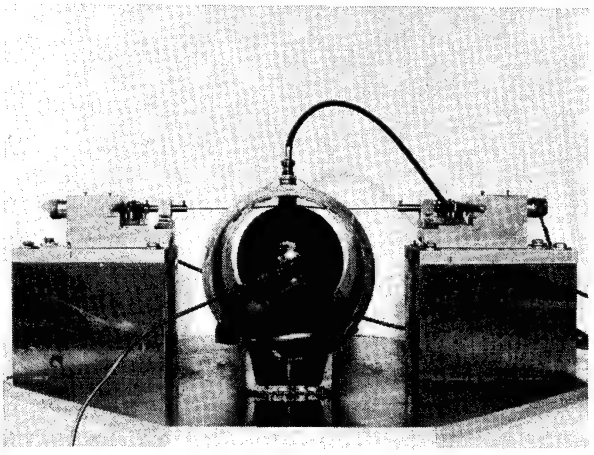

Fig. 23. Details of vessel pressurization.

The strain in the axial direction was measured by a commercial (standard) resistance wire strain gage bonded to the cylindrical portion of the vessel. The strain in the hoop direction was measured by two potentiometers with a music wire that looped around the cylindrical section of the vessel. We also used the same commercial wire gage bonded to the vessel to measure the strain in the hoop direction. The difference in strain as measured by the two methods was negligible. The signals from the strain measurements were recorded as a function of pressure on an x-y recorder.

RESULTS AND DISCUSSION

Balanced-Hoop/Axial-Fiber Ratio

Our definition of a balanced-hoop/axial-fiber ratio vessel is one that fails randomly under pressure. A balanced vessel is assumed to have uniform strength, and hence the best efficiency. An empirical approach is the simplest for determining this ratio for a particular vessel design.

We varied the hoop/axial-fiber ratio from 1.5 to 1.8 using 30 of our standard 10.2-cm model vessels.[7] We found that the optimum fiber ratio for this particular design (no reinforcements) was between 1.7 and 1.75. When the equators and knuckles of the vessel are reinforced we

believe that the optimum ratio is around 1.81, excluding the reinforcements.

Effect of Pressurization Rate on Vessel Performance

We wound 12 identical vessels at the early stage of our process and pattern development, and tested them at two different pressurization rates. Table 9 is a summary of the test results. These results have been analyzed (in two separate groups or one combined group) in terms of burst pressure, vessel performance factors, or failure stress; they did not reveal a rate effect. This conclusion is consistent with our previous

Table 9. Effect of pressurization rate on Kevlar 49/epoxy vessel performance.

Pressurization rate (kPa·s)	287	2,870
Number of specimens	6	6
Burst pressure[a]		
Mean, kPa (psi)	16 400 (2380)	16 700 (2420)
95% confidence limits, kPa (psi)	930 (140)	930 (140)
Std. dev., kPa (psi)	920 (130)	930 (140)
CV, %	5.6	5.6
Mass of composite, W_c, g(lb)	43.3 (0.0953)	43.1 (0.0949)
CV, %	3.5	1.6
Mass of fiber, W_f, g(lb)	31.3 (0.0689)	31.1 (0.0684)
CV, %	0.9	0.8
Vessel performance, PV/W_f		
Mean, $kPa \cdot m^3/kg$	507	499
95% confidence limits	3	3
CV, %	0.5	0.5
Vessel performance, PV/W_c		
Mean, $kPa \cdot m^3/kg$	368	360
95% confidence limits	22	22
CV, %	6.1	6.0
Fiber content by vol, %	68.4	68.4
CV, %	4.0	2.1
Hoop-fiber failure stress[b]		
Mean, MPa (ksi)	2 720 (395)	2 680 (389)
95% confidence limit	160 (23)	160 (23)
Std. dev.	150 (22)	150 (22)
CV, %	5.5	5.7

[a]All specimens were std. 10.2-cm model vessels with a volume of 9.49×10^{-4} m^3, 1.5 hoop/axial-fiber ratio, made identically with vacuum winding, tested at 21°C, failed in hoop.

[b]Estimated, based on netting analysis.

work on the Kevlar 49 fiber-epoxy strands.

Note that these 12 vessels were not of the most efficient design, since they were purposely wound unbalanced (to control the location of failure) and were deprived of localized reinforcements. Nevertheless, as shown in Table 9, their quality was very consistent with a CV < 6%.

Effect of Dimensions on Vessel Performance

The effect of vessel dimensions, dome contour in particular, on the vessel performance has been controversial for years. For various reasons, such as unreliable material properties, questionable processing and testing techniques, and, most important of all, the lack of a reasonable specimen size, there were no clear answers on these subjects in the literature. In our study we tried to avoid these pitfalls. We wound at least 10 vessels for each vessel design except for the group of vessels having an L/D of 3. We had slippage problems in winding and an uncontrolled mode of failure during burst tests. Whenever applicable, we processed and handled all vessels in as identical a manner as possible. Table 10 summarizes all test results of vessels of various designs.

Note that all these vessels were wound with a 1.6 hoop/axial-fiber ratio, excluding the hoop reinforcement at the equators of the vessel.

Data Scatter

We fabricated 21 standard 10.2-cm vessels with the established winding process. We had difficulty controlling the fiber/resin ratio of the initial six vessels in this control group. As shown in Table 10, column 1, this group was a sufficiently large sample size to establish the variance of the data. A CV < 5%, as compared to 6.3% for the starting fiber/epoxy strands, indicates that our process was well under control.

Effect of L/D

The experimental results on the effect of L/D are summarized in Table 10 under columns 1, 2, and 3. In terms of burst pressure, P, no statistically significant difference at the 0.05 probability level occurs when the L/D is varied up to 3.0. Theoretically, for a larger L one would expect a slightly higher P because of the reduced polar winding angle for a given vessel, diameter D, with a fixed boss diameter, d. However, in practice, this gain can be easily offset with a very long vessel by increased winding problems such as slippage, and the large variation of fiber tension on the mandrel.

For the fixed 10.2-cm vessel diameter with in-plane dome contour, the calculated average volume per 2.5 cm of vessel is 192 cm^3 for the cylindrical section and 14.7 cm^3 for the dome section. The corresponding fiber required is 2.4 g/cm in the cylindrical section and 2.2 g/cm in the dome section of the vessel. This means that a unit weight of fiber can wrap 8.2% more volume on the cylindrical section than on the dome section.

In the absence of winding problems, the overall L/D effect on the vessel performance in terms of PV/W_f is that the higher the L/D ratio the better the vessel performance. In practice, however, we believe that winding problems cannot be eliminated, and hence the optimum L/D ratio should be kept to < 3.

Table 10. Test results of rubber-lined 10.2-cm Kevlar 49/epoxy vessels.

	Control[a]	Various length/ diam.ratios		Various boss/ diam ratios		Various dome contours	
	1	2	3	4	5	6	7
Design							
Winding angle, θ	13°	9°	5°15'	7°30'	10°	7°30	5°55'
Dome contour	In-plane	In-plane	In-plane	In-plane	In-plane	Helical	Hemispherical
Boss/diameter, d/D	0.935/4	0.935/4	0.935/4	0.415/4	0.665/4	0.415/4	0.415/4
Length/diameter, L/D	5.5/4	8.0/4	12/4	5.5/4	5.5/4	5.5/4	5.5/4
Slip-angle	-2°	2°	12°	4°	1°	4°	5°
Burst Pressure[b], P							
Mean, kPa (psi)	18 600 (2700)	17 700 (2570)	17 200 (2490)	18 500 (2690)	19 100 (2770)	17 100 (2490)	6 070 (880)
95% confidence limits kPa (psi)	330 (48)	860 (124)	1 850 (269)	340 (49)	410 (60)	710 (103)	330 (48)
Standard deviation kPa (psi)	720 (104)	1 100 (161)	1 500 (216)	440 (64)	500 (72)	920 (134)	430 (62)
CV, %	3.9	6.3	8.7	2.4	2.6	5.4	7.1
Number of specimens	21	9	5	9	8	9	9
Failure[c]	(17H+4F)	(8H+1K)	(3H+2K)	9H	(7H+1K)	(5H+4K)	He equator
Composite modulus, GPa (10^6 psi)							
Axial direction	33 (4.8)	34 (4.9)	36 (5.2)	35 (5.0)	35 (5.0)	35 (5.0)	35 (5.0)
Hoop direction	57 (8.2)	54 (7.8)	59 (8.6)	58 (8.4)	58 (8.4)	57 (8.2)	52 (7.5)
Rupture strain, %							
Axial direction	1.68	1.60	1.45	1.66	1.68	1.52	0.54
Hoop direction	1.98	2.00	1.84	1.96	2.02	1.88	0.72
Mass of composite, W_c, g	44.8	66.2	97.6	45.3	46.4	45.2	50.8
CV, %	3.0	1.9	3.0	3.5	2.5	1.4	2.3
Number of specimens	15	10	8	10	10	10	10
Mass of fiber, W_f, g	32.1	46.8	71.2	32.6	32.7	31.5	35.7
CV, %	2.7	1.9	0.9	1.3	1.3	1.3	2.0
Number of specimens	15	10	8	10	10	10	10
Vol of vessel, V, cm^3	949	1 420	2 200	926	928	939	1 120
CV, %	0.3	0.3	0.2	0.2	0.5	0.2	0.2
Number of specimens	72	10	7	9	9	9	9
Vessel performance, PV/W_f							
Mean, kPa·m^3/kg	547	537	537	527	542	507	186
95% confidence limits	12	25	52	12	12	22	15
Standard deviation	20	35	42	17	17	25	20
CV, %	3.4	6.6	7.7	3.1	3.2	5.5	10
Number of specimens	13	9	5	9	8	9	9
Vessel performance, PV/W_c							
Mean, kPa·m^3/kg	390	380	382	380	382	358	162
95% confidence limits	12	20	35	10	15	15	20
Standard deviation	20	27	27	12	17	17	25
CV, %	4.8	7.3	7.4	3.3	4.8	5.0	15.9
Number of specimens	13	9	5	9	8	9	9
Fiber content by vol, %	67.8	66.7	69.1	68.0	66.7	65.9	66.3
CV, %	5.0	3.6	3.2	3.4	2.4	1.7	3.0
Number of specimens	15	10	8	10	10	10	10
Density, g/cm^3 22°C	1.375	1.377	1.382	1.382	1.386	1.372	1.382
Vessel thickness, cm	0.083	0.083	0.081	0.081	0.081	0.081	0.082
Axial winding	0.035	0.035	0.031	0.033	0.032	0.030	0.034
Hoop winding	0.049	0.048	0.049	0.049	0.052	0.051	0.047
Calc. fiber-hoop failure stress							
Mean, kPa (ksi)	2 940 (427)	2 890 (419)	2 870 (416)	2 990 (433)	3 050 (443)	2 260 (400)	903 (131)
95% confidence limits	50 (7.0)	70 (10.0)	300 (40)	50 (7.4)	60 (9.0)	110 (15.5)	40 (5.2)
Standard deviation	110 (15)	90 (12)	240 (35)	70 (9.6)	80 (11.0)	140 (20)	50 (6.8
CV, %	3.8	3.0	8.7	2.4	2.6	5.4	5.8
Number of specimens	21	8	5	9	8	9	9

[a] Standard 10.2-cm model vessels.

[b] Tested at ambient temperature and at a rate of 0.12 kPa·s.

[c] Normal failure locations are: (1) H for hoop, K for knuckle, and F for fitting; thus 2H and 1K indicate two vessels failed in hoop and one at knuckle.

Effect of d/D

The experimental results on the effect of d/D are summarized in Table 10 under columns 1, 4, and 5. We could not find any significant difference on the vessel performance by varying the vessel boss diameter d from 10 to 23% of its diameter D. However, we recommend that d/D should be kept to a minimum whenever possible. A small d/D should reduce the weight of the bosses as well as the polar winding angle.

Effect of Dome Contours

The vessel performance from three dome contours are compared in Table 10, columns 4, 6, and 7. There is little doubt that in-plane contour is the most efficient, but the helical contour ranks a close second. The difference in performance between the in-plane and the helical contours, however, is only about 8%. For a vessel with a very high L/D ratio, helical dome contour is sometimes preferred for winding. The hemispherical dome contour should be eliminated in vessel design.

Interspersed vs Noninterspersed Winding Pattern

For various reasons, researchers have tried to intersperse the hoop and axial windings for pressure vessel design. In the case of an S-glass/epoxy pressure vessel, we found that interspersed winding gave poor vessel performance.[7] We further studied this subject on the present fiber composite system, again using the standard vessels. Burst results from the two groups of vessels are shown in Table 11. We cannot see any difference on the vessel performance between the interspersed and noninterspersed winding patterns. We believe, however, that the performance of an interspersed vessel is mainly dependent on the brittleness and the abrasive nature of the fiber, and the balance of the hoop-to-axial winding ratio, which in turn controls the uniformity of the vessel deformation. In general, we see no overall advantage in using an interspersed pattern for winding thin-walled vessels.

10.2-cm Vessel of the Best Design

Based on what we learned from the various vessel designs, we estimated that the best vessel design should have a combination of the following:

- $L/D < 3$,
- $d/D < 0.1$,
- in-plane dome contour,
- reinforced equators and knuckles, and
- hoop/axial-fiber ratio of over 1.80.

We have several hundred standard 10.2-cm-model mandrels that essentially meet the requirements (with the exception that the d/D is 0.234). Consequently, we decided to wind some vessels to check our assumptions. We fabricated and tested two vessels each for two designs. The results are shown in Table 12. We have obtained very high vessel performance: $PV/W_f = 611\ kPa \cdot m^3/kg$, $PV/W_c = 457\ kPa \cdot m^3/kg$, and a fiber failure stress of 3080 MPa (446 ksi). Note that, depending on the vessel design, one can expect the axial fibers to fail at the same stress level as the hoop fibers.

CONCLUSIONS

A properly designed and carefully wound vessel with a Kevlar 49 fiber/epoxy material system can have a minimum

Table 11. Cylindrical (10 cm) Kevlar 49/epoxy vessel (0.5-mm rubber liner, test temperature 21°C),[a]

Vessel	Noninterspersed winding			Interspersed winding		
1. Number	P-163	P-164	P-165	P-166	P-167	P-168
2. Volume, V, m^3 ($in.^3$)	0.949×10^{-3} (57.93)					
3. Burst pressure: MPa	18.1	17.8	17.7	17.9	17.2	18.1
(ksi)	(2.61)	(2.56)	(2.54)	(2.58)	(2.50)	(2.61)
4. Failure location[b]	H	H	F	F	F	F
5. Performance factor:						
Fiber, PV/W_f, $kPa \cdot m^3/kg$	535	518	498	520	495	520
(10^6 in.)	(2.26)	(2.08)	(2.00)	(2.09)	(1.99)	(2.09)
Composite, PV/W_c, $kPa \cdot m^3/kg$	348	341	326	343	314	351
(10^6 in.)	(1.40)	(1.37)	(1.31)	(1.38)	(1.26)	(1.41)
Composite						
1. Mass, g						
Composite, W_c	49.4	49.3	51.5	49.5	52.3	49.0
Fiber, W_f	32.1	32.6	33.7	32.7	33.1	33.1
2. Fiber content, vol%	60.5	61.6	60.8	61.6	59.7	63.3
Calc. fiber stress GPa						
Hoop	2.606	2.558	2.544	2.579	2.482	2.613
Longo	2.372	2.324	2.310	2.344	2.255	2.372
Winding						
1. Longo angle	13°					
2. Hoop/longo fiber ratio	1.79					
3. Pattern	36 bands, closed, helically reinforced at ends					
4. Hoop	6 layers					
Layers, interspersing	6(2 + 4)[c]			6(2 + 2 + 2)[d]		
Total winding revolutions	966					
5. Longo	4 layers					
Layers, interspersing	None[c]			4(2 + 2)[d]		
Total winding revolutions	1 080					
6. Extra reinforcement						
Equators(revolutions)	0	0	80	0	0	80
Knuckles(revolutions)	92[c]			92[d]		
Resin System (Ratio)	DER 332/T-403 (100/36)					
1. Gelling (h/°C)	16/room temperature					
2. Curing (h/°C)	3/73.9					

[a] 115 kPa/s (1 ksig/min) test rate.

[b] H - Hoop failure, F - Fitting failure, K - Knuckle failure.

[c] P-163, P-164, and P-165 only.

[d] P-166, P-167, and P-168 only.

Table 12. 10.2-cm vessels of improved designs.

Hoop/axial-fiber ratio	Burst pressure[a], kPa	(psig)	Vessel performance PV/W_f, $kPa \cdot m^3/k_s$	Vessel performance PV/W_c, $kPa \cdot m^3/k_s$	Mode of failure	Fiber-failure stress, MPa	(ksi)
1.90	21 800	(3170)	600	410	Mixed[b]	2850	(410)[b]
1.81	22 600	(3275)	611	457	Hoop	3080	(450)

[a]Average of two vessels for each design, wound on the standard 10.2-cm-model mandrels.

[b]The failure mode was mixed hoop and axial. The fiber failure stress was almost identical in both axial and hoop directions.

average hoop-fiber failure stress of 3080 MPa (446 ksi). Given a composite specific gravity of approximately 1.38, the Kevlar 49 fiber-epoxy composite is indeed attractive for pressure vessels.

The winding process and the pattern are the key factors affecting the quality and the consistency of vessel performance. A well controlled process should produce vessels with the data scatter less than that of the starting material, i.e., a CV of approximately 6% in this case.

In the absence of dimensional restraints, we believe that the best design of a cylindrical vessel is from the following combination:

- wide-band winding,
- "in-plane" dome contour,
- $d/D < 0.1$,
- $L/D < 3$,
- hoop/axial-fiber ratio ~1.81, and
- added reinforcement at equators and knuckles of the vessel.

Pressure testing rates of from 287 to 2870 kPa/s have a negligible effect on the burst pressure of the vessel.

Filament-Wound Pressure Vessels, 20.3 cm Diameter

We had several objectives in the following study:

- To scale up the vessel size to 20.3 cm in diameter
- To compare the performance between cylindrical and spherical vessels
- To obtain some preliminary vessel data at both room and liquid hydrogen temperatures.

To remove the material variability and processing effects, we used the original batch of pre-production single-end roving (the properties were known) and fabricated the 20.3-cm cylindrical and spherical vessels with two well-controlled filament winding processes. Both types of vessels were tested for short term burst and cyclic fatigue.

EXPERIMENTAL

Materials

We used two epoxy matrices interchangeably: Epoxy A (the previously described ERL 2258 system) is a blend of cycloaliphatic and bis-phenol A resin cured with mixed aromatic amines at relatively high temperature; epoxy B (the previously described DER 332 system) is a pure bis-phenol A resin cured with an aliphatic polyether triamine either at moderate or room temperature. We principally used epoxy B as the matrix material. We continued to use the same pre-production fiber.

Cylindrical Vessel Design

The 20.3-cm cylindrical vessel design was largely based on our previous work[10]: A vessel length-to-diameter ratio of 1.65; an outside diameter of the bosses to the vessel diameter ratio of 0.11; in-plane dome contour (ASTM D-2585-68); reinforced equators and knuckles of the vessel; and a hoop-to-axial fiber ratio (in terms of winding circuits) of between 1.7 to 1.8. The design burst pressure of the vessel is approximately 13.8 MPa (2000 psi). The volume of the vessel is $9.3 \times 10^{-3} m^3$.

We used two types of mandrels:

1. Water soluble mandrel with 0.5-mm rubber coating which becomes the liner of the vessel when the mandrel is washed away,
2. 0.76-mm thin aluminum mandrel internally supported with a plaster (Ultrical 30) for rigidness during winding.

The mandrel designs are shown in Fig. 24. The rubber-lined vessels were for the tests at 21°C; the aluminum-lined vessels were for the tests at both 21°C and LH_2 temperature. We sandblasted the surface of the aluminum liner and used a flexible epoxy adhesive to ensure good bonding between the liner and the composite.

Spherical Vessel Design

The design burst pressure of the 20.3-cm spheres was more than two times higher than the cylindrical vessels. We were limited to this high burst pressure primarily by a fixed vessel thickness, which in turn was controlled by our winding pattern and the fiber lay-down thickness. The volume of the sphere was $4.1 \times 10^{-3} m^3$.

We used two mandrel designs: a single-boss sphere, and a simulated double-boss sphere. The double-boss sphere had a 0.76-mm aluminum mandrel internally supported with plaster; the single-boss sphere had a 2.0-mm-thick aluminum liner. Figure 25 shows these designs.

Filament Winding

Cylindrical vessels were fabricated using a numerically controlled winding machine as previously stated. We used about 4.5 N tension for winding of the single-end strand. In axial winding, we used a wide band pattern[9]; 36 sequential bands of 1.78 cm width completely cover the bare mandrel.

Spheres were wound on a custom-made horizontal machine using a single spool of fiber. No vacuum impregnation chamber was available in this process. A wide band, multi-angle pattern was used for the spheres. Winding starts from the boss of the vessel; this layer is put on

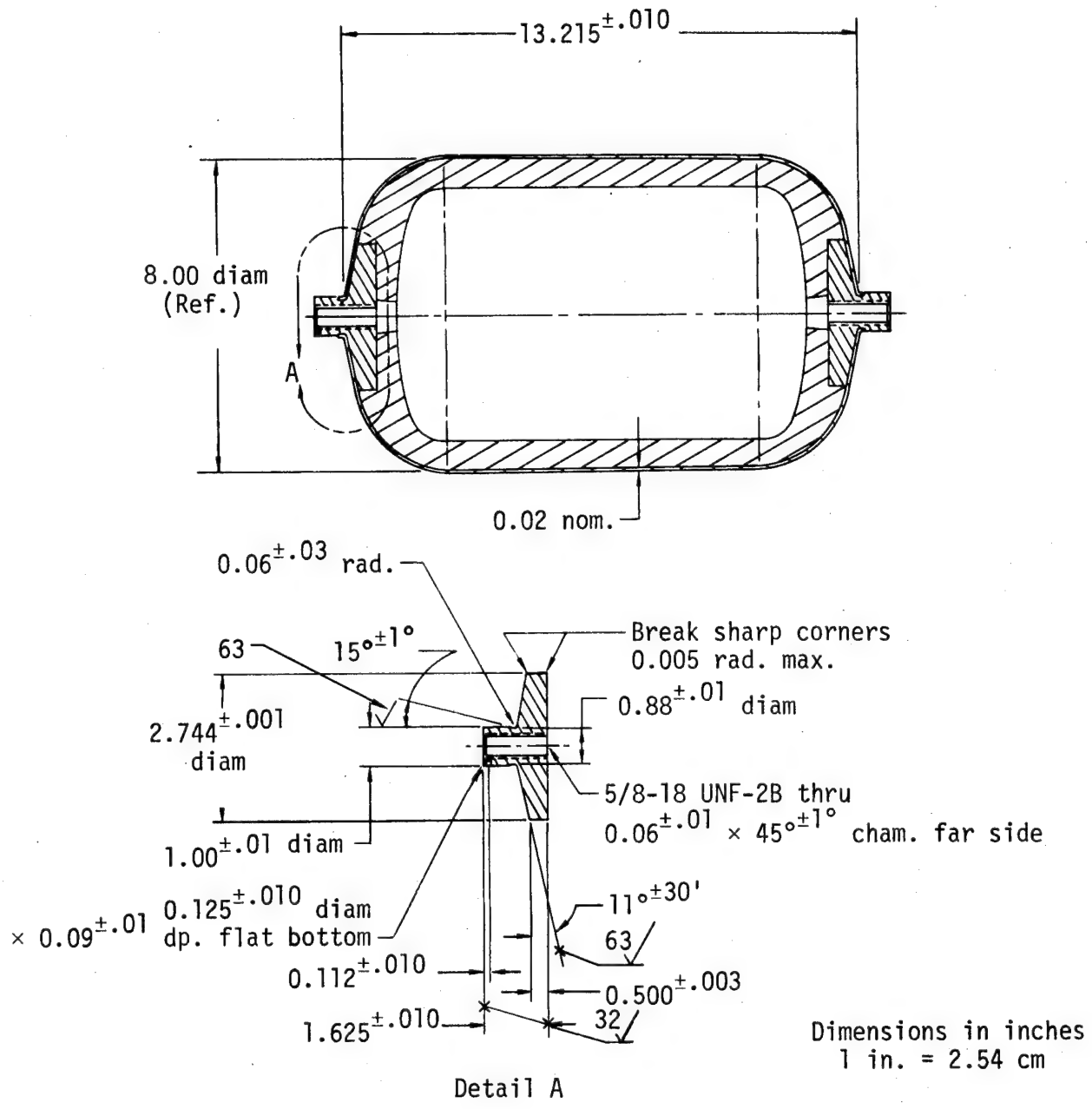

Fig. 24. Mandrel designs for a 20.3-cm cylindrical vessel; (a) 0.5-mm rubber-lined water-soluble mandrel, (b) thin, aluminum mandrel supported with plaster.

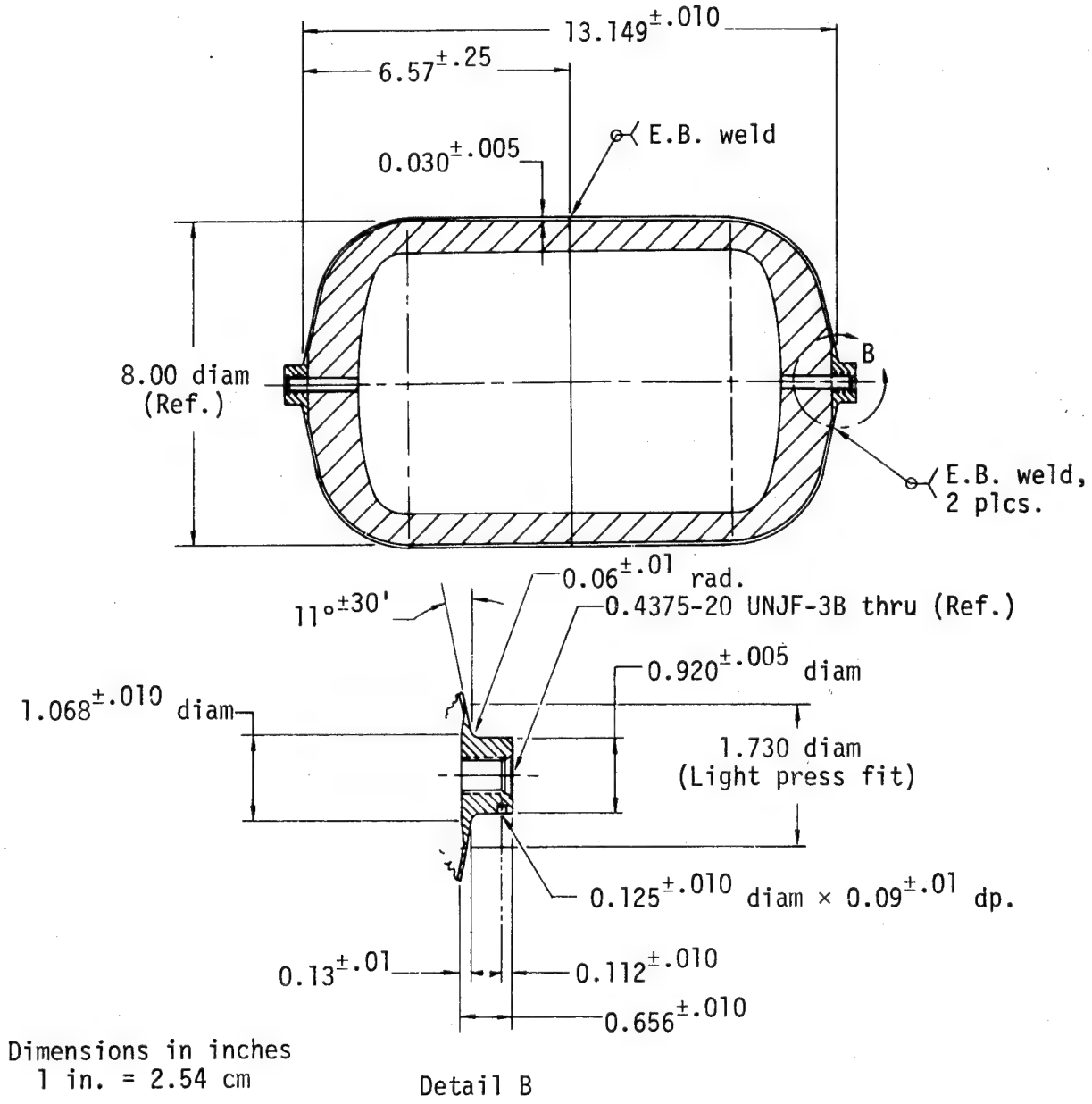

Fig. 24. (Continued)

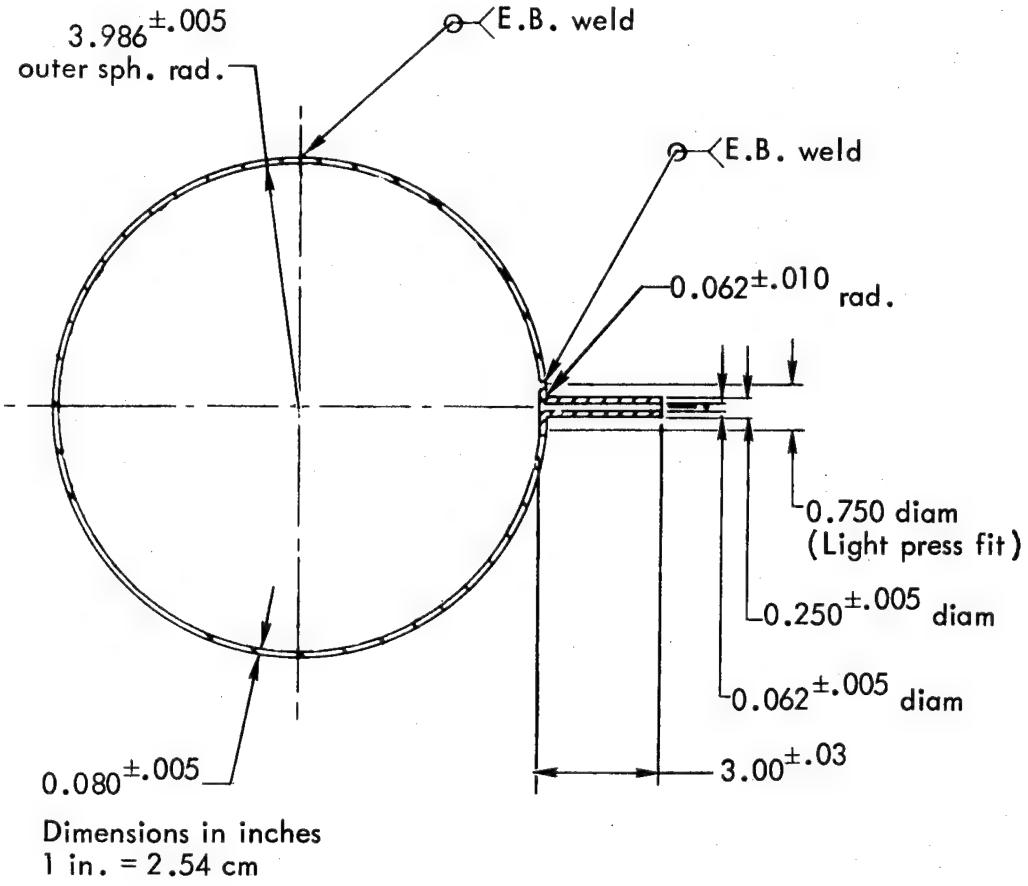

(a)

Fig. 25. Mandrel designs of the 20.3-cm spheres; (a) single-boss spherical mandrel, (b) double-boss spherical mandrel.

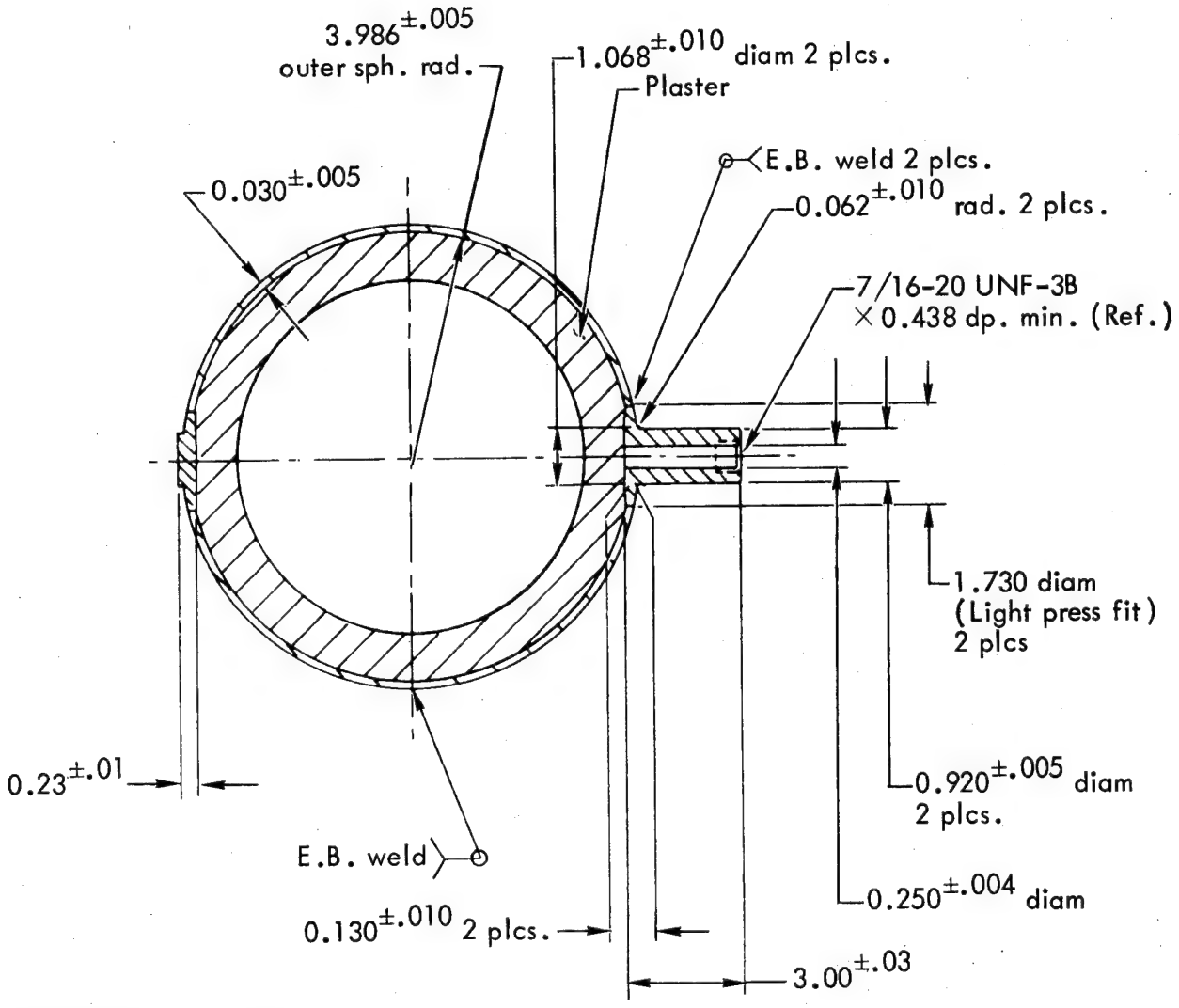

(b)

Fig. 25. (Continued)

with the smallest winding angle. Stepwise, the winding angle is increased to 90°; each winding angle completely covers the mandrel once. A complete pattern is from the boss of the vessel to the equator and back. In Table 13 we summarize two typical winding patterns; a complete pattern in each case has a minimum of 14 layers.

Testing at Room Temperature and Liquid Hydrogen Temperature

Both burst and fatigue tests of the cylindrical and spherical vessels were carried out at 21°C and LH_2 temperature (no fatigue data on spheres at 21°C, however).

The vessels tested at 21°C were pressurized with fluid using the previously described control system. For the cylindrical vessel burst tests, the test rate was 0.12 MPa/s, except as noted in Tables 14 and 15. The test rate for the spheres was 0.16 MPa/s except as noted in Table 16. During the cyclic fatigue tests of the cylinders, the test rate was 0.16 MPa/s. The cyclic pressure range was 0.69 to 9.7 MPa. Each vessel was

Table 13. Winding procedure for spheres.

Large double boss design				Small single boss design		
Helix angle (°)	Band width (cm)	No. of bands	Sequence	Helix angle (°)	Band width (cm)	No. of bands
10.2	1.27	50	1	6.9	2.11	30
10.2	1.27	26	1A[a]	7.8	0.32	26
20.8	2.47	24	2	20.7	2.46	24
36.6	2.49	21	3	34.5	2.46	21
48.5	2.47	19	4	48.3	2.46	17
62.3	2.44	12	5	62.1	2.46	12
76.2	2.43	6	6	75.9	2.46	6
90.0	2.44	1	7	90.0	2.46	1
90.0	2.44	1	7	90.0	2.46	1
76.2	2.43	6	6	75.9	2.46	6
.	.	.	.	.	.	.
.	.	.	.	.	.	.
.	.	.	.	.	.	.
10.2	1.27	50	1	6.9	2.11	30

[a]Single occurrence; local reinforcement layer.

Table 14. Cylindrical (20 cm) Kevlar 49/epoxy vessel (0.5 mm rubber liner, test temperature.

Vessel											
1. Number	P-142	P-144	P-148	P-151	P-152[b]	P-153[b]	P-156[b]	P-157[b]	P-158[b]	P-159[b]	P-160[b]
2. Volume, V, m^3 ($in.^3$)			9.28×10^{-3}		(566)						
3. Burst pressure, MPa	14.2	14.2	15.4	14.2	13.0	12.9	15.6	14.9	14.1	13.1	14.7
(ksi)	(2.06)	(2.05)	(2.24)	(2.06)	(1.89)	(1.88)	(2.27)	(2.17)	(2.04)	(1.90)	(2.13)
4. Failure location[a]	H	F	F	F	K + F	F	F	F	F	F	F
5. Performance factor:											
Fiber, PV/W_f, $kPa \cdot m^3/kg$	488	483	520	485	453	428	530	503	478	438	485
(10^6 in.)	(1.96)	(1.94)	(2.09)	(1.95)	(1.82)	(1.72)	(2.13)	(2.02)	(1.92)	(1.76)	(1.95)
Composite, PV/W_c, $kPa \cdot m^3/kg$	358	368	363	381	324	316	398	383	341	319	376
(10^6 in.)	(1.44)	(1.48)	(1.46)	(1.53)	(1.30)	(1.27)	(1.60)	(1.54)	(1.37)	(1.28)	(1.51)
Composite											
1. Wall thickness, mm	1.40	1.45	1.40	1.37	1.35	1.40	1.35	1.37	1.32	1.37	1.35
Longo, mm	0.56	0.56	0.53	0.51	0.51	0.53	0.51	0.51	0.48	0.51	0.51
Hoop, mm	0.84	0.89	0.86	0.86	0.84	0.86	0.84	0.86	0.84	0.86	0.84
2. Mass, g											
Composite, W_c	368.0	355.0	395.0	347.0	375.0	380.0	364.0	362.0	382.0	381.0	362.0
Fiber, W_f	269.5	270.5	275.6	272.0	267.2	280.8	274.0	275.4	273.5	278.1	279.5
3. Fiber content vol%	69.4	72.4	65.8	75.0	67.3	70.1	71.6	72.4	67.8	69.2	73.8
Calc. fiber stress, GPa											
Hoop	2.468	2.434	2.668	2.455	2.254	2.234	2.703	2.579	2.434	2.261	2.530
Longo	2.213	2.199	2.406	2.213	2.027	2.013	2.441	2.323	2.193	2.041	2.282
Winding											
1. Longo angle					7°10'						
2. Hoop/longo fiber ratio	1.78[c]				1.79						
3. Pattern	Closed, 36 bands										
4. Hoop	10 layers										
Layers, interspersing	10(4 + 6)[d]				10(4 + 2 + 2 + 2)						
Total winding revolutions	4 098[c]				4 121						
5. Longo	6 layers										
Layers, interspersing	None[d]				6(2 + 2 + 2)						
Total winding revolutions	3 564										
6. Extra Reinforcement:											
Equators (revolutions)	164[c]				80						
Knuckles (revolutions)	280[c]				190						
Resin system (ratio)	DER 332/T-403 (100/36)		2258/0820 (100/30)[e]		DER 332/T-403 (100/36)						
1. Gelling (h/°C)	16/Rm. temp.		90/Rm. temp.[e]		16/Rm. temp.						
2. Curing (h/°C)	3/73.9		2/73.9[e]		3/73.9						

[a] H - Hoop failure; F - Fitting failure; K - Knuckle failure.

[b] 69 kPa/ (600 psig/min) test rate.

[c] P-142 only.

[d] P-142, P-144, and P-180 only.

[e] P-148 only.

instrumented for strain. On the cylinders, two strain gages (BLH A-1 wire gage) were bonded onto the outside of the hoop wraps. One gage measured the axial strain of the hoop wraps and the other the hoop strain. On the sphere, a single "belly band" was used which measured the circumferential growth of the sphere on a great circle at 45° to the girth welding line.

The tests at LH_2 temperature were carried out by soaking the pressure vessels in liquid hydrogen for a minimum of 30 min until thermocouple readings indicated the test temperature had stabilized. Gaseous hydrogen backed by gaseous helium was used to pressurize the vessels. As a safety precaution, before cooling the vessels they were filled with Freon TF to reduce the gaseous volume. The test setup is shown schematically in Fig. 26 and photographically in Fig. 27. For the burst tests and the first cycle of the fatigue tests, the pressurization rate was 0.092 ± 0.02 MPa/s. After the first cycle, the cyclic vessels were pressurized at 0.23 ± 0.06 MPa/s. Each vessel was instrumented with two strain gages

Table 15. Cylindrical (20 cm) Kevlar 49/epoxy vessels (0.76 mm Aluminum liner, test temperature 21°C).

Vessel						
1. Number	P-143	P-145	P-147	P-149	P-177[b]	P-180[b]
2. Volume, V, m^3 ($in.^3$)		9.28×10^{-3} (566)				
3. Burst pressure, MPa	14.3	14.7	14.0	17.1	15.2	14.2
(ksi)	(2.08)	(2.13)	(2.04)	(2.48)	(2.20)	(2.06)
4. Failure location[a]	H	H	F	H	F	H
5. Performance factor:						
Fiber, PV/W_f, $kPa \cdot m^3/kg$	493	508	485	595	548	533
(10^6 in.)	(1.98)	(2.04)	(1.95)	(2.39)	(2.20)	(2.14)
Composite, PV/W_c, $kPa \cdot m^3/kg$	353	376	353	441	411	391
(10^6 in.)	(1.42)	(1.51)	(1.42)	(1.77)	(1.65)	(1.57)
Composite						
1. Wall thickness, mm	1.47	1.42	1.45	1.37	1.40	1.37
Longo, mm	0.61	0.53	0.51	0.51	0.51	0.51
Hoop, mm	0.86	0.89	0.94	0.86	0.89	0.86
2. Mass, g						
Composite, W_c	377	362	369	359	343	337
Fiber, W_f	270	267	267	266	257	248
3. Fiber content, vol %	67.5	69.9	68.6	70.3	71.3	69.7
Calc. Fiber stress, GPa						
Hoop	2.496	2.530	2.427	2.951	2.765	2.586
Longo	2.234	2.282	2.186	2.661	2.365	2.213

Table 15. (Continued).

Winding			
1. Longo angle		7°10'	
2. Hoop/longo fiber ratio	1.78[c]	1.79	1.70[d]
3. Pattern	Closed, 36 bands		
4. Hoop	10 layers		
Layers, interspersing	10(4 + 6)		
Total winding revolutions	4 098[c]	4 121	3 840[d]
5. Longo	6 layers		
Layers, interspersing	None		
Total winding revolutions	3 564		
6. Extra reinforcement:			
Equators(revolutions)	160[c]	80	
Knuckles(revolutions)	280[c]	190	
Resin system (ratio)	DER 332/T-403 (100/36)		
1. Gelling (h/°C)	16/Rm. temp.		
2. Curing (h/°C)	3/73.9		

[a]H - Hoop failure; F - Fitting failure; K - Knuckle failure.
[b]69 kPa/s (600 psig/min) test rate.
[c]P-143 only.
[d]P-177 and P-180 only.

(BLH-FSM-350). On the cylinder, the gages were oriented in the hoop and longitudinal directions on the hoop wraps. On the spheres, the gages were oriented parallel and perpendicular to the plane of the weld of the two hemispheres.

RESULTS AND DISCUSSION

Burst Pressure of Various Vessel Designs

The burst pressures of cylindrical vessels of various designs are summarized in Tables 14 and 15; similar data covering several groups of spherical vessels are summarized in Table 16. No attempt was made to statistically treat all the data because, in some cases, the sample size for any particular design was insufficient. The performance of the larger vessels seemed to be comparable to the 10.2-cm vessels. Until better statistical data is available, we are not willing to comment on the possible vessel size effect.

Pressure-Deformation Relations

We measured the vessel pressure vs deformation on a group of eight cylindrical vessels. The results are summarized in Fig. 28. It is evident that the deformation of a vessel in both the axial and the hoop directions is almost the same up to rupture;

Table 16. Spherical (20.3 cm) Kevlar 49/epoxy vessel.

Vessel						
1. Liner	0.76 mm Al.		2 mm Al.[a]		Rubber[b,c]	
2. Boss type	Large double		Small single		Small single	
3. Number of vessels	10		6		4	
4. Volume, V, m^3 ($in.^3$)	4.1×10^{-3}		(250)			
Test data	**Average**	**St. Dev.**	**Average**	**St. Dev.**	**Average**	**St. Dev.**
1. Burst pressure, MPa	28.7	2.5	39.0[d]	1.1	35.5	1.2
(ksi)	(4.17)	(0.36)	(5.65)	(0.15)	(5.14)	(0.18)
2. Performance factor:						
Fiber, PV/W_f, $kPa \cdot m^3/kg$	450	40	575[e]	17	562	25
(10^6 in.)	(1.81)	(0.16)	(2.31)	(0.07)	(2.26)	(0.10)
Composite, PV/W_c, $kPa \cdot m^3/kg$	334	42	413[e]	17	406	12
(10^6 in.)	(1.34)	(0.17)	(1.66)	(0.07)	(1.63)	(0.05)
Composite						
1. Wall thickness, mm	2.20	0.05	2.06	0.04	2.17	0.08
2. Mass of composite, g	355	19	340	5	358	8
3. Mass of fiber, g	260	8	244	3	258	4.0
4. Fiber content, vol%	69.9	4.8	67.9	1.6	68.1	2.6
Resin system (ratio)	DOW DER 332/Jeffamine T-403 (100/36)					
Cure conditions	Approximately 8 weeks at room temperature					

[a] 86 kPa/s (750 psig/min) test rate.
[b] Rubber liner over perforated aluminum.
[c] 115 kPa/s (1 ksig/min) test rate.
[d] Liner effect was not considered in the calculations.
[e] Data were corrected for liner effect as shown in Fig. 30.

and that the scatter bands are quite narrow up to 0.5% strain. Therefore, we think that a secant modulus based on the average stress from a typical pressure-deformation curve at 0.5% strain can typically represent this group of vessels. Thus, the apparent composite modulus for our 20.3-cm Kevlar 49/epoxy vessels is 69.6 GPa in the hoop direction and 39.3 GPa in the axial direction.

The pressure-deformation relations of the spherical vessels are summarized in Fig. 29. There are several points worth commenting on:

- Other than the failure strains, the two bands in Fig. 29 are not directly comparable because of the difference in vessel designs and winding patterns.

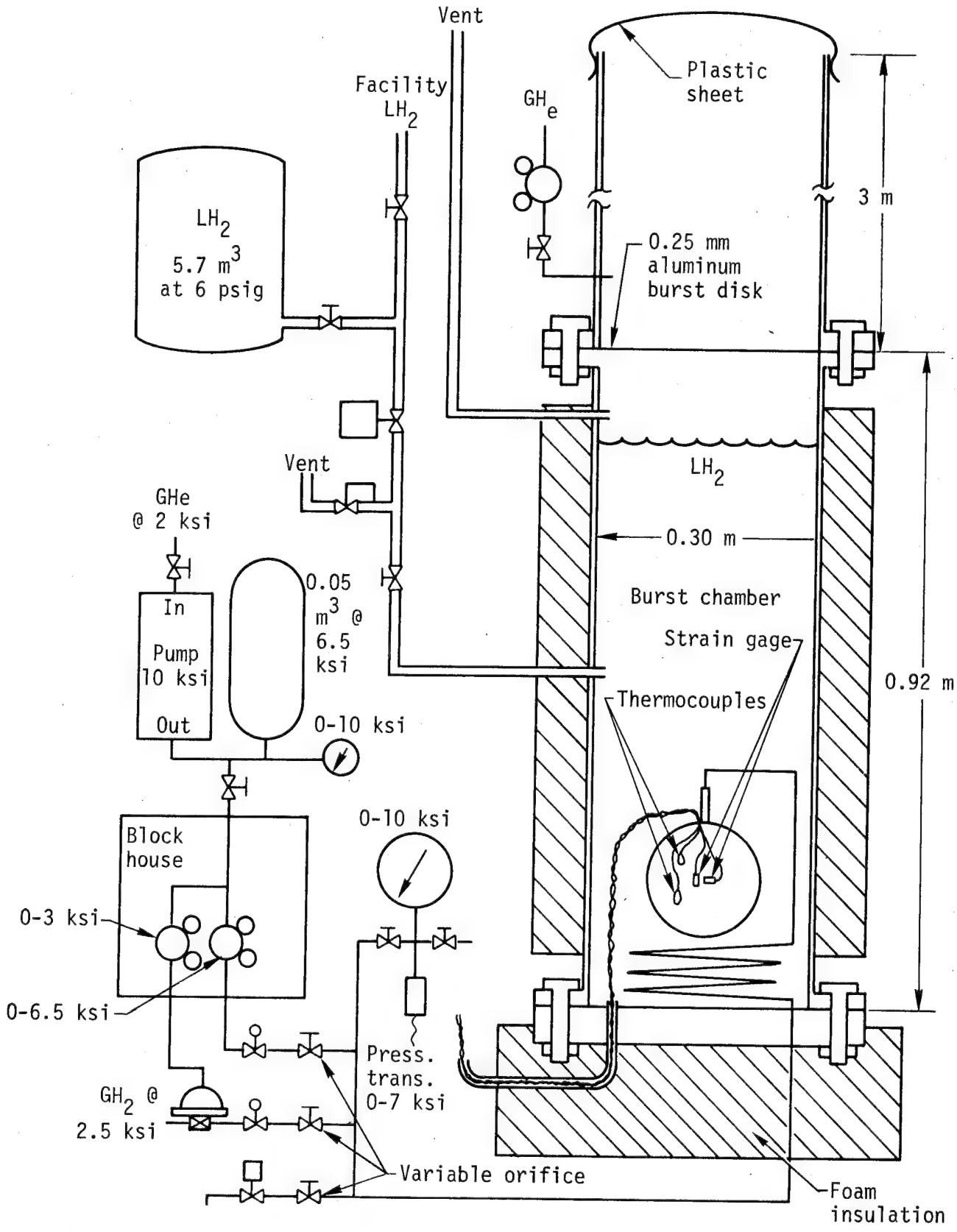

Fig. 26. LH_2 pressure cycling and burst setup for 20.3-cm-diam filament-wound bottles.

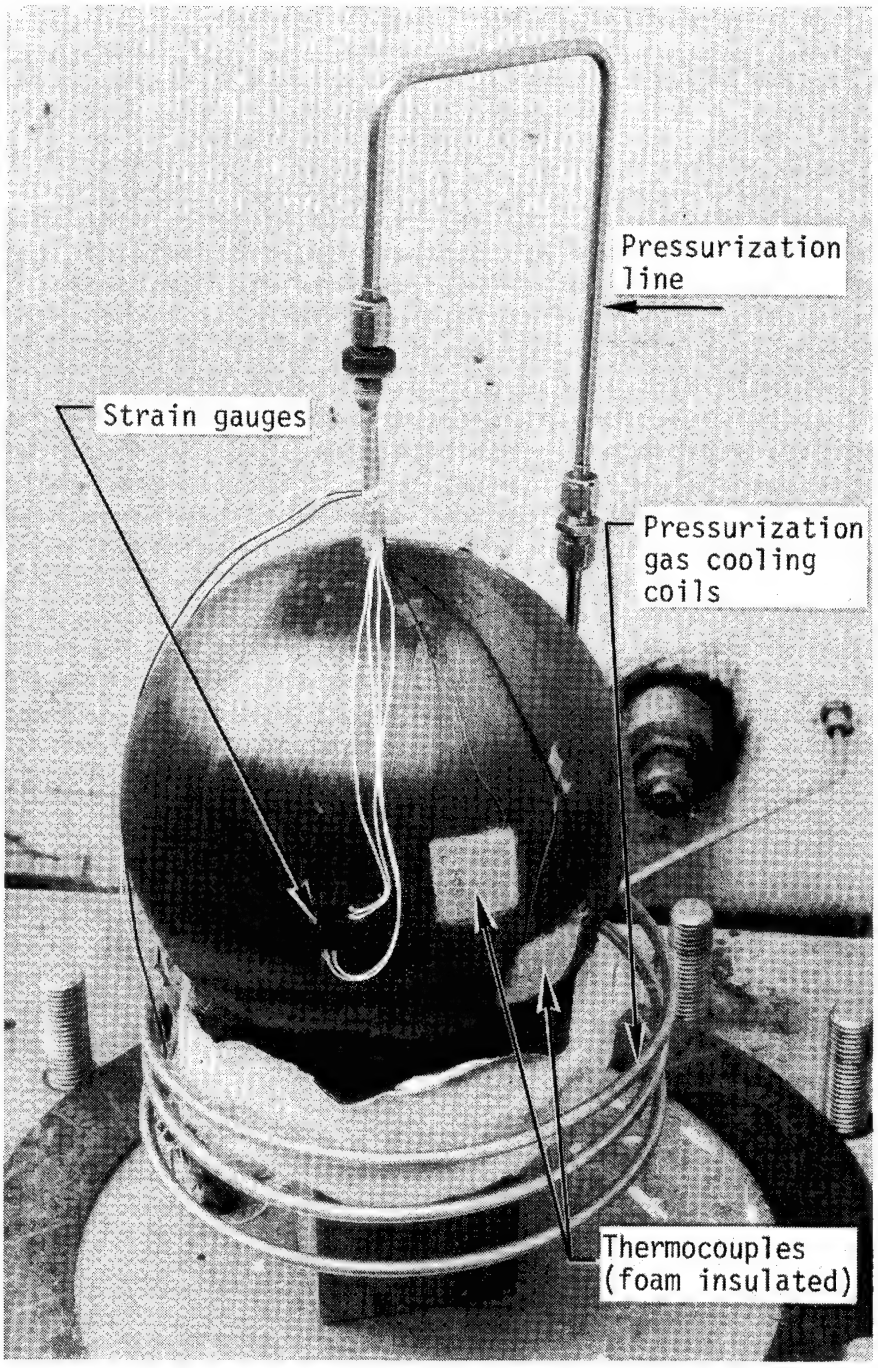

Fig. 27. LH_2 burst test apparatus.

- We believe that the knee of the curves indicates the yielding of the aluminum bladder.
- The apparent composite modulus of the spherical vessels cannot be estimated directly since we lack a reliable orthotropic analysis.

Effect of Epoxy System on Vessel Performance

We do not believe that the two different epoxies used in this study can significantly affect the burst result (tensile performance) of the vessel so long as their handling characteristics, during winding, are comparable. Previously, we substantiated this point sufficiently on S-glass/epoxy strands under simple tension.[11] In this study we further checked this point by making one vessel (P-148) from the high performance Epoxy-A and comparing it with the performance of two other vessels (P-142 and P-144) made, otherwise identically, from Epoxy-B. From the test data summarized in Table 14, it is evident that the performance of these three vessels are essentially the same in terms of the burst pressure times volume divided by the vessel mass. However, we prefer Epoxy-B, the room temperature curable system, for this particular fiber because we assume that the lower the vessel cure temperature, the lower the composite residual stresses. This relationship is a result of the great mismatch of thermal properties between the fiber and the matrix. The basis for our assumption is a delamination problem with Kevlar 49/epoxy vessels cured at 120°C without gelling.

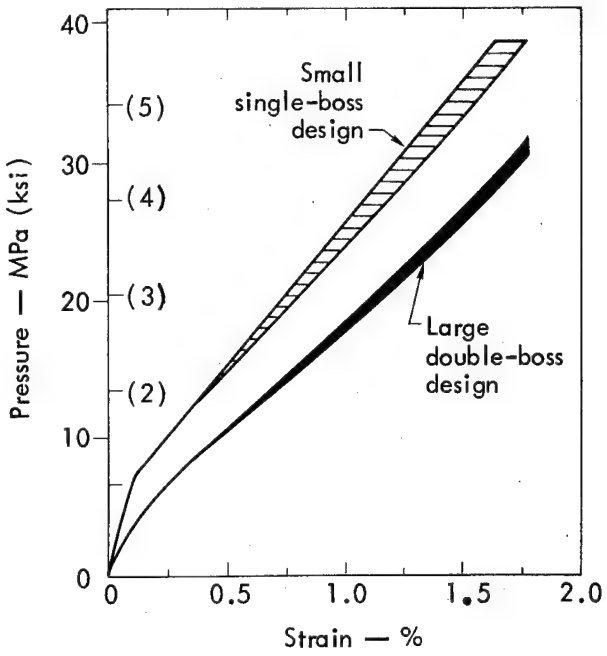

Fig. 29. Scatter bands of pressure vs deformation of 20.3-cm Kevlar 49/epoxy spheres at 21°C.

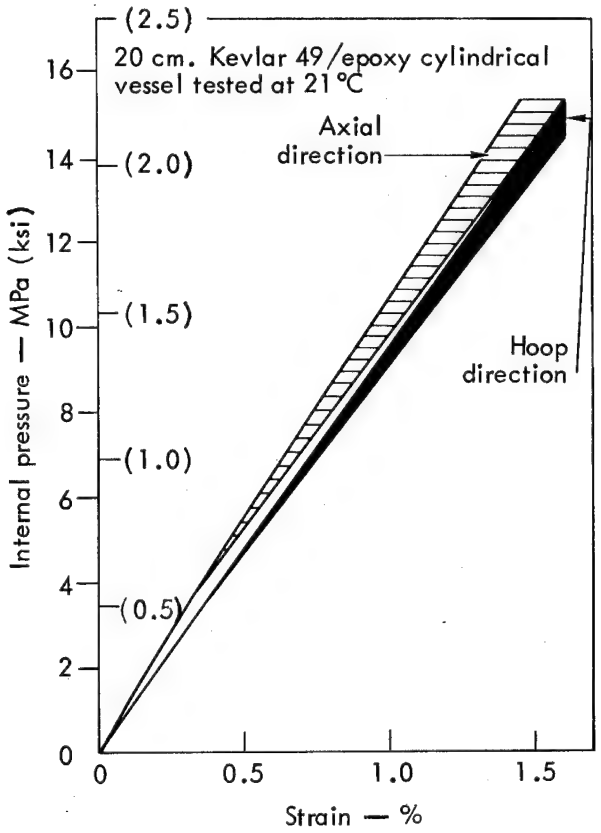

Fig. 28. Scatter bands of pressure vs deformation of 20.3-cm Kevlar 49/epoxy cylindrical vessels at 21°C.

Rubber and Aluminum Liners

We used thin rubber and aluminum liners for the cylindrical vessels. The effect of the 0.76-mm aluminum liner on the burst pressure of a vessel was not significant. We arrived at this conclusion by comparing the performance of one group of vessels (P-142 and P-144) against another (P-143, P-145, and P-147). Both groups of vessels were wound under similar conditions.

For spherical vessels, we used both 0.76-mm and 2.0-mm aluminum liners. In the case of the fairly thick liner, its effect on the burst pressure of the vessel cannot be ignored. This effect can be estimated from the relationship in Fig. 30. The curve represents the results of a spherically symmetric finite element computer calculation. We tried experimentally to verify this relationship by testing four spherical vessels made from rubber-coated perforated aluminum mandrels. We assumed that these vessels would perform exactly like rubber-lined vessels with negligible liner strength.

In Table 16, we summarized the test results. These data check well with vessel performance results if they are corrected according to Fig. 30 for aluminum liner influence. It is clear that the contribution of 2.0-mm aluminum liner to the vessel performance is approximately 11%.

Vessel Performance

The vessel performance factor PV/W (the product of the pressure times volume divided by mass) has long been used successfully to examine vessel efficiency. However, instead of using the composite vessel mass, we think a better approach is to use the mass of fiber in the vessel to calculate the performance factor. There are several good reasons for this approach:

- The fiber content in a vessel varies; thus, to compare vessels by composite vessel mass, on an equal basis, the fiber content of each vessel should be corrected to a constant value.
- The fiber rupture stress can easily and accurately be measured using matrix-impregnated fiber strands to obtain reliable values for the fiber strength-to-density ratio, which in turn is related to vessel PV/W_f. This relationship is given in Ref. 12. It allows one to quickly estimate the maximum possible fiber performance factor for a material system.

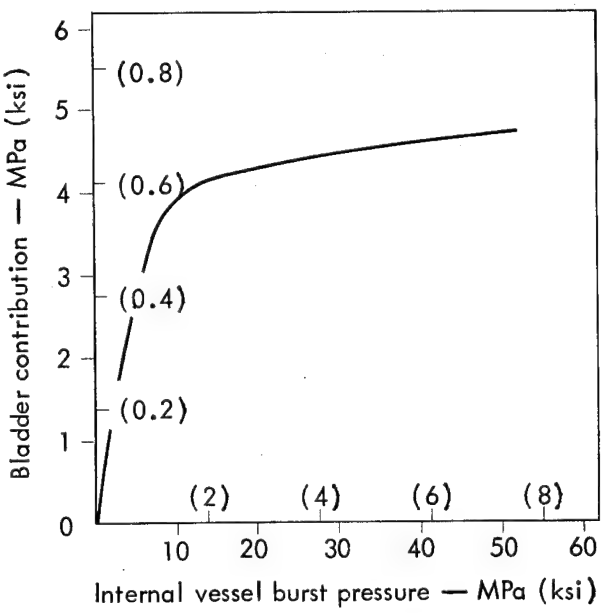

Fig. 30. Contribution of the 2.0-mm-thick Al-1100-o bladder to 2.0-mm-thick Kevlar 49 epoxy 20.3-cm spherical pressure vessel. The calculation is based on the following composite properties: the hoop modulus of 40 GPa (8.5×10^6 psi); the through-the-thickness modulus of 23.77 GPa (0.5×10^6 psi); and the Poisson's ratio of 0.25.

The vessel performances at LH_2 for various vessel designs are summarized in Table 17. These data can be compared to the results shown in Table 15 (cylindrical vessels at 21°C) and Table 16 (spherical vessels with a 0.76-mm and a 2.0-mm aluminum liner). Statistical analysis does not show any effect of LH_2 temperature on 0.76-mm aluminum-lined cylindrical and spherical vessels. In the case of 2.0-mm aluminum-lined spherical vessels, the single value burst pressure at LH_2 [failure shown in Fig. 31(a)] is about 11% higher than the average burst value at 21°C. This value seems statistically significant; however, we attribute the bulk of this difference to the contribution of 2.0-mm aluminum liner. The increase in

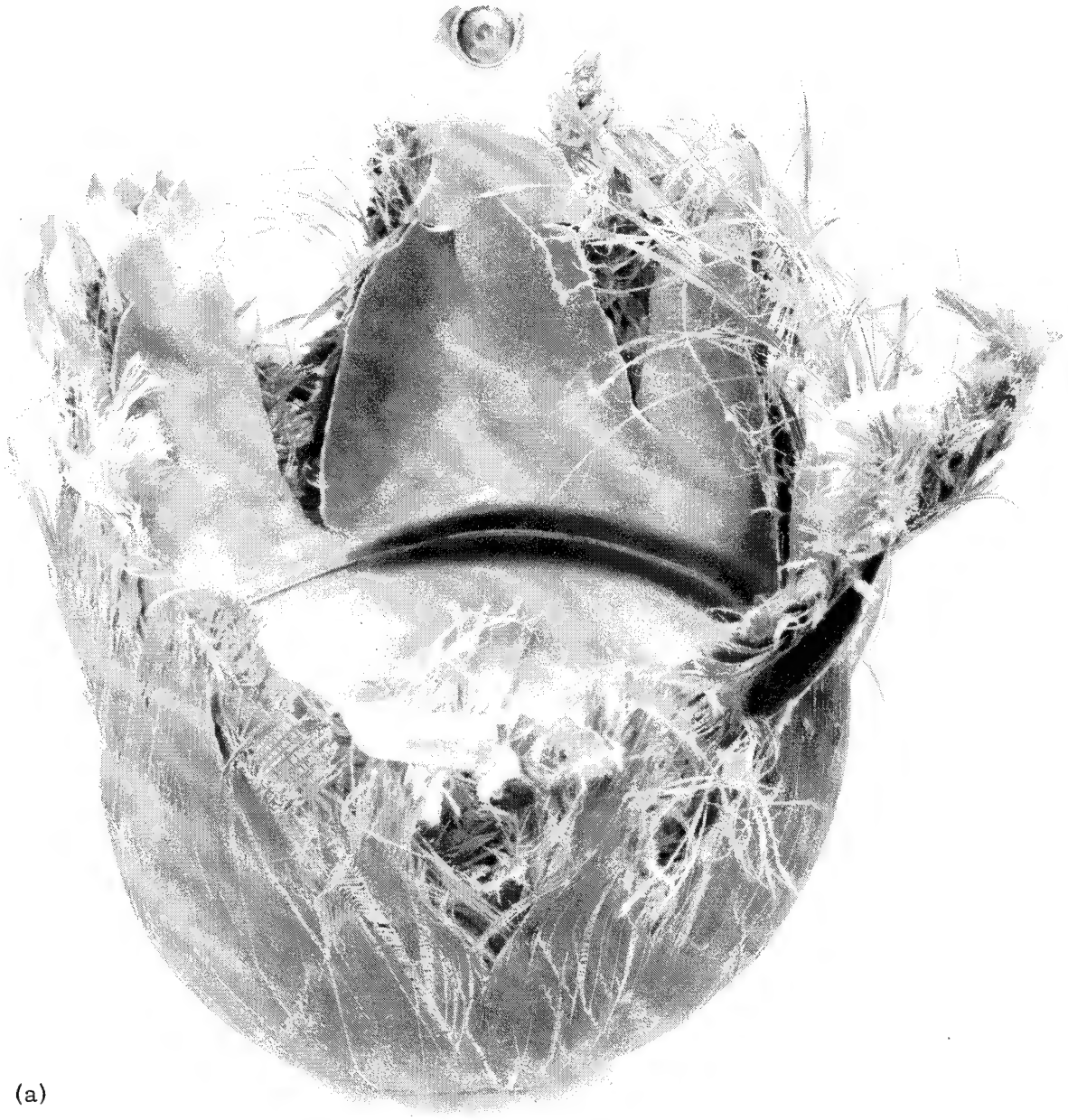

(a)

Fig. 31. Vessel failure; (a) burst of 2.0-mm Al-lined sphere at LH_2 temperature, (b) burst of 0.5-mm rubber-lined cylindrical vessel at 21°C.

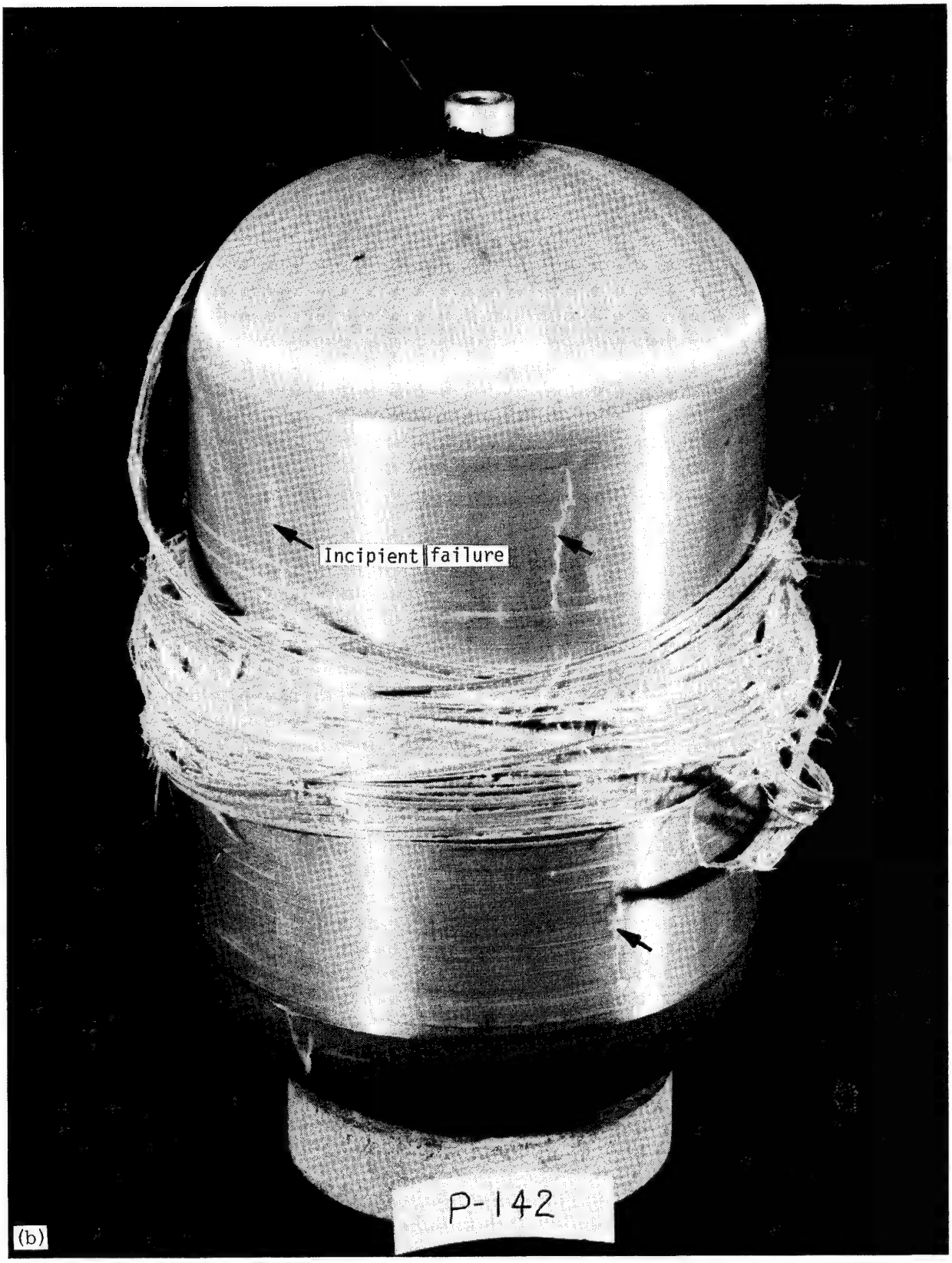

Fig. 31. (Continued)

Table 17. Effect of LH_2 temperature on performance of spherical and cylindrical (20 cm) Kevlar 49/epoxy vessels (test temperature -253°C).

Vessel	Cylindrical (0.76 mm liner)		Spherical (0.76 mm liner)		Spherical (2 mm liner)
1. Number	P-154	P-155	0423	0434	0686
2. Volume, V, $10^{-3}m^3$ ($in.^3$)	9.28 (566)		4.09 (250)		4.09 (250)
3. Burst pressure: MPa	15.5	16.5	31.9	30.0	43.3
(ksi)	(2.25)	(2.40)	(4.63)	(4.35)	(6.28)
4. Failure location[a]	H	H	I	I	I
5. Performance factor:					
Fiber, PV/W_f, $kPa \cdot m^3/kg$	535	570	495	441	692
(10^6 in.)	(2.15)	(2.29)	(1.99)	(1.77)	(2.78)[b]
Composite, PV/W_f, $kPa \cdot m^3/kg$	398	423	391	336	513
(10^6 in.)	(1.60)	(1.70)	(1.57)	(1.35)	(2.06)[b]
Composite					
1. Wall thickness, mm	1.40	1.40	2.24	2.21	2.06
2. Mass, g					
Composite, W_c	360.9	364.9	334.5	365.6	345.0
Fiber, W_f	268.7	268.9	263.6	279.0	255.7
3. Fiber content, vol%	70.8	69.7	75.6	72.8	70.2
Winding					
1. Longo angle	7°10'[c]		13.8°		
2. Hoop/longo fiber ratio	1.79				
3. Pattern	Closed, 36 bands		13.8° bandwidth		
4. Hoop	10 layers				
Layers, interspersing	10(4 + 2 + 2 + 2)				
Total winding revolutions	4 121				
5. Longo	6 layers				
Layers, interspersing	6(2 + 2 + 2)				

Table 17, Continued.

Total winding revolutions	3 564	
6. Extra reinforcement		
Equators (revolutions)	80	
Knuckles (revolutions)	190	
Resin system (ratio)	DER 332/T-403(100/36)	DER 332/T-403(100/36)
1. Gelling (h/°C)	3/60[c]	Room temp.
2. Curing (h/°C)	3/73.9[c]	Room temp.

[a]H - Hoop failure, F - Fitting failure, K - Knuckle failure, I - Intermediate.
[b]No correction for liner contribution.
[c]P-154 and P-155 only.

strength of 1100 aluminum at LH_2 temperature is shown to be a factor of 2 to 3 higher (depending on the strain level) than its room temperature strength.[13] From this evidence and our previous results on the effect of LN_2 temperature on the strength of Kevlar 49/epoxy strands, we conclude that, outside of metal liner effects, cryogenic temperature has no significant effect on vessel performance factors.

Cylindrical vs Spherical Vessel

Since it is a well recognized fact that a sphere is the most efficient shape for metallic pressure vessels, this concept has often been mistakenly extended to filament-wound vessels. On the other hand, in the early days of filament winding some who tried to wind spheres did not achieve vessel performances comparable to cylindrical vessels. Thus, confusion over the performance of filament-wound spheres vs cylinders began. Analytical treatment by R. H. Reid and F. J. Darm in 1963 and later verified by Feldman, et al.,[12] indicated the maximum expected vessel performance is PV/W = 1/3 (failure stress/density). This expression applies without exception to all filament-wound shapes whose filaments are uniformly loaded.

Comparing the cylindrical and spherical vessels, our data from Tables 14 and 16 essentially confirms the fact that shape has no effect on the performance factor of filament wound vessels.

We think that one should choose the vessel shape based on factors such as space limitations or winding machine availability rather than on vessel performance. Any experimental difference in performance factor between various vessel shapes is likely a result of processing factors, vessel design, or both.

There are several points that are critical in winding high performance

vessels. Wide band winding[9] does minimize fiber cross-overs as well as heavy buildup adjacent to any fitting. This point is particularly critical to the spherical vessel. While the weak link for a sphere is at the poles, there are three weak areas for a cylindrical vessel: the edge of the fitting on the dome, the knuckle, and the end of hoop winding on the cylindrical section. The failure of a vessel is often controlled by one of these localized weak spots, which must be eliminated by some means. We have tried localized reinforcement on the cylindrical vessels with some success. Figure 31(b) shows a vessel that did not fail at the localized weak spots.

Cyclic Fatigue

Two cylindrical vessels (P-182 and P-183) with a 0.76-mm aluminum liner were pressure cycled at 21°C and at approximately 70% of the ultimate burst [between 0.69 and 9.65 MPa (100 and 1400 psi)]. Premature failures (14 and 15 cycles, respectively) of the aluminum liner prevented us from determining the fatigue behavior of the Kevlar 49/epoxy composite.

At LH_2 temperatures, two spherical vessels were fatigue tested. One vessel with a 2.0-mm aluminum liner was cycled 581 times to 16.5 ± 0.3 MPa (2400 ± 50 psig, 67% of the ultimate burst), at which time it was found to be leaking through the windings. Another vessel with the same liner was cycled 498 times to the same pressure with no evidence of leaking. After 57 additional cycles (total of 555) it was also found to be leaking through the windings in numerous locations.

Clearly the cyclic life of this vessel liner system is not outstanding. These lives do not indicate a fatigue problem with Kevlar 49, but rather a liner fatigue problem. All tests were terminated because of excess leakage through the metal liners.

The liners in these vessels were not selected for optimum fatigue performance. Thus, the use of rather weak 1100 aluminum led to a relatively large amount of plastic strain in the liner during each cycle. It is well known that low cycle fatigue depends on the amount of plastic deformation per cycle.

The relatively poor fatigue performance of the cylindrical vessels is primarily the result of local corrosion at the weld at the center of the cylindrical portion of the liner. The source of this corrosion was a corrosive salt (Paraplast 33) that was used to support the cylindrical metal mandrels during winding. After testing was completed, we noticed that the weld regions at the center of the cylinder had been preferentially attacked by the salt solution. This led to a reduction in thickness, and, as a result, the two cylinders both cracked in these welds. Since the fitting welds, which experience only small strains during each cycle, showed significantly less corrosion, we concluded that the weld corrosion was strain enhanced at the center of the cylinders.

CONCLUSIONS

Our data show that the vessel performance factor is approximately the same for both spherical and cylindrical vessels. Thus, we agree with theoretical predictions.

The best vessel performance factor (PV/W) is 600 kPa · m^3/kg, based on fiber mass; it is 450 kPa · m^3/kg based on composite mass. We did not have enough vessels in some designs to allow study of the reproducibility.

The effect of LH_2 temperature on the vessel performance is negligible.

For cryogenic applications or gas containment at room temperature, the choice of vessel liner is likely to be a light weight metal. The reliability of a thin, weak aluminum liner for cyclic loading is questionable. In this study, because the liners failed prematurely, we were unable to gather good fatigue data for the various pressure vessels.

Acoustic Emission

Acoustic emission data from the 10.2-cm bottles, 20.3-cm bottles and 20.3-cm spheres are discussed as well as data from organic fiber elongated NOL rings and fiber/epoxy strands. Acoustic emission results obtained during these tests have been primarily used as a tool to help understand the microscopic damage that occurs in a composite organic filament-wound pressure vessel as it is pressurized to failure. Without acoustic emission data it would be impossible to gain this same understanding. The acoustic emission data have also been useful in determining when a cylindrical pressure vessel has the proper ratio of hoop wraps to longitudinal wraps. Such a ratio gives a balanced vessel in which the hoop wraps are highly loaded before failure occurs.

ACOUSTIC EMISSION SYSTEM

A commercial acoustic emission system was used for all tests. This system allowed either one or two channels of acoustic emission information to be obtained.

Commercial, piezoelectric acoustic emission transducers (transducer "rings" at a characteristic frequency) were used. The acoustic signal was processed through a preamplifier, a filter (usually set to pass 100 to 300 kHz), and a power amplifier. In total, the system provided some 70 to 80 dB of electronic gain as needed. The acoustic signal was presented visually in two ways. First, the signal was displayed on an oscilloscope as a function of time. In addition, a count was made of the number of times the amplitude of the acoustic signal exceeded a voltage bias (nominally set at 1 Vdc). This count was recorded on an X-Y plotter as a function of convenient test parameters, both as a count rate (usually averaged over 1 or 2 sec) and as a cumulative total of counts. The coupling agent for the acoustic emission transducer was a viscous resin. During the 10.2-cm and 20.3-cm bottle tests the transducer was coupled to the cylindrical portion of the bottles. In a few cases a transducer was also coupled to the "head" region of the bottles. For the elongated NOL ring tests the transducer was coupled to the ring near the mid-point of the straight section (Fig. 2), and for the strand tests the transducer was coupled to one of the specimen grips.

FIBER STRESS RATIO

To discuss the use of acoustic emission data as a tool to balance the bottle pressure vessel design, we must first define a term called the fiber stress ratio. That is the ratio of longitudinal fiber stress σ_L to hoop fiber stress σ_H. This ratio was determined from a simple netting analysis applied to the cylindrical portion of the bottle; it gave an approximate measure of the ratio of the fiber stresses in the two different wraps at a given pressure. Hence, a bottle wound with a balanced design (based on the netting analysis) would have a fiber stress ratio $\sigma_L/\sigma_H = 1.0$.

ACOUSTIC EMISSION TESTS

Kevlar 49 Fiber/Epoxy Vessels, 10.2-cm and 20.3-cm Cylinders

Figures 32 and 33 illustrate the two broad types of acoustic-emission records that can be obtained from testing 10.2-cm organic fiber composite bottles. The two types, count rate and summation of counts, are shown as a function of internal pressure. The typical predominate failure modes that are associated with these two types of acoustic-emission responses are the so-called hoop failure (Fig. 34) and end failure (Fig. 35). The difference in acoustic emission and failure behavior between these two bottles is associated with how the bottle was wound. The behavior shown in Figs. 33 and 35 results from one of the following: (a) a large stress ratio σ_L/σ_H (unbalanced design), (b) a weakness in the fitting region, or (c) failure to reinforce the ends of the hoop wraps. The behavior shown in Figs. 32 and 34 results from a sufficiently low stress ratio σ_L/σ_H, adequately reinforced hoop wraps, and no weakness in the fitting region. The typical geometric patterns of acoustic emission shown in Figs. 32 and 34 did not significantly change

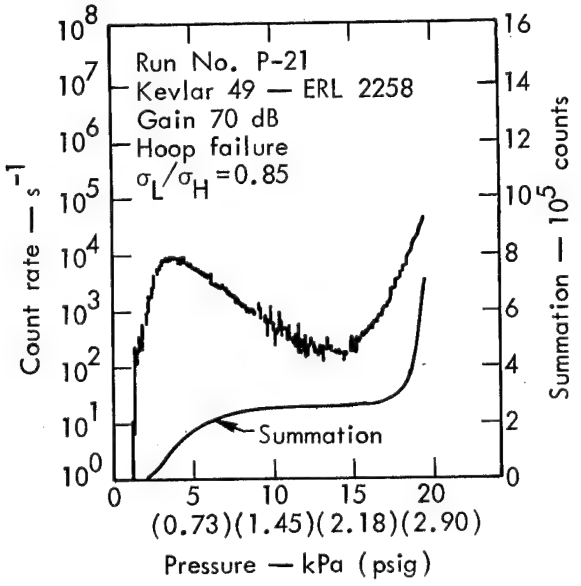

Fig. 32. Acoustic emission from an organic-fiber 10.2-cm bottle that experienced hoop failure.

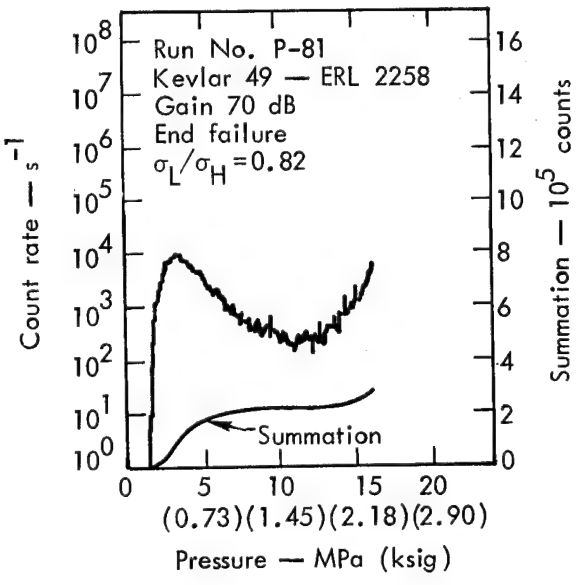

Fig. 33. Acoustic emission from an organic-fiber 10.2-cm bottle that experienced end failure.

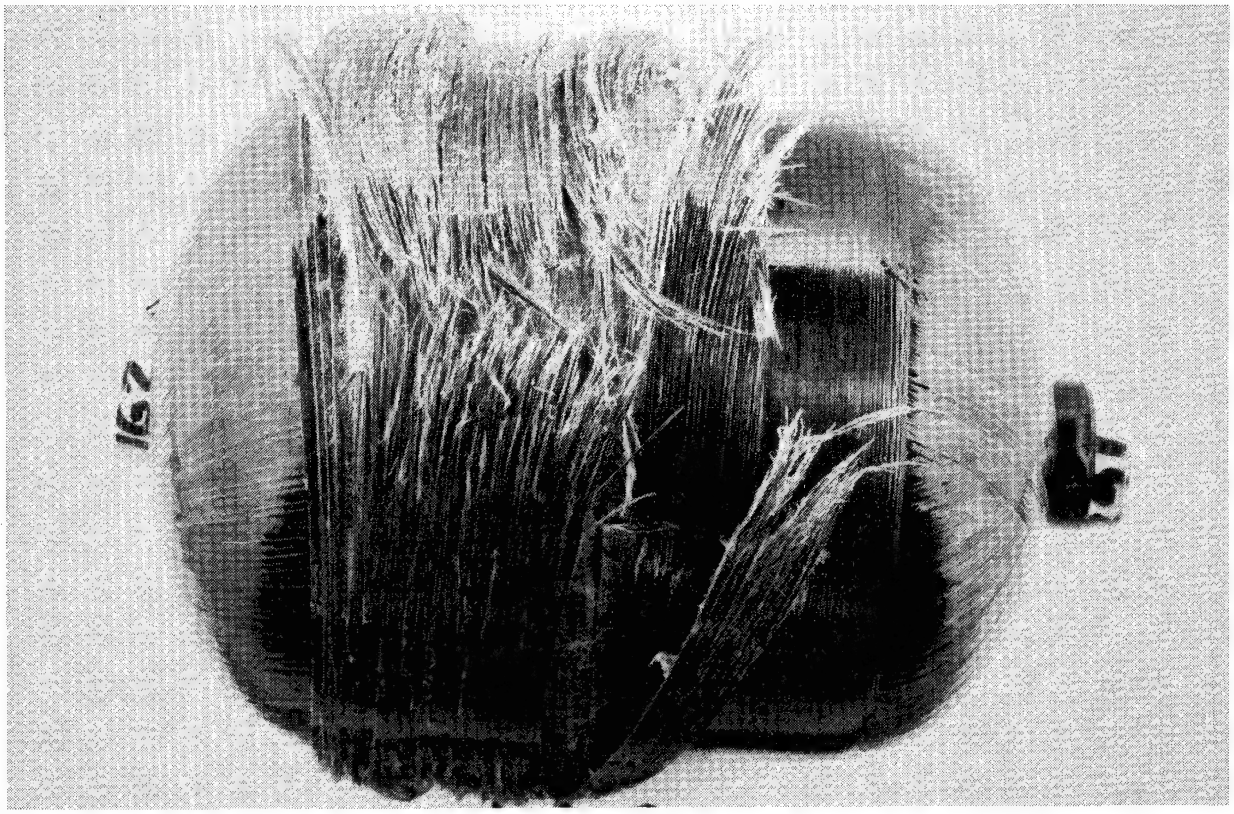

Fig. 34. Typical hoop failure of a 10.2-cm organic-fiber-reinforced pressure bottle.

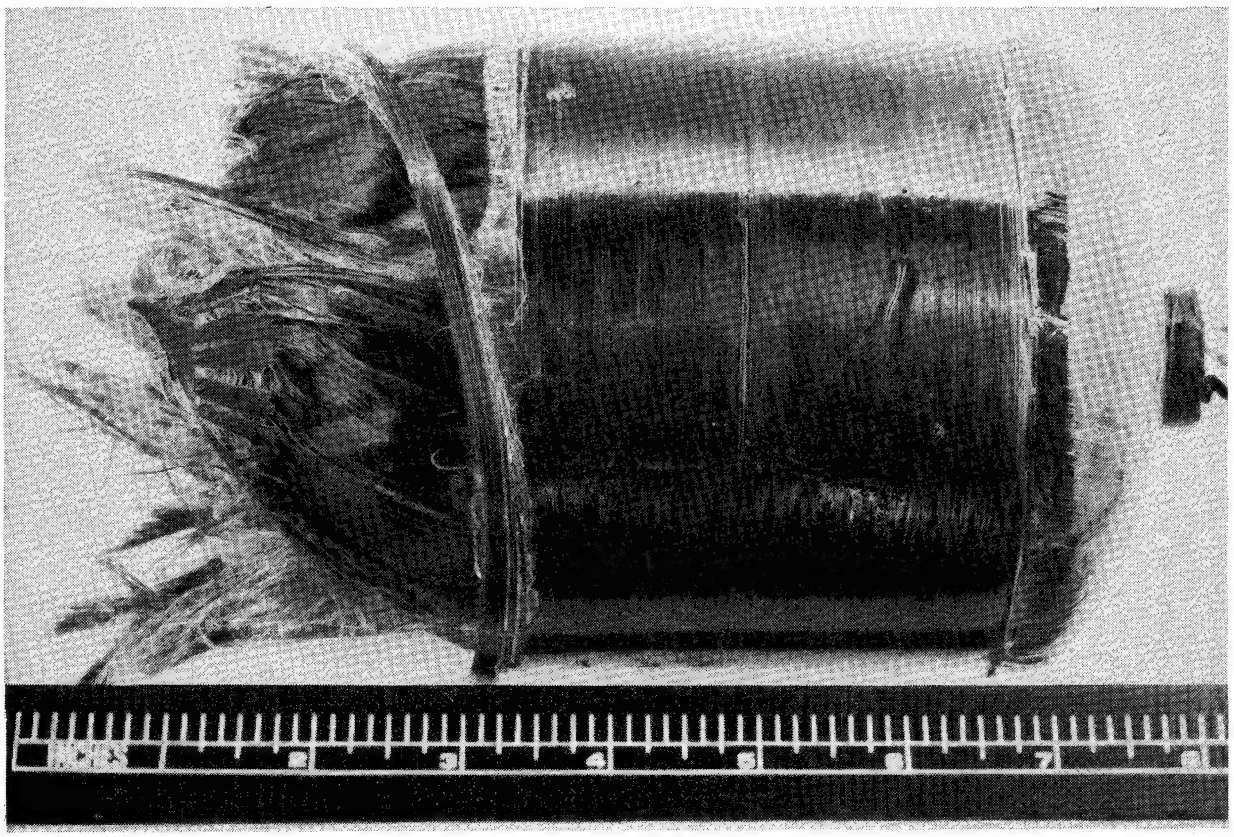

Fig. 35. Typical end failure of a 10.2-cm organic-fiber-reinforced pressure bottle.

when the wrapping pattern was changed to the so-called interspersed pattern. The interspersed pattern bottle was wound by the following wrapping sequence: two hoop layers, two longitudinal layers, two hoop layers, two longitudinal layers, and, finally, two hoop layers. The noninterspersed bottle was wound by first laying down four longitudinal layers and then six hoop layers. All of the above statements apply to 20.3-cm pressure bottles as well except that there are more layers involved.

Figure 36 shows the differences in the summation of acoustic emission vs internal pressure between unflawed 10.2-cm bottles that typically experienced end failures and 10.2-cm bottles with various indicated flaws. Two acoustic emission transducers were used. The transducer on the cylindrical portion of the bottle was called the hoop transducer, and the one on the

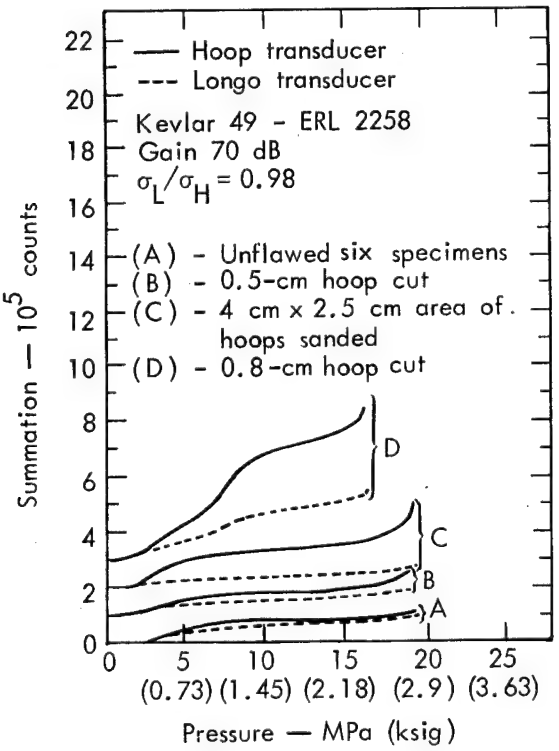

Fig. 36. Acoustic emission from flawed 10.2-cm organic-fiber bottles.

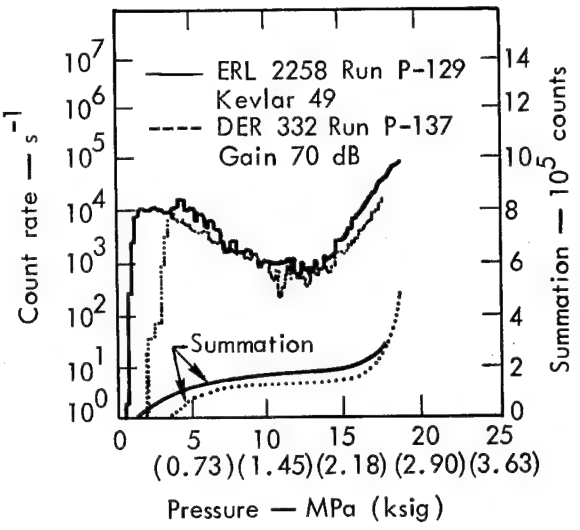

Fig. 37. Acoustic emission from 10.2-cm organic-fiber bottles with different epoxies.

"head" portion was called the longo transducer. The curves labeled (A) represent the typical summation of counts from both transducers for unflawed specimens. Curves (B), (C), and (D) show the typical emission from specimens with flaws: a 0.5-cm cut in the outer hoop wraps (B), a 4.0 × 2.5 cm region of the outer hoop wraps sanded with emery paper (C), and a 0.8-cm cut in the outer hoop wraps (D). To clarify the presentation, the zero summation line has been moved up one major division for curves (B), (C), and (D). In case (B), the flaw did not control the failure of the bottle. This bottle failed in the end of "head" region, as did the unflawed specimens. The failure location in the other two specimens, curves (C) and (D), was controlled by the artificial flaws.

Figure 37 compares the acoustic emission from two 10.2-cm specimens that differ significantly only in the type of epoxy resin used. In one case the resin was the ERL 2258 system, while in the other case it was the lower-cure-temperature DER 332 system.

The only significant deviation from the acoustic emission (AE) bottle data shown so far was a large increase in the early acoustic emission. The increase occurred at the distinct peak in acoustic emission count-rate data, and it normally occurs at approximately 20 to 25% of the bottle failure pressure. The increase at the first count rate peak seems to be more predominate in 20.3-cm bottles than in 10.2-cm bottles. Figure 38 illustrates the summation, count rate, and strain data for a typical 20.3-cm-diam organic-fiber composite vessel that showed this large increase in the amount of AE generated during the early peak. Vessels that generated this acoustic emission pattern were observed to have regularly spaced cracks on the hoop wraps. These cracks have also been seen on some 10.2-cm vessels that had an increase in AE during the early peak. For the 10.2-cm vessels, these cracks (Fig. 39) ran parallel to the hoop wraps for distances of up to approximately one-half or three-fourths the circumference of the vessels. Typically, they were spaced at about 0.10-cm increments or about 10 cracks/cm. They also were more apparent to visual inspection on one-half of the hoop wraps than they were on the other half. On 20.3-cm vessels the cracks were spaced at about 0.11-cm intervals. For comparison purposes a 10.2-cm bottle, which did not have the exaggerated early peak, is shown in Fig. 40. Axial strain data for this bottle had a change of slope at about the acoustic emission peak just as did the 20.3-cm bottle with the exaggerated first peak.

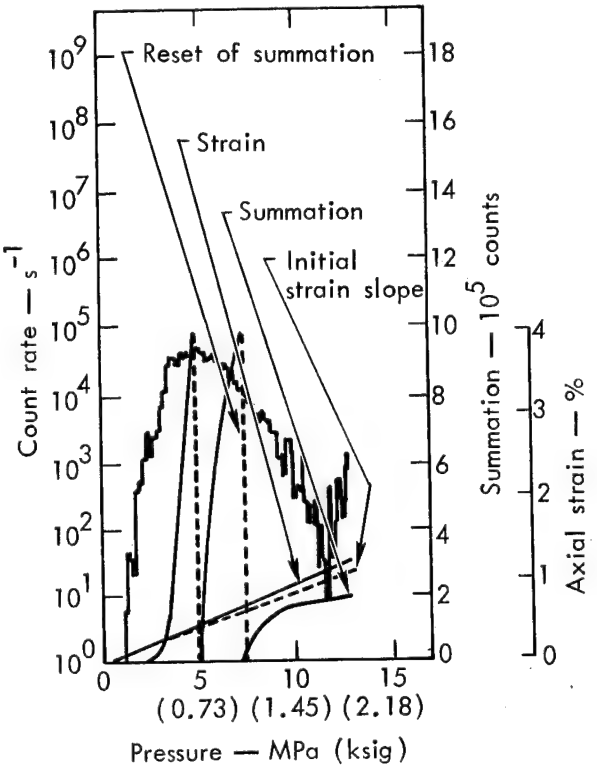

Fig. 38. Acoustic emission and axial hoop strain vs pressure for a 20.3-cm vessel with a large, early acoustic emission peak. (Run P-159, Kevlar 49, DER 332, gain is equal to 70 dB, averaging time is equal to 2 s.)

Kevlar 49 Fiber/Epoxy Rings and Strands

During tests of the elongated organic-fiber/epoxy NOL rings, the same AE characteristics appeared as in the vessel tests. Typical AE vs load data are shown in Fig. 41(a). Note that the summation of AE builds up rapidly at low loads, then levels off, and finally increases rapidly just before failure. The count-rate AE data also clearly show an early peak in the modified NOL rings.

Figure 41(b) shows the summation of AE vs load for a tensile test of a single strand (285 filaments) of organic fiber/epoxy. The significant fact here is that the early peak in AE has been eliminated, and we observe only the rapid increase in summation of counts just before strand failure.

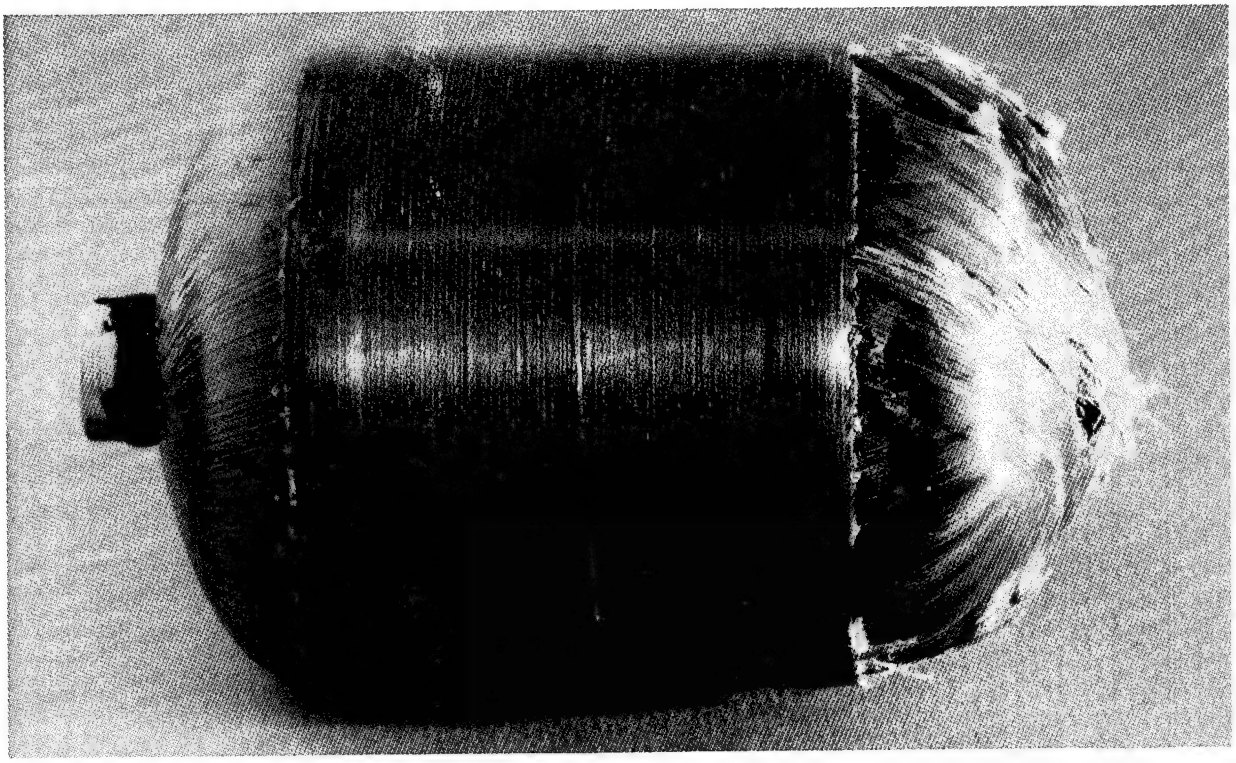

Fig. 39. Typical cracks in hoop wraps of a 10.2-cm organic-fiber vessel.

SOURCE OF ACOUSTIC EMISSION

The discussion and the interpretation of all acoustic emission results are based on the conclusion that the large majority of acoustic-emission data gathered at the gain levels used in these tests comes from, or is associated with, fiber failure. This conclusion is based in part on the fact that a fracture-toughness, epoxy double-cantilever beam (DCB), strengthened with approximately 50 strands of single-end S-glass situated perpendicular to the cleavage plane, produced some 13 000 to 15 000 counts during testing to failure, while an epoxy DCB without strands produced approximately 400 to 600 counts during testing to failure. See Ref. 14 for further discussion of these tests. Although these tests primarily refer to S-glass-reinforced epoxies, the basic

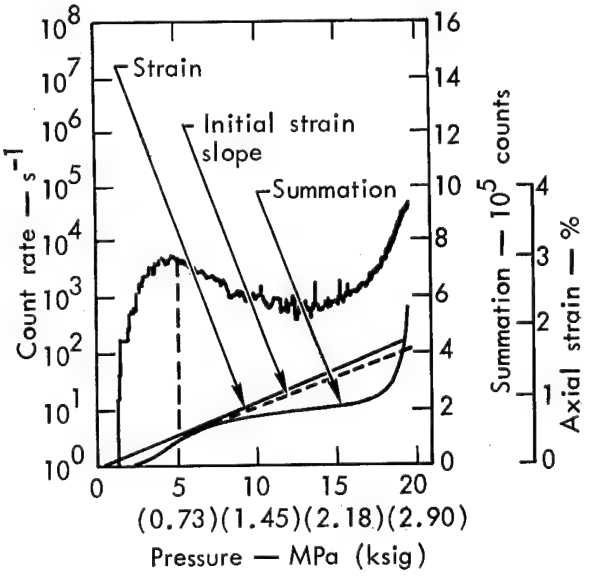

Fig. 40. Acoustic emission as a function of pressure from a typical 10.2-cm organic-fiber bottle. (Run P-24, Kevlar 49, ERL 2258, gain is equal to 70 dB, averaging time is equal to 1 s.)

significant finding carries through to organic-reinforced epoxies. Namely, the

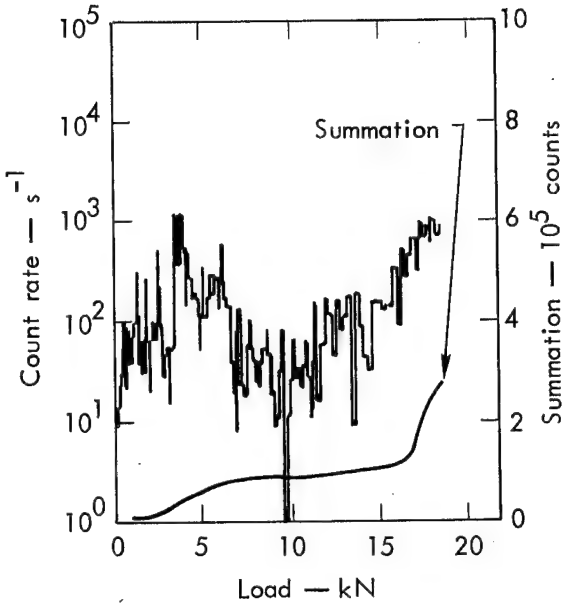

Fig. 41(a). Typical acoustic emission vs load from an elongated organic-fiber NOL ring. (Run 3, Kevlar 49, ERL 2258, gain is equal to 70 dB, averaging time is equal to 1 s.)

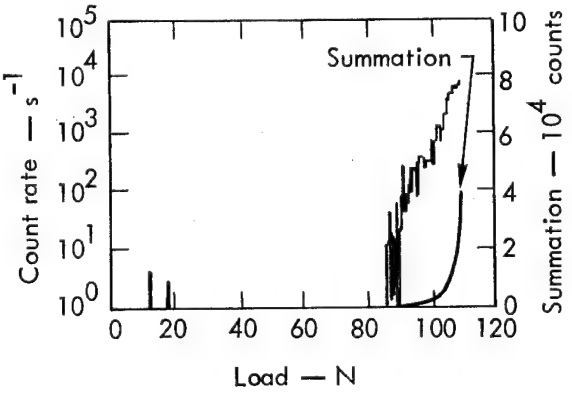

Fig. 41(b). Typical acoustic emission vs load from an organic-fiber/epoxy strand. (Run 15, Kevlar 49, ERL 2258, gain is equal to 80 dB, averaging time is equal to 0.2 s.)

fiber failure stresses are much higher than matrix failure or interfacial debonding stresses, and hence the energy released by these latter mechanisms is much less than that released by fiber failure.

DISCUSSION OF VESSELS, RINGS, AND STRANDS

The contrast between summation of counts and count rate shown in Figs. 32 and 33 illustrates, for organic fiber-reinforced epoxies, one of the key applications of acoustic emission to composite pressure bottle design. As was pointed out in Ref. 12 (for S-glass-reinforced epoxies), the rapid rise in summation of counts and count rate just before failure (shown in Fig. 32) results from the many fiber breaks that occur in the relatively uniformly-stressed hoop wraps. Thus, the acoustic emission data can be used for organic and S-glass bottles to distinguish between bottle designs that efficiently load the hoop wraps before failure and those that do not. The acoustic emission behavior shown in Fig. 33 indicates that failure in this bottle occurred before the hoop wraps were highly loaded. The three basic causes for this behavior were pointed out in a previous section.

The organic fiber rings and strands also show this rapid rise in summation of counts and count rate just before failure (Figs. 41). This indicates that many fibers are being broken as the failure load is being approached.

We observed that the basic geometry of the acoustic emission patterns for the organic-fiber bottles was not significantly altered when the interspersed winding sequence was used. This result implies that, for this fiber, the interspersed pattern will probably not degrade the performance of such vessels significantly, and may even offer a slight improvement. It was pointed out in Ref. 13 that the use of the interspersed pattern in S-glass led

to a significantly different acoustic emission pattern. This pattern indicated a degraded bottle and, indeed, the experimental failure pressures were degraded by some 14 to 18% below those found for bottles having the noninterspersed pattern.

Figure 37 (organic-fiber bottles) shows that the use of the lower-cure-temperature epoxy system led to an increase in the internal pressure at which a significant amount of acoustic emission began (defined as the pressure where the summation of counts rises above the zero line). The increase is on the order of two to four times the pressure at which acoustic emission begins in the high-cure-temperature resin bottle. At this point it is only possible to speculate on the cause for this change in acoustic-emission response. It may be that this phenomenon is related to the residual stresses, the fiber matrix configurations that are induced during the cure cycle, or the matrix fracture toughness.

The results shown in Fig. 36 for the flawed organic-fiber bottles indicate that it is possible to detect a flawed bottle when the flaw is controlling the bottle failure. Such flaws may be detected at approximately one-half the normal failure pressure. Note that in test (B), where the flaw did not control the bottle failure, the summation of acoustic emission gave little indication that the flaw was present. It is also clear from test (C) that the location of the acoustic-emission transducer with respect to the flaw location is important. In this case the longo transducer gave no visible indication that the flaw was present. In case (D) both transducers gave adequate indication of the presence of the flaw. The reason for this difference can be partly explained by a difference in the mechanism of propagation of the flaws in cases (C) and (D). When the acoustic emission signals from the hoop transducer in these two cases were viewed on an oscilloscope, the indication was that the flaw growth was proceeding in a different manner in each case. The acoustic emission signals had very large amplitudes in case (D). Often the signals completely saturated the electronic equipment. This observation indicated that the flaw growth was proceeding by events involving large energy releases. In case (C) the acoustic emission signals tended to be comparatively small (indicating growth by small energy releases). These rather small signals, which originated in the hoop wraps for case (C), were attenuated during propagation to the longo transducer and hence did not have enough amplitude to be counted by the longo acoustic emission channel. One further point should be made with regard to these tests. In spite of relatively gross flaws, in case (B) the flaw did not control the failure, in case (C) the bottle failure pressure was not significantly degraded, and in case (D) the failure pressure was degraded only some 15%. Hence, it would seem that the organic-fiber bottle is relatively resistant to artificial flaws.

THE EARLY PEAK IN COUNT RATE DATA

Microscopic Investigation of Cracks

Micrographs of the outer surface of the hoop wrap cracks are shown in Fig. 42. Notice the loose filament ends that consistently appear along the cracks. These broken filaments indicate that as the cracks form, acoustic emission (AE) will

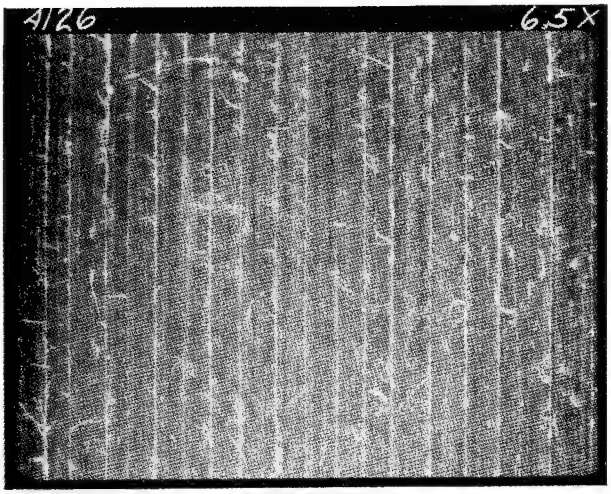

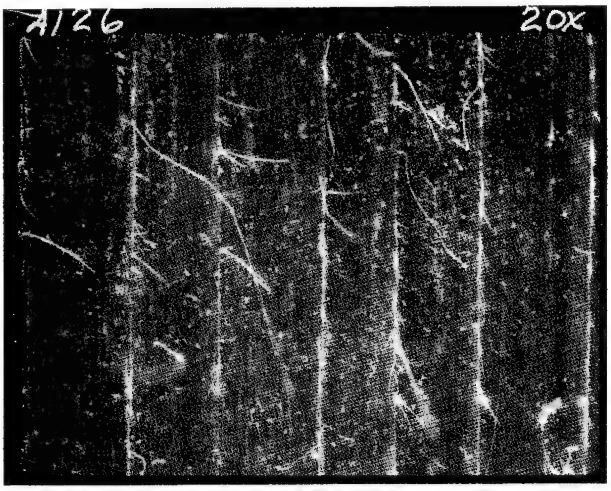

Fig. 42. Micrographs of cracks on outer hoop wraps of a 10.2-cm organic-fiber vessel.

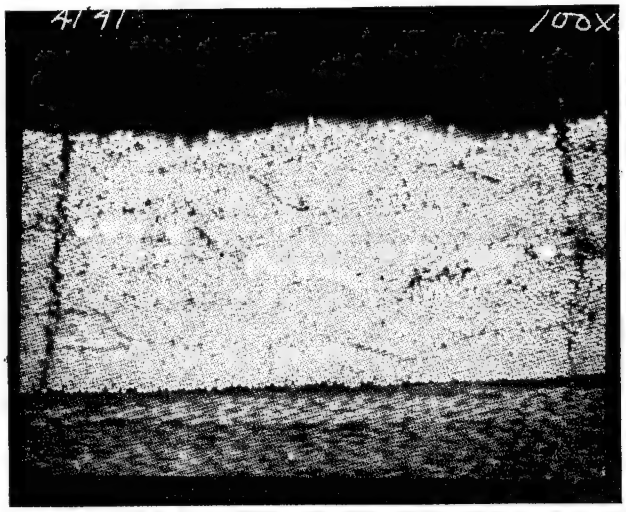

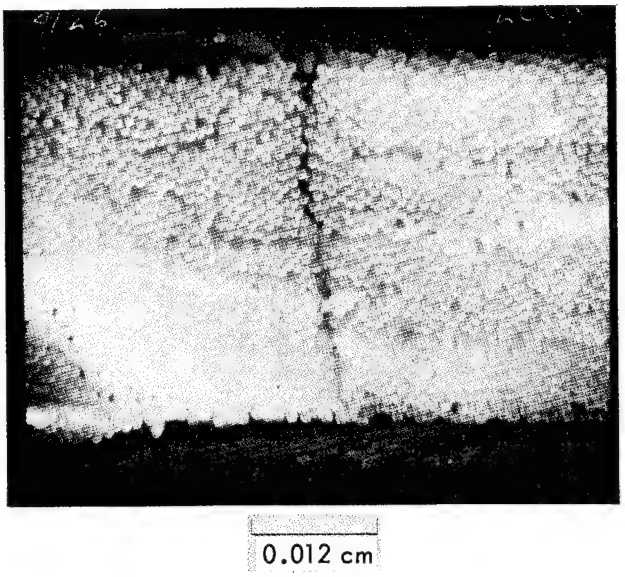

Fig. 43. Micrographs of a cross section of the hoop wraps that show crack propagation through the hoop wrap layers (10.2-cm bottle).

be generated. After the surface inspections, samples were prepared to characterize the depth of the cracks. The micrographs in Fig. 43 demonstrate that these cracks typically extend completely through the four outer layers of the hoop wraps. This fact implies that there are very likely broken filaments (similar to those shown in Fig. 42) that extend completely through the thickness of the hoop wraps. These filament breaks evidently occur because, locally, the matrix cracks are not parallel to all filaments.

A low magnification inspection of the longo wraps did not show matrix cracks similar to those in the hoop wraps. The reason is probably that the matrix cracking is much less severe in these wraps because the fibers are helically wound at

13°. Hence, the fibers give reinforcement in two directions in the longo wraps.

A Physical Model for the Early Peak

As the composite pressure vessel is pressurized, the axial deformation in the longo layers causes axial deformation and stresses in the hoop wraps. Thus, the axial hoop-layer stresses are controlled by the longo deformation. At first this axial deformation in the hoop wraps is elastic; that is, the matrix material shows a tensile elastic strain. But with further expansion, the matrix material in the hoop wraps begins to crack parallel to the direction of the hoop fiber strands. This cracking reaches a peak at about 0.45% axial strain (see Fig. 38) in the hoop outer layer. With increased straining beyond 0.45%, the rate of formation of new cracks decreases to a minimal value. The reason for the decrease is that there are now a sufficient number of cracks to allow essentially unimpeded axial expansion of the hoop layers. This description is supported by the AE and strain data of Figs. 38 and 40. In both figures the strain curve has a small "knee" that corresponds to the AE count-rate peak. This knee indicates that a decrease in the modulus of the composite hoop wraps in the axial direction takes place at approximately the AE peak.

The source of the AE that shows a count rate peak at about 0.45% strain is not matrix cracking but the filament breakage shown in Fig. 42, which accompanies the matrix cracking. The fact that this filament breakage occurs almost completely over all hoop wraps of the vessels means that a substantial amount of AE is generated during this period. The conclusion that the matrix cracking alone does not generate significant acoustic emission is based on the epoxy DCB tests that were mentioned earlier in this report. These tests indicated that a small proportion of the AE (detected at the electronic gain levels used) resulted from matrix fractures.

The fact that the early peak in AE does not appear in the strand tensile test shown in Fig. 41(b) emphasizes that a biaxial stress field is necessary. In particular, there must be significant local stress in a direction perpendicular to the fiber direction. It is interesting that the early peak in AE also appears on the elongated NOL ring test shown in Fig. 41(a). This result implies that local stresses perpendicular to the fiber direction are present and cause cracking similar to that in the hoop wraps of the bottles.

Matrix Cracking Parameters

There are a number of composite properties that may control the strain level at which the matrix cracking reaches a peak. Among those that may be most important are: (1) the matrix failure elongation, (2) the fiber volume percentage, (3) the fracture toughness of the matrix material, and (4) the size and number of small matrix flaws induced during the gel and cure of the fiber/epoxy composite. The fact that factors (1) and (3) may change when the epoxy is cured in the presence of fibers serves to complicate the determination of which of the above four factors might be most significant. The simplest way to pick the significant factors may be to conduct AE studies of vessels that have controlled

changes in these four factors. Determination of the strain level at which the AE count-rate peak occurs may allow one to determine the most significant factors and then develop a mathematical model. Hopefully, this would eventually lead to fiber/matrix systems with minimal fiber fracture due to matrix cracking.

SUMMARY: CYLINDRICAL VESSELS, RINGS, AND STRANDS

- For organic filament-wound pressure bottles, acoustic emission can be used to determine if the hoop wraps are highly loaded before vessel failure occurs.
- Acoustic emission can sort out flawed organic fiber vessels if the flaw controls the vessel failure.
- Use of a lower-cure-temperature epoxy matrix increased by a factor of between two and four the pressure at which organic-fiber vessels first produce significant acoustic emission.

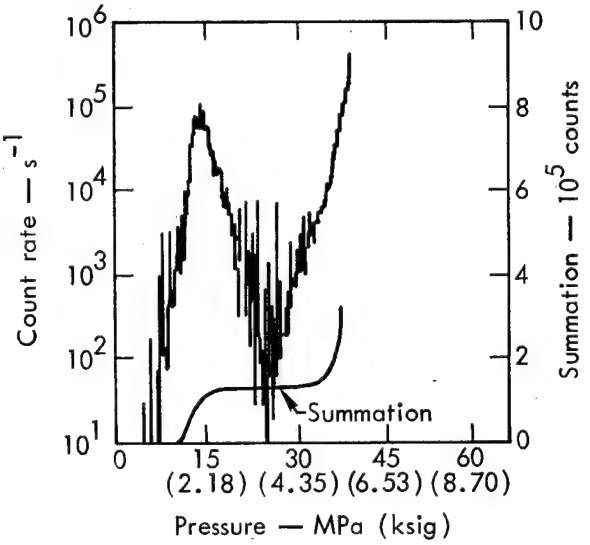

Fig. 44. Acoustic emission vs internal pressure for 20.3-cm small boss Kevlar 49 fiber/epoxy sphere. (Resin DER 332, gain is equal to 70 dB.)

- Micrographs indicate that filament failure resulting from matrix cracking is the source of the first AE count-rate peak in organic-fiber/epoxy pressure vessels. This peak corresponds to the knee in the curve showing axial hoop wrap strain vs internal pressure.
- Significant stresses perpendicular to the local fiber direction are required for the first AE count-rate peak to occur.
- Acoustic emission testing is particularly suited to studies aimed at finding the factors that most significantly control matrix cracking in organic-fiber/matrix pressure vessels.

FIBER/EPOXY 20.3-cm SPHERES

Acoustic emission from the 20.3-cm spheres has the same form as a well-designed cylindrical bottle. Figures 44 and 45 show the typical acoustic emission data for the single boss and double boss mandrel designs. All spherical vessels tested showed the rapid rise in count rate and summation of counts just before failure. This indicates that, as in the well-designed bottle, there are many fibers that are breaking just before failure, and hence the winding design gives rise to relatively uniform stresses in the composite wall. The 20.3-cm spheres also have the characteristic early peak in count rate data. It is likely due to the biaxial stress state and results from a mechanism similar to that in the bottles. Since the spherical winding pattern is similar to that used in the longitudinal wraps of the bottles, it is not likely that highly visible cracks will appear on the

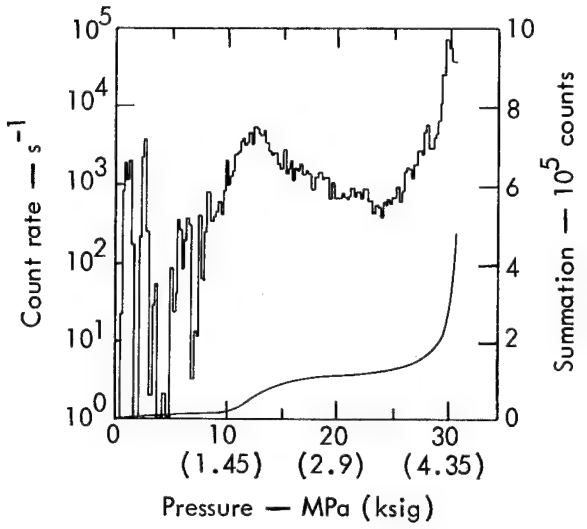

Fig. 45. Acoustic emission vs pressure for a typical 20.3-cm large boss sphere (Kevlar 49, DER 332, gain is equal to 80 dB).

sphere as they do on the hoop wraps of the cylinder.

FATIGUE TESTS, 20.3-cm CYLINDERS

Acoustic emission data was obtained during two cylindrical fatigue tests at room temperature. The summation of counts was recorded as a function of the number of cycles. Since the bottles leaked prematurely (15 and 16 cycles), it was difficult to obtain any meaningful information from the acoustic emission data, except that acoustic emission is a very sensitive leak detector. Figure 46 shows one of the curves. The only characteristic is that the summation of acoustic emission increased approximately linearly until leaking began.

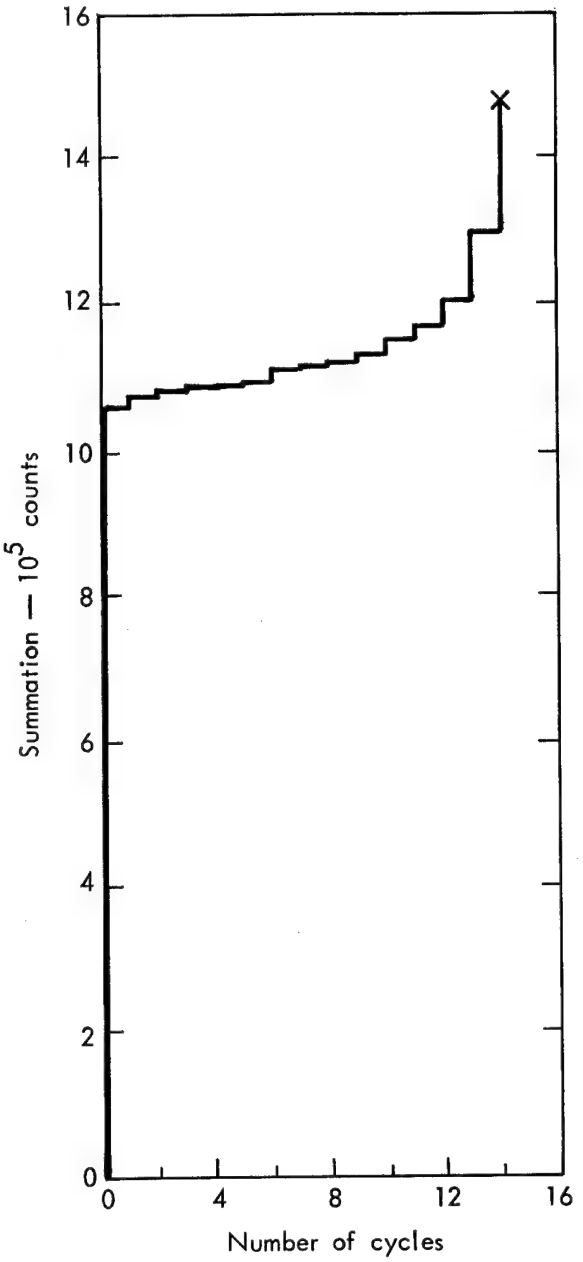

Fig. 46. Summation of acoustic emission vs number of cycles. Fatigue of 20.3-cm Kevlar 49 cylinder. (Cycled from 690 to 9 650 kPa, gain is equal to 70 dB, DER 332.)

CONCLUSIONS: ACOUSTIC EMISSION

The results presented here show that acoustic emission can help us understand the microdamage that occurs during the testing of filamentary/epoxy composites. This information can be used to make design modifications which can improve the composites.

With the understanding that has been gained to date, the next task is to fully

investigate the use of acoustic emission as a nondestructive test technique for filamentary composites. The most rewarding approaches would be (1) acoustic emission amplitude analysis and (2) a systematic study of artificially flawed pressure vessels.

Fiber Microstructural Characterization

INTRODUCTION

The objective of this work was to characterize fibers; i.e., shape, size, structure, fracture mode, behavior in a composite, and unique features.

The fracture appearance of bare fibers, epoxy impregnated tensile strand specimens, NOL rings, and pressure vessels was studied. The composites consisted of Kevlar 49 fiber and the epoxy resin, Union Carbide ERL 2258/ZZL 0802 (100/30).

RESULTS

A scanning electron microscope (SEM) photomicrograph of a typical organic single bare filament is shown in Fig. 47. The filament has been cut with a sharp razor blade. The surface of the filament is smooth, and we believe that the small particles adhering to the surface are artifacts and are not an intrinsic part of the structure.

In Fig. 48 the typical fracture surface of a strand tensile specimen obtained by SEM is shown. At the lower magnifications (Figs. 48a and b) it can be seen that, upon fracture, the organic strand breaks down into both individual filaments and bundles ranging from about 10 to 20 filaments. The end of an individual 12-μm-diam filament is shown at high magnification in Fig. 48c. Note that upon fracture the end is further shredded in a fibrous manner into as many as 15 to 20 sub-filaments. All sub-filament elements tend to come to a point, with the radius of curvature at the tip of some of them being less than 0.1 μm (Fig. 48d).

In Fig. 49c particles or defects can be seen within the shredded sub-filament. These defects, which were observed often, do not appear to be artifacts, but are an inherent characteristic of the filament.

The appearance of the fracture areas of other organic composites was similar to that of the tensile specimen. Figure 49 shows the fracture area from a cylindrical pressure vessel which was tested to failure in a catastrophic manner, and

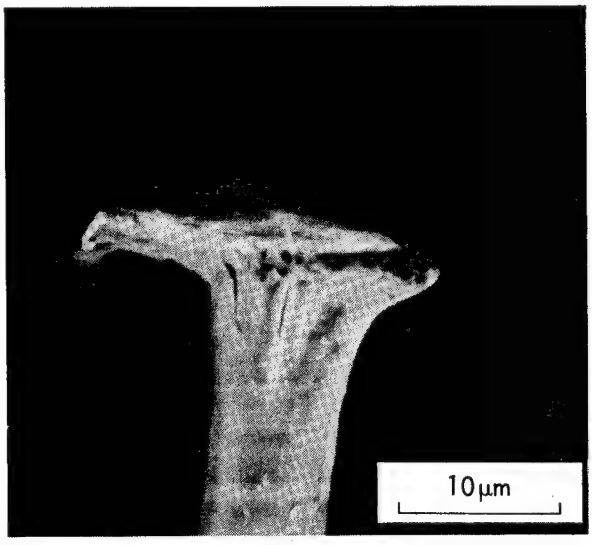

Fig. 47. A typical organic filament which has been cut with a razor blade (SEM).

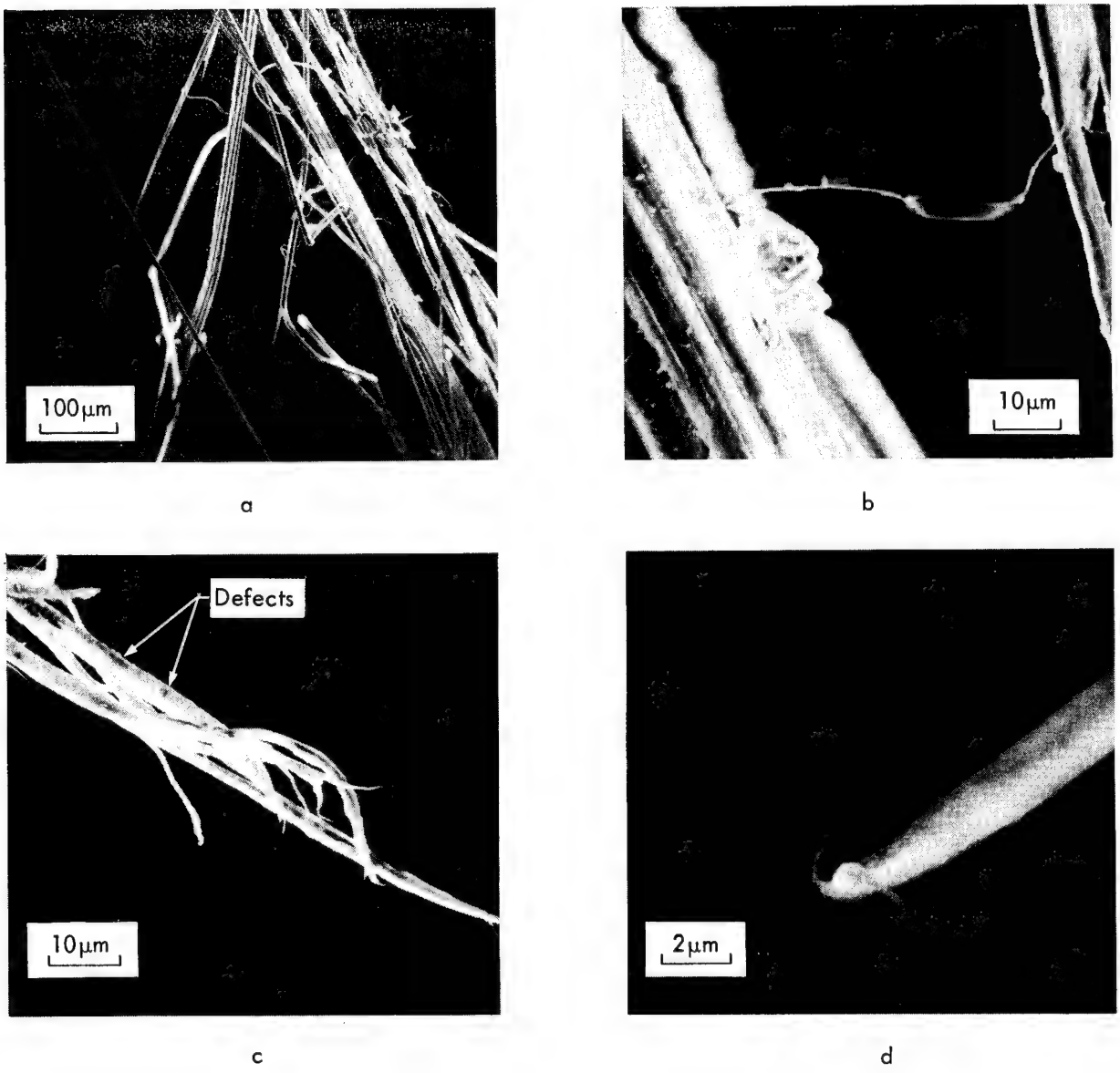

Fig. 48. Fracture ends of an organic fiber/epoxy strand tensile specimen (SEM); (a, b) several filaments, (c) end of a single filament, (d) end of a subfilament.

Fig. 50 shows the fracture area from a NOL ring. Both the splitting of individual filaments and the defects of unknown origin can be clearly seen in Figs. 49 and 50.

In one case (Fig. 51), a Kevlar 49 filament from the fracture area of a pressure vessel was split along the axis; it appeared that epoxy was on the inside fracture surface. This would indicate that the fiber was damaged before winding and that upon winding with epoxy some epoxy was deposited on the fracture surface. This phenomenon was atypical.

To increase the breadth of the investigative techniques an attempt was made to use transmission electron microscopy (TEM) to view bare single filaments. Charging of the fibers did create beam instability, but several TEM micrographs were possible (Figs. 52, 53).

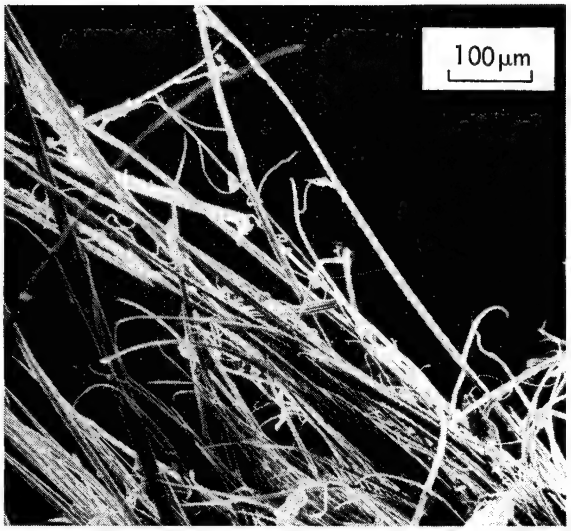

a

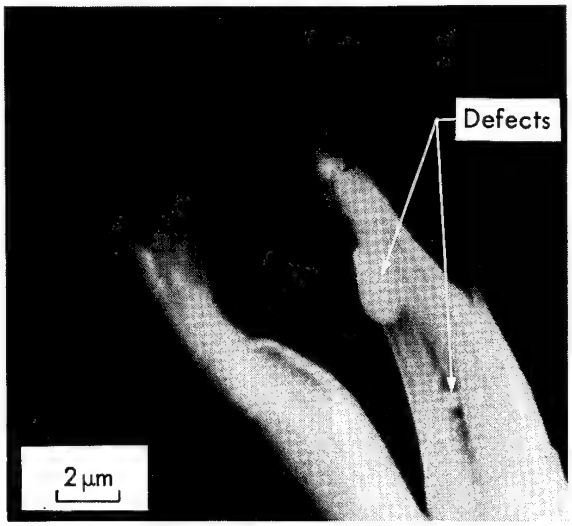

b

Fig. 49. Fracture ends of an organic fiber from a pressure vessel tested to failure (SEM); (a) several filaments, (b) split subfilaments.

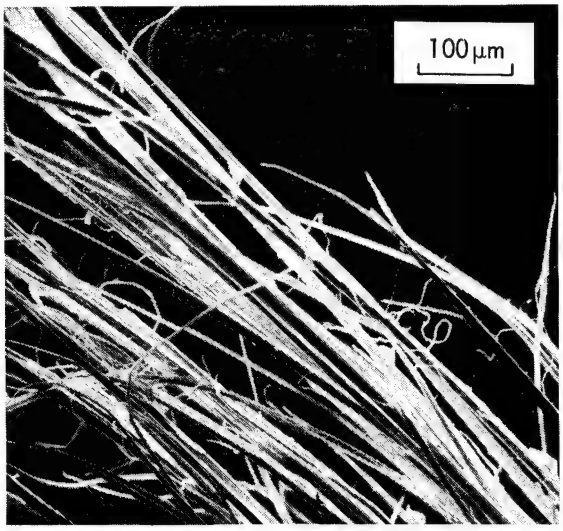

a

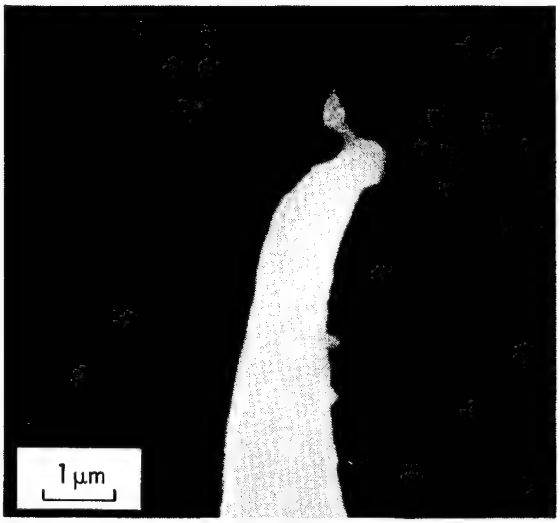

b

Fig. 50. Typical filament ends from a fractured NOL ring (SEM); (a) several filaments, (b) a single subfilament.

The typical microstructure in transmission is shown in Fig. 52. Both high and low density areas are easily delineated. Stereo pairs of these areas clearly showed that at least some of these defects were within the fiber, rather than on the surface. This substantiates the existence of either a second phase or inherent defects observed in the SEM studies.

Figure 53 shows TEM micrographs of the typical tensile fracture ends of single filaments. The very fine points of the sub-filaments are similar to those

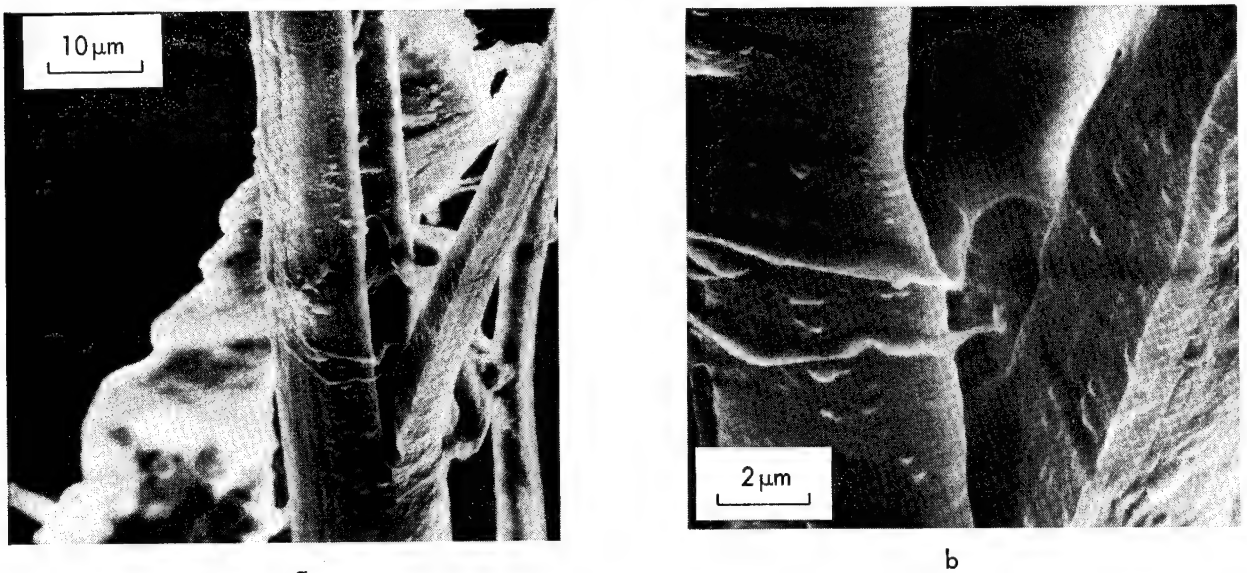

a b

Fig. 51. Atypical filament ends from the fracture area of a pressure vessel (SEM).

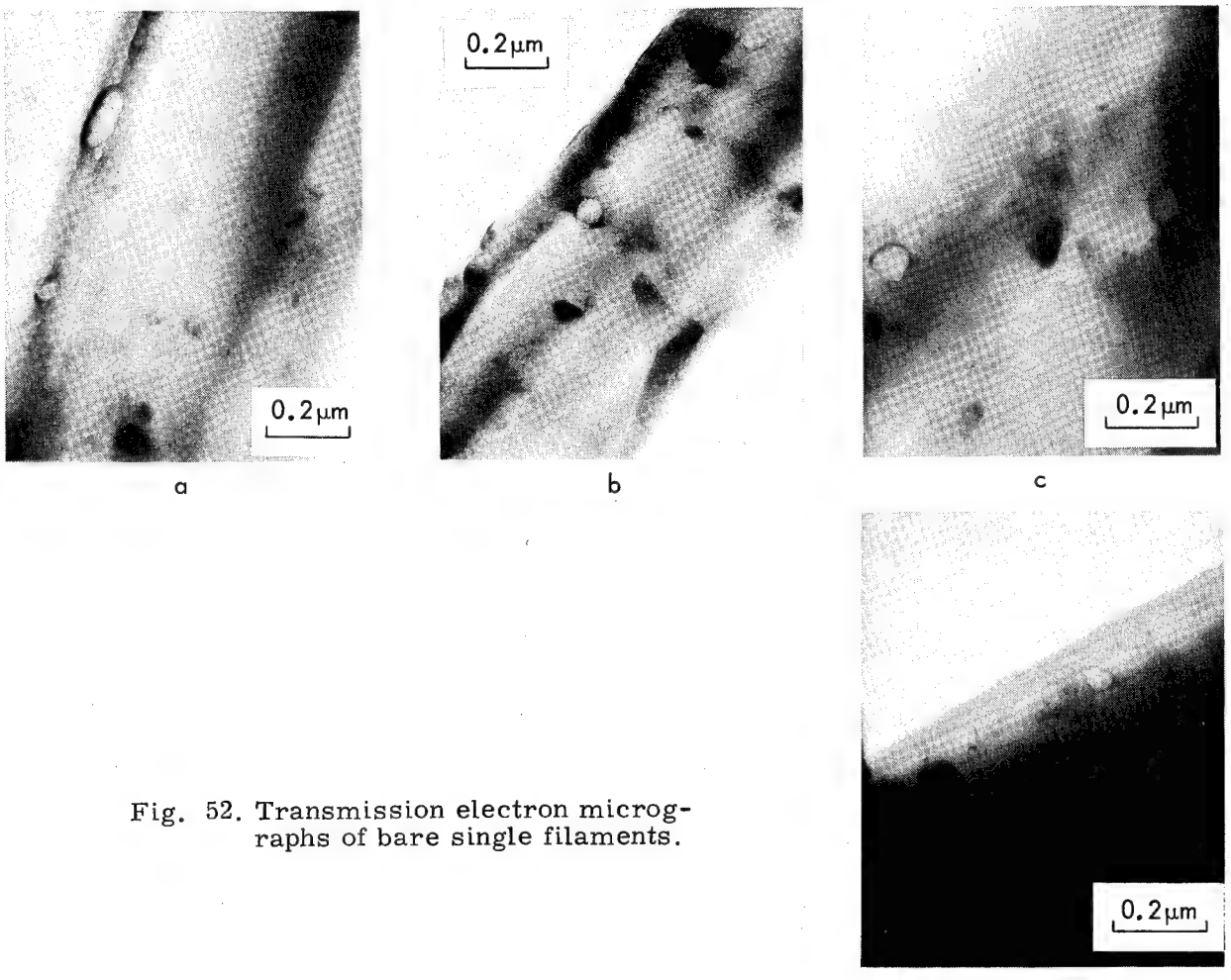

a b c d

Fig. 52. Transmission electron micrographs of bare single filaments.

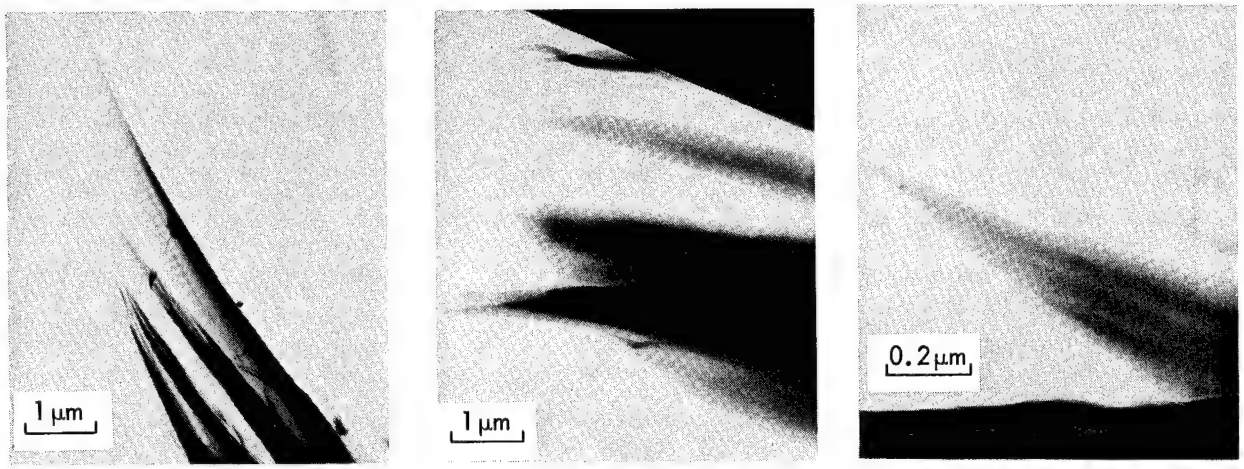

Fig. 53. Transmission electron micrographs of fracture ends of bare single filaments.

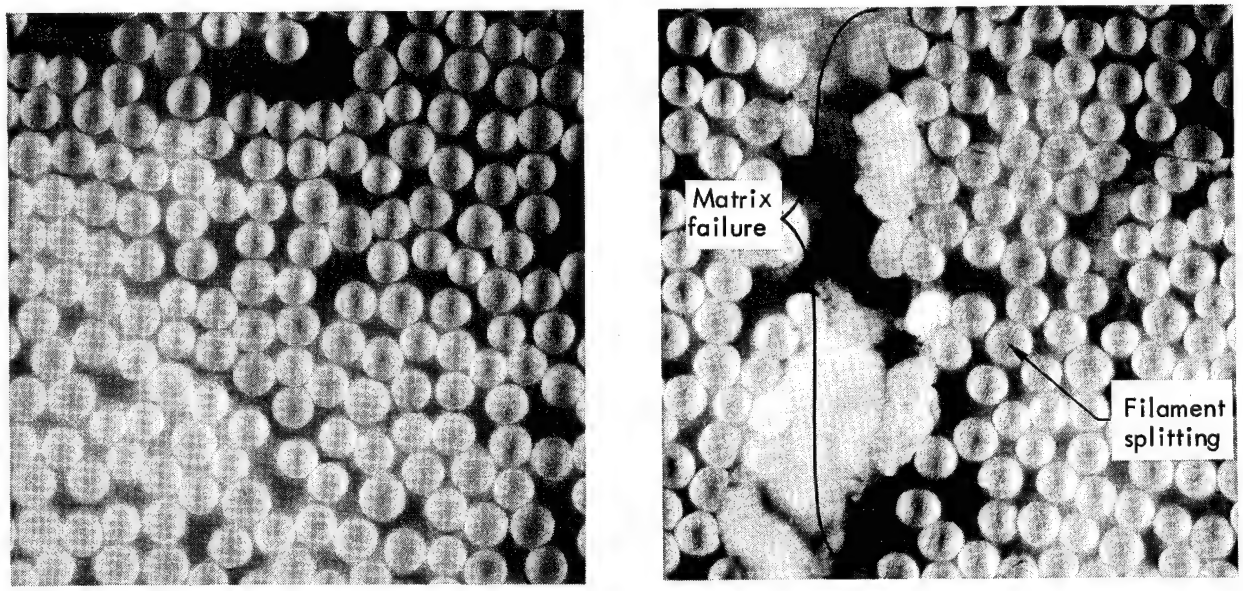

a) Cross section away from failure area.

b) Cross section in a failure area.

Fig. 54. Cross section of the organic fiber/epoxy composite used in a pressure vessel tested to failure (500X); (a) cross section away from failure area, (b) cross section in a failure area.

observed by SEM. A limited number of fracture ends were observed and found to be fairly clean, i.e., there was not a preponderance of the internal defects associated with the fracture ends.

Further characterization of the organic fiber failure mode was possible by optical microscopy. Typical cross sections of an organic composite are shown in Fig. 54. The particular specimens were from a pressure vessel, but the microstructure was similar in simple strands and NOL rings. The pressure vessel was tested to failure and in Fig. 53a, a cross section at a considerable distance from the area of failure is shown. The epoxy

matrix is intact and the fibers show relatively little evidence of damage and defects. In Fig. 54b, a cross section of the composite in the failure area is shown. A large fracture in the epoxy matrix is present and considerable splitting of the filaments along their axes is visible. The splitting is particularly prevalent in the area immediately adjacent to the matrix fracture. The splitting in the fractured area appears to be a common phenomenon, but care must be exercised in specimen preparation as it is conceivable that some polishing procedures would lead to such splitting. The splitting of the filaments observed by optical microscopy is in agreement with the splitting tendency of the fibers upon failure seen by SEM and TEM.

SUMMARY

- Transmission and scanning electron microscopy can be utilized to advantage in studying organic fibers.
- The internal microstructure of single organic filaments is not homogeneous but contains second phases or inclusions.
- Evidence for microvoids was not found but the possibility of their existence was not eliminated.
- The fracture mode of the organic fibers consisted of spitting individual filaments along the filament axis and stretching individual components of the organic fibers to failure.

Final Conclusions

The typical fiber failure stress of the fiber/epoxy strands is 3510 MPa (509 ksi); the typical fiber modulus is 140 GPa (20×10^6 psi); and the typical composite density is 1.4 g/cm^3 at ambient temperatures. We consider the fiber uniformity to be acceptable for an engineering material.

The vessel performance factor is approximately the same for both spherical and cylindrical vessels. The choice between the two vessel shapes should be based on dimensional requirements and the availability of the type of winding machine. We believe that the best design of a cylindrical vessel is from the following combination: wide-band winding (to minimize fiber cross-over), "in-plane" dome contour, fitting diameter approximately 10% of the vessel diameter, of vessel length-to-diameter ratio of no more than three, a hoop/axial-filber winding ratio of around 1.75, and localized reinforcement at the equators and knuckles of the vessel.

The best vessel performance factor based on fiber mass (PV/W_f) is around 600 kPa $\cdot$ m^3/kg (2.4×10^6 in.). We do not see any obvious size effect between 10.2-cm and 20.3-cm-diameter vessels. Both cryogenic temperatures and strain rate have little effect on the fiber failure stress or the vessel performance factor.

For cryogenic temperatures or gas containment, when fatigue resistance is necessary, a soft Al liner for a vessel is unreliable. A fatigue-resistant metal liner is needed before the composite metal-liner-vessel system can be used for these applications.

Acoustic emission is a useful tool for detection of the microscopic failure events that occur during pressurization of an organic fiber/epoxy pressure vessel. Acoustic emission can show if the hoop wraps of a cylindrical vessel are highly loaded before failure. It also can distinguish between different epoxies. And finally, acoustic emission can sort out artificially flawed organic fiber cylindrical pressure vessels if the flaw controls the failure.

The character of the fracture mode of this organic fiber/epoxy composite and the absence of finish to aid interfacial bonding leads one to be cautious about using this composite in applications where the loading is not largely tensile. For tensile-critical applications, however, this organic fiber/epoxy system is attractive.

Microstructural characteristics of the fiber indicate that:

- There are microscopic inhomogeneities within the organic filament.
- The failure mode of the filaments in this organic fiber/epoxy composite, under tensile loading, consists of the splitting of individual filaments along the filament axis.

Acknowledgment

This work was performed under the joint auspices of the National Aeronautic and Space Administration and the U.S. Atomic Energy Commission.

References

1. Chem. and Eng. News 50, 33 (1972).
2. T. T. Chiao and . P. Althouse, "Characterization of an Epoxy System for Filament Winding," in Proc. 4th National SAMPE Technical Conf., 1972 (SAMPE, Palo Alto, California, 1972), pp. 161-168.
3. R. L. Moore and J. K. Lepper, "Strain-Measure Techniques for Modulus Determination," submitted to the J. of Testing and Evaluation, Aug. 1973.
4. W. H. Gloor, Estimation of True Fiber Modulus from Instron Data, Air Force Material Laboratory, Rept. TM-Man-68-15 (1968).
5. T. T. Chiao and R. L. Moore, J. Composite Materials 5, 2 (1971).
6. N. F. Dow, "Materials, and Engineering Problems," in Mechanics of Composite Materials, F. W. Wendt, H. Liefowitz, and N. Ferrone, Eds. (Pergamon Press, Oxford, 1970), p. 23.
7. T. T. Chiao and A. D. Commins, "Fiber Strength of S-Glass/Epoxy Composites Under Biaxial Loading," in Proc. 4th National SAMPE Technical Conf., 1972 (SAMPE, Palo Alto, California, 1972), pp. 169-177.
8. T. T. Chiao and R. L. Moore, "A Room-Temperature-Curable Epoxy for Advanced Fiber Composites," to be presented at the SPI Reinforced Plastics/ Composites Institute 29th Annual Technical and Management Conf., Washington, D.C., 1974.
9. D. A. Stang, "The Use of Planar Ribbon Winding for Control of Polar Build-up in Filament-Wound Tankage," in Proc. 14th National SAMPE Technical Conf., 1968 (SAMPE, Coco Beach, Florida, 1968), p. 11.
10. T. T. Chiao and M. A. Marcon, "Filament-Wound Vessel from an Organic Fiber/ Epoxy System," S.P.I. Reinforced Plastics/Composites Division Proceedings, Sect. 9-B, 1973.
11. T. T. Chiao, J. K. Lepper, N. W. Hetherington, and R. L. Moore, J. of Composite Materials 6, 360 (1972).
12. A. Feldman, A. J. Giguere, and D. A. Stang, "Design Application of High Modulus Filament-Wound Composites to Aerospace Propellant and Pressurization Tanks," in Proc. 15th National SAMPE Technical Conf., 1969 (SAMPE, Los Angeles, California, 1969), p. 157.
13. F. R. Schwartzberg, Cryogenics Materials Data Handbook, Martin Marietta Corp., Denver, Colorado, Rept. AFML-TDR-64-280 (1970).
14. M. A. Hamstad, "Acoustic Emission from Filament-Wound Pressure Bottles," in Proc. 4th National SAMPE Technical Conf., 1972 (SAMPE, Palo Alto, California, 1972), pp. 321-331.

Distribution

LLL Internal Distribution

Roger E. Batzel
R. B. Barker
E. R. Bissell
G. A. Broadman/R. B. Carr
R. H. Bulmer
W. H. Chapman
T. T. Chiao — 50
W. J. Comfort
R. G. Dong
T. N. Faddis
B. L. Garner
M. A. Hamstad — 20
J. E. Hanafee/F. J. Fulton
J. A. Hoffman
J. S. Kane
J. Kury
J. K. Lepper
R. A. Larder
M. A. Marcon — 5
L. M. McGrew
R. L. Moore — 2
P. H. Moulthrop/W. B. Crowley
R. L. Morton/R. B. Engle
W. E. Nelson
T. Perlman/R. Wasley
K. Ristad
R. G. Stone
C. A. Tatro
R. J. Wasley
J. White
TID File — 30

External Distribution

D. M. Schuster — 5
Sandia Laboratories
Albuquerque, New Mexico

G. C. Deutsch
J. J. Gangler
N. J. Mayer
B. Achhammer
National Aeronautics and Space Administration
Washington, D.C.

J. M. Stuckey
H. M. Walker
D. Kornfeld
National Aeronautics and Space Administration
Marshall Space Flight Center
Alabama

J. T. Hoggatt
The Boeing Company
Seattle, Washington

W. T. Freeman, Jr. — 3
Hercules, Incorporated
Allegheny Ballistics Laboratory
Cumberland, Maryland

E. Morris
Structural Composites Industries, Inc.
Azusa, California

NASA Representative
Science and Technical Information Facility
College Park, Maryland

F. R. Barnet
R. Simon
U.S. Navy Ordnance Laboratory
Silver Spring, Maryland

Technology Utilization Office
National Aeronautics and Space Administration
Cleveland, Ohio

J. Carter
Brunswick Corporation
Lincoln, Nebraska

B. Aleck
Grumman Aerospace Corporation
Bethpage, Long Island, New York

A. Cozewith
ARDE, Inc.
Mahwah, New Jersey

External Distribution (Continued)

W. S. Dritt
Union Carbide Corporation Y-12
Oak Ridge, Tennessee

R. E. Lewis 2
Army Materials and Mechanics
Research Center
Watertown, Massachusetts

R. H. Johns
G. T. Smith
R. F. Lark 2
R. H. Kemp
J. R. Faddoul
National Aeronautics and Space
Administration
Cleveland, Ohio

W. Jensen
E. Y. Robinson
Jet Propulsion Laboratory
Pasadena, California

J. D. Ray
W. H. Gloor
H. S. Schwartz
G. P. Peterson
W. J. Schulz
S. Litvak
A. Olevitch
L. J. Obery
E. J. Morrisey
Department of the Air Force
Wright-Patterson AFB, Ohio

R. L. Johnston
R. E. Johnson
S. V. Glorioso
B. D. Kendrick
R. N. Prince
L. G. St. Leger
NASA-Lyndon B. Johnson Space
Center
Houston, Texas 77001

N. S. Khot
R. D. Joblove
G. P. Sendeckyj
Air Force Flight Dynamics
Laboratory
Wright Patterson Air Force Base
Ohio 45433

B. M. Halpin, Jr.
Department of the Army
Watertown Arsenal
Watertown, Maryland 02172

R. J. Thompson
Department of the Army
Redstone Arsenal
Huntsville, Alabama 35809

P. Goodwin
C. Bersch
M. Stander
Naval Air-Systems Command
U.S. Navy Department
Washington, D. C. 20360

B. Drimmer
M. Kinna
Naval Ordnance Systems Command
U.S. Navy Department
Washington, D. C. 20360

R. Morse
Brunswick Corporation
4300 Industrial Ave.
Lincoln, Nebraska 68504

C. Zwenben, E 262
J. W. Moore
L. Miner
E. I. duPont de Nemours & Co.
duPont Experimental Station
Wilmington, Delaware 19898

S. P. Prosen
The Fiberite Corporation
512 W. Fourth Street
Winona, Minnesota 55987

A. Feldman
Martin Marietta Corporation
Denver, Colorado

M. Nabler
L. Korb
North American Rockwell
Corporation
12214 Lakewood Blvd.
Downey, California 90241

L. J. Ashton
Fiber Science, Inc.
245 East 157th Street
Gardena, California 90248

I. E. Figge, Sr.
R. Barrisford
U.S. Army Air Mobility
R&D Lab.
Fort Eustis, Virginia

TID-4500 Distribution, UC-4
Chemistry 169

RE-RUN
7/24/74 100

MSG/lc/edas

☆ GPO 790-191